DEVELOPMENT, IMPLEMENTATION AND VALIDATION OF A NON-DIMENSIONAL PUMP MODEL IN ENERGYPLUS

By

KAUSTUBH P. PHALAK

Bachelor of Technology in Mechanical Engineering

University of Pune

Pune, Maharashtra, India

2007

Submitted to the Faculty of the
Graduate College of the
Oklahoma State University
in partial fulfillment of
the requirements for
the Degree of
MASTER OF SCIENCE
December, 2011

DEVELOPMENT, IMPLEMENTATION AND

VALIDATION OF A NON-DIMENSIONAL PUMP

MODEL IN ENERGYPLUS

Thesis Approved:

Dr. Daniel Fisher

Thesis Adviser

Dr. Jeffrey Spitler

Dr. Lorenzo Cremaschi

Dr. Sheryl A. Tucker

Dean of the Graduate College

Table of Contents

List of Figures

List of Symbols

Following is the list of most generally used symbols used in the discussions. Special notations are explained at specific places.

A_2	-	Impeller exit cross-sectional area
A_{CS}	-	Impeller cross-sectional area
C	-	Absolute velocity of the fluid in pump / Equivalent system pressure constant
C_2	-	Absolute velocity of the fluid exiting impeller
C_3	-	Absolute average velocity of the fluid inside volute
$C_{s\,1}$	-	Fluid shock velocity at the entrance of the impeller
$C_{s\,2}$	-	Fluid shock velocity at the exit of the impeller
$C_{t\,1}$	-	Tangential component of absolute velocity of the fluid entering impeller
$C_{t\,2}$	-	Tangential component of absolute velocity of the fluid exiting impeller
$C_{t\,2}'$	-	Average flow velocity in the volute
D	-	Diameter / hydraulic diameter
d_1	-	Impeller inlet diameter (inches)
D_1	-	Impeller inlet diameter (m)
d_2	-	Impeller outlet diameter (inches)
D_2	-	Impeller outlet diameter (m)
D_h	-	Impeller hub diameter
D_i	-	Impeller inlet hydraulic diameter
e_P	-	Pressure measurement uncertainty

e_{RPM}	-	Tachometer uncertainty
e_V	-	Flow-meter uncertainty
$e_{V\,Fluke}$	-	Fluke/NetDAQ logger voltage uncertainty
e_W	-	Watt transducer uncertainty
f	-	Friction factor / Input frequency to electric motor
g	-	Gravitational acceleration
H	-	Pressure head
h_{in12}	-	Velocity shock at the entrance
h_{in23}	-	Velocity head loss inside volute
h_{diff}	-	Diffusion head loss
$H_{\text{effective}}$	-	Effective pressure head
h_{sf12}	-	Surface friction head loss inside impeller
h_{sf23}	-	Surface friction head loss inside volute
H_{th}	-	Theoretical head
K	-	Pressure constant
K_1 , K_2	-	Theoretical pump head coefficients
L	-	Pipe length
m	-	Mass flow rate
n	-	Rotational speed (rpm)
N	-	Rotational speed (rps)
Ns	-	Specific speed of pump
p	-	Pressure rise
P	-	Power
P_{CS}	-	Impeller cross-sectional perimeter
Δp	-	Change in pressure

PLR	-	Part load ratio
q	-	Volumetric flow rate (gpm)
Q	-	Volumetric flow rate (m^3/s)
Q_{BEP}	-	Volumetric flow rate at best efficiency point
r_1	-	Impeller inlet radius
r_2	-	Impeller exit radius
Re	-	Reynolds number
s	-	Percentage slip (the lag between rotor speed and magnetic field)
t	-	Impeller blade thickness
U	-	Impeller tangential velocity
U_1	-	Impeller inlet tangential velocity
U_2	-	Impeller exit tangential velocity
V	-	Average velocity of the fluid
W	-	Velocity of the fluid relative to the impeller
w	-	Impeller width
W_1	-	Fluid relative velocity (impeller at inlet)
W_2	-	Fluid relative velocity (impeller at exit)
W_{m2}	-	Radial component of fluid relative velocity (impeller exit)
W_{t2}	-	Tangential component of fluid relative velocity (impeller exit)
Z	-	Number of poles in motor winding / Number of impeller blades
β	-	Damping factor
β_1	-	Impeller inlet blade angle
β_2	-	Impeller exit blade angle
ϵ	-	Relative roughness
ζ	-	Equivalent loss coefficient

ζ_2	-	Shock loss coefficient at exit of impeller
ζ_r	-	Impeller friction loss coefficient
ζ_v	-	Volute friction loss coefficient
η	-	Efficiency
μ	-	Dynamic Viscosity
ν	-	Kinematic viscosity
π_1 , π_2, π_3	-	Non-dimensional products
ρ	-	Fluid density
σ	-	Fluid slip factor
τ	-	Torque
φ	-	Non-dimensional flow coefficient
ψ	-	Non-dimensional pressure coefficient
ω	-	Angular velocity of impeller

Chapter 1. Introduction and Objectives

1.1 Introduction

Nationally electric motors consume 50-60% to total electrical energy of which about 46% is used in HVAC equipments like fans, pumps and compressor. Thus approximately one quarter of total electrical energy consumption in United States is due to fans and pumps (Elliot & Nadel, 2003).

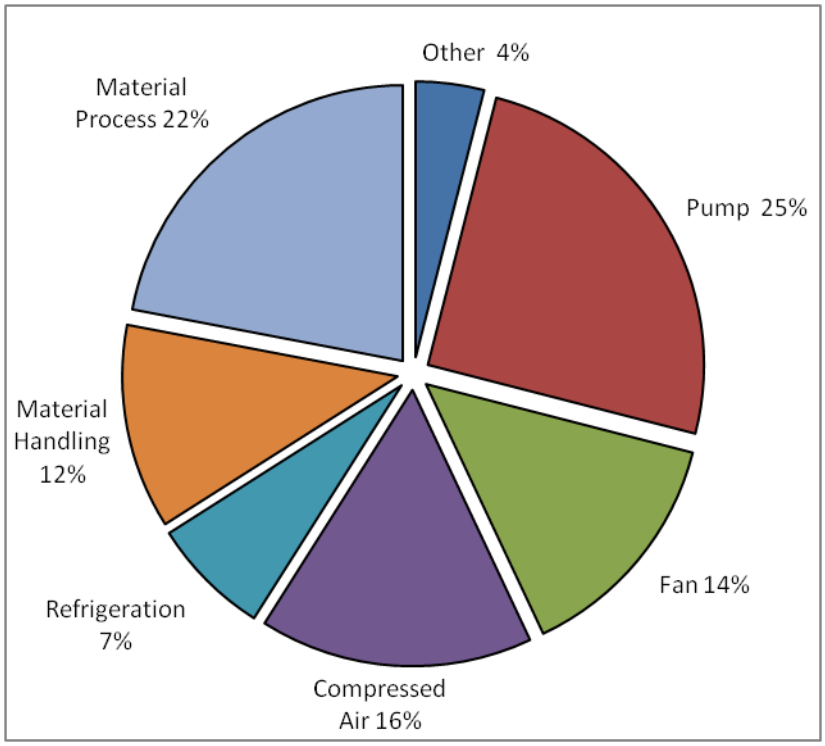

Figure 1-1 National Industrial Motor Systems Energy End-Use

Following Elliot & Nadel (2003)

In HVAC systems, pumps or fans are often selected on the basis of maximum fluid flow required. In most systems flow requirements vary throughout the day and year. Thus, pumps often run at partial flow conditions. Desired flow is achieved by increasing system flow resistance, bypass

loops or controlling pump performance.

According to affinity laws for pumps (McQuiston, Parker, & Spitler, 2005), pump flow varies in direct proportion to rotational speed while power varies by cube of rotational speed. If this relation holds for power, reduction in speed should result in substantial energy savings. Thus reduction in the rotational speed of the pump using a variable frequency drive (VFD) is advised over using valves (dampers in case of fans) to control the flow rate. Valves and dampers increase (or decrease in case of bypass control) system resistance to adjust flow as per requirement. This adjusts the system curve to achieve required flow per load demand (as shown in Figure 2-9 and Figure 2-10 and explained in section 2.3). Use of VFD is scaling down (or up) the pump (or fan) curve i.e. adjustment of pump (or fan) curve to provide required flow. Decrease rotational speed of pump and fan results in reduction in input energy. Thus use of VFD should result in energy savings.

A number of software packages allow the simulation of building energy and related HVAC systems in order to predict total energy consumption by components to satisfy the building load. Pumps are an integral part of HVAC system. In cases of frequent fluid flow variation, using a rated power consumption value of pumping system may result in substantial inaccuracies in pump power usage. If the pump power is a major contributor to the overall energy consumption, accurate pump power prediction becomes important.

1.2 Objectives

Research objectives of the work are outlined as follows:

1.2.1 Theoretical Study for Confirmation of Non-dimensional Model

Affinity laws are used to predict changes in pump performance with respect to changes in pump parameters. When results of non-dimensional models are compared to pump affinity laws divergence is observed. The first objective of this research is to find the reason for divergence and

suggest a generalized non-dimensional model that satisfies the affinity laws and is based on manufacturers' pump data. To support this model, this research includes a study of the effects of pump parameters on performance curves using energy conservation and velocity vector analysis.

1.2.2 Experimental Verification of Affinity Laws

Often the energy savings predicted by affinity laws appear overly optimistic. One of the objectives of this research is to verify the accuracy of these laws using an experimental facility. The focus of this research is the energy consumption's dependence on rotational speed.

1.2.3 Implementation of Pump Model in EnergyPlus

The previous section described the importance of accurate pump power prediction in HVAC systems. This carries over to HVAC system and plant simulation software. A realistic pump model is required to carry out pressure based simulation, which will govern flow rate in the system and predict accurate power consumption. The objective is to develop and implement in EnergyPlus a pump model which will reliably predict accurate values of energy usage for typical pumping systems.

1.3 Thesis Organization

Overall organization of the document is discussed in this section.

Chapter 2 provides basic theory required for understanding of subsequent chapters. It provides information about pump performance curves, stable and unstable pump operation, basics of working of variable frequency drives, introduction to EnergyPlus. Chapter 3 and 4 deal with the first objective discussed in Section 1.2.1. Chapter 5 and 6 are concerned with Section 1.2.2 and 1.2.3 respectively. Since each chapter has its own objective, there is no separate chapter for a literature review. For the respective discussions a separate literature review is provided within each chapter. Similarly a section for results and discussion is provided at the end of chapter. Chapter 7 provides conclusions related to each objective discussed in Chapter 1.

Document Organization

Chapter 3 discusses two theoretical pump models in which pump performance is studied with respect to pump geometrical and operational parameters. Equations for pump head are derived and a VBA code is developed for each model. Using these codes pump head vs. flow rate curves are generated and compared with the curve provided by manufacturers.

From the results of the theoretical pump models it was concluded that for simulation purposes a simplified non-dimensional model rather than a detailed model, as discussed in Chapter 3 is needed. Thus, Chapter 4 talks about non-dimensional analysis, significant variables in the analysis and pump affinity laws and derives non-dimensional numbers from variables that affect pump performance. Results of non-dimensionalization are compared with affinity laws.

Power savings predicted by affinity laws for power savings seem overly optimistic. To verify the power savings predicted by affinity laws an experiment is run on existing facility with variable frequency drive. Procedure and results are discussed in Chapter 5.

In energy simulations, power consumed by pumping systems can play an important role in many configurations. This power consumption is dependent on pressure drop in the loop and the flow through it. Thus pressure based simulation has been introduced in EnergyPlus. For pressure based simulation a flow resolver function is added to which non-dimensional pump characteristic curve can be added. Variable frequency drive control logic has also been introduced in the PlantPumps module which scales the pump curve according to input RPM schedule or required mass flow rate by the demand side of plant loop. Chapter 6 discusses this flow resolution method and various VFD control techniques.

Chapter 2. Background

2.1 General Centrifugal Pump Theory

2.1.1 Centrifugal Pump Construction and Fluid Mechanics

Centrifugal pumps are the most widely used impeller pumps in the HVAC industry. The basic operation is of pump is to convert kinetic energy to potential energy. There are several types of centrifugal pumps, classified according to their construction, application, performance and stages.

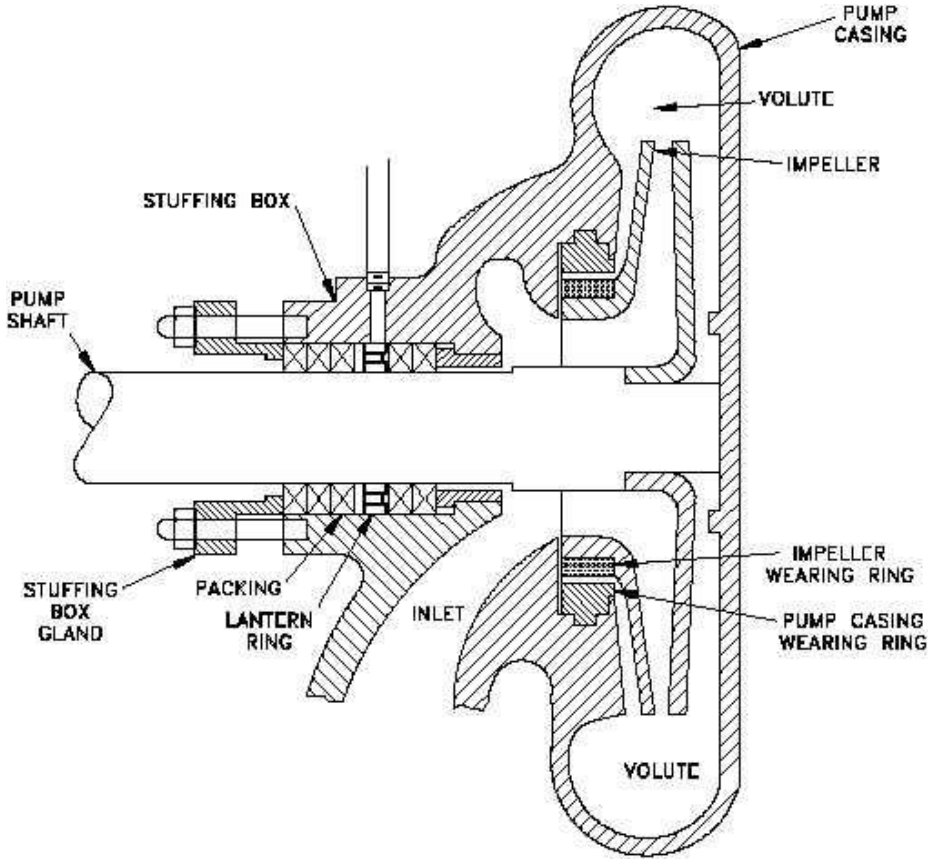

Figure 2-1 Cross-section of Single Stage Centrifugal Pump

Courtesy of Integrated Publishing, Inc. (1993)

Figure 2-1 shows the basic construction of a single stage centrifugal pump.

The impeller is mounted on a rotating shaft as shown in Figure 2-1, increases the momentum of liquid. The rotating element (i.e. the impeller) sets the liquid in a motion in a radial outward direction. This applies a centrifugal force to the liquid creating a velocity head. Blades on the impeller (and diffuser ring[1]) then direct the fluid into the volute. The volute has continuously increasing cross-sectional area in the flow direction which reduces the velocity of the liquid. According to Bernoulli's principle, reduction in velocity results in an increase in pressure. Since there are comparatively negligible losses, the pressure head increases continuously as volute cross-sectional area increases.

2.1.2 Pump and Motor Selection

Pump selection can be based on several parameters which might be broadly classified under process requirement, mechanical considerations and hydraulic performance. Process requirements are based on hazardous environment, pump location, temperatures etc. Mechanical considerations include material, bearings, seals, vibrations, noise, installation, maintenance etc. Selection based on hydraulic performance includes consideration of nominal flow, head, efficiency, power and rotational speed.

For rotational drive pumps, electric motors are generally preferred. However, in case of outdoor, emergency, or remote locations internal combustion engines are used. They offer limited operational range of rotational speed with very limited flexibility in variation. Electric motors for pumps are selected with a certain service factor (close to and generally greater than 1). Service factor determines the horse power rating of the motor.

$$Electric\ motor\ power\ rating\ = service\ factor\ \times\ pump\ input\ power\ requirement$$

[1] Diffuser ring (not shown in the figure) is a series of stationary guide passages surrounding the impeller having gradually increasing cross-section area.

[2] NPSH is the difference between fluid pressure and vapor pressure at given temperature. Fluid starts

Service factor depends upon the type of application and shows the spare power or power margin i.e. the additional power the motor can provide in case of overload. When pumps are sold with a motor the service factor is usually close to 1.

2.1.3 Pump Performance Curves and System Curve

Pump performance curves display the dependence of flow on pressure head, efficiency, Net Positive Suction Head (NPSH)[2] and power. These curves are given by pump manufacturers after collecting experimental data on a given pump for four to five impeller diameters. Sometimes manufacturers provide a band instead of a curve. To achieve specified pump performance, the impeller is often physically trimmed which results in scaling down of the pump curves.

The operating point of the system is determined by the intersection of the pressure rise and pressure drop curves. The pressure drop inside a pipe for average velocity (V) is given by Equation 2-1 (Darcy-Weisbach equation):

$$\Delta p = f \frac{L}{D} \frac{\rho V^2}{2g} \qquad (2\text{-}1)$$

The friction or Darcy factor (f) is determined by the Moody chart or by Colebrook's equation. Colebrook's equation is an implicit equation, which adds a complication to solving this system; however numerous explicit curve-fit equations are available which provide a sufficiently accurate value of the friction factor.

The pressure drop across pipe fittings is given by Equation 2-2:

$$\Delta p = K \frac{\rho V^2}{2g} \qquad (2\text{-}2)$$

The pressure constant (K) of several types of fittings is given in reference books and journals.

[2] NPSH is the difference between fluid pressure and vapor pressure at given temperature. Fluid starts boiling whenever fluid pressure drops below vapor pressure and this lead to cavitation causing damage to impeller and volute casing.

This pressure constant is assumed to be independent of flow conditions, depending only on the fitting geometry.

If Equation 2-1 and Equation 2-2 are added for the entire series piping network then the resulting equation will provide the overall pressure drop in the system.

$$\Delta p = \frac{\rho V^2}{2g}\left[\sum\left(f\frac{L}{D}\right) + \sum K\right] \qquad (2\text{-}3)$$

In Equation 2-3 density (ρ), gravitational acceleration (g), pipe length (L), hydraulic diameter (D) and pressure constant (K) are either geometric characteristics of the system or constants. Friction factor is a function of relative roughness (which is a material property; thus constant) and Reynolds number. In the Moody chart it can be observed that friction factor (f) is almost independent of Reynolds number (and thus independent of flow) in the turbulent region. After combining all the constants and replacing average velocity (V) by flow (Q) we can write;

$$\Delta p = CQ^2 \qquad (2\text{-}4)$$

It can be observed that system pressure drop curve is parabolic in nature. Intersection of pump and system curve is operating point.

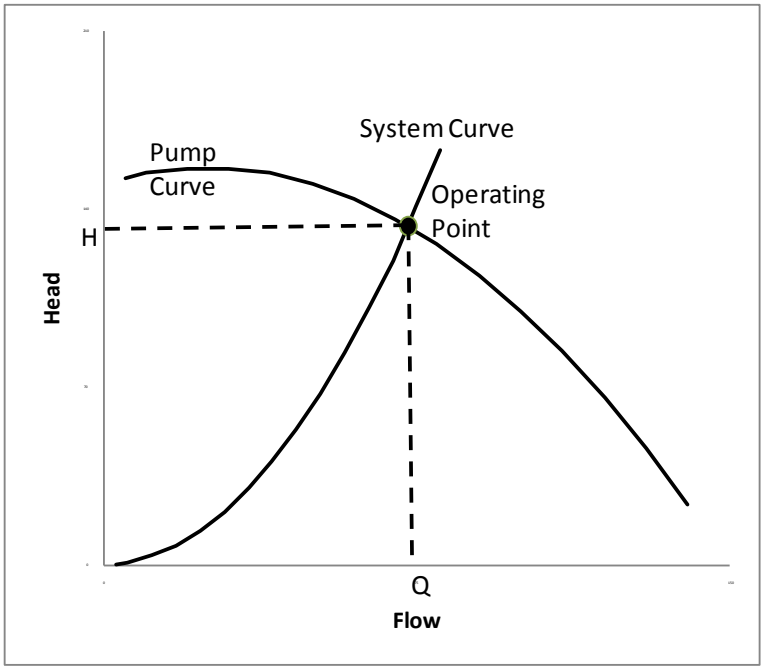

Figure 2-2 Pump curve, System curve and Operating point

Often a minimum flow rate requirement is imposed on a pump to prevent low flow rate instability and excessive recirculation. Instability at low flow rates can be explained as follows:

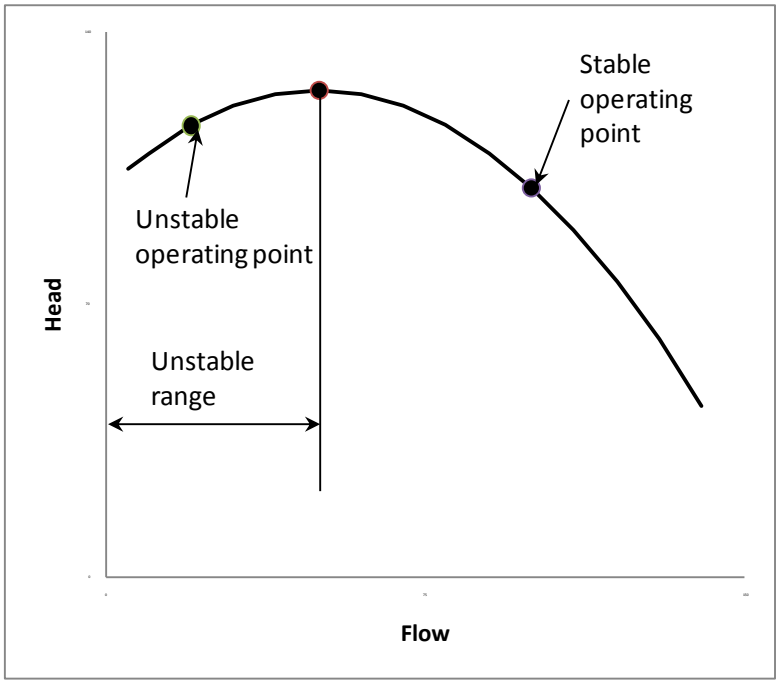

Figure 2-3 Pump curve showing unstable operating range

The pump is considered to be in a stable operation mode if it attains steady state even after a slight disturbance to its original operating condition. If the operating point is located in on the part of the curve where the slope is positive, then a slight increase in pressure will result in an increase in flow rate which will tend to increase the pressure again. Thus, the operating point will move towards the critical point. Similarly it will move towards shut-off head if there is slight reduction in flow[3]. On the other hand a negative slope will result in, increased flow with reduced supplied head which will tend to reduce the flow in the system and the system will thus reach steady state condition.

2.2 Variable Frequency Drives

Variable frequency drives (VFDs) are the devices which control the speed of AC electric motors by changing the input frequency of the power supply. VFDs are widely used to save energy in HVAC systems.

Figure 2-4 (Europump And Hydraullic Institute, 2004) shows types of variable speed drives according to types of motors. Variable speed drives (VSD) can be classified according to type of control as electrical and mechanical type drives. Electrical VSDs offer better control over speed of the motor. In most of the applications AC asynchronous induction motors are used and pulse width modulation (PWM) is preferred over slip recovery.

[3] Operation in this mode is called surge (or compressor stall in case of compressors) and the point separating the stable and unstable modes of operation is called the surge point.

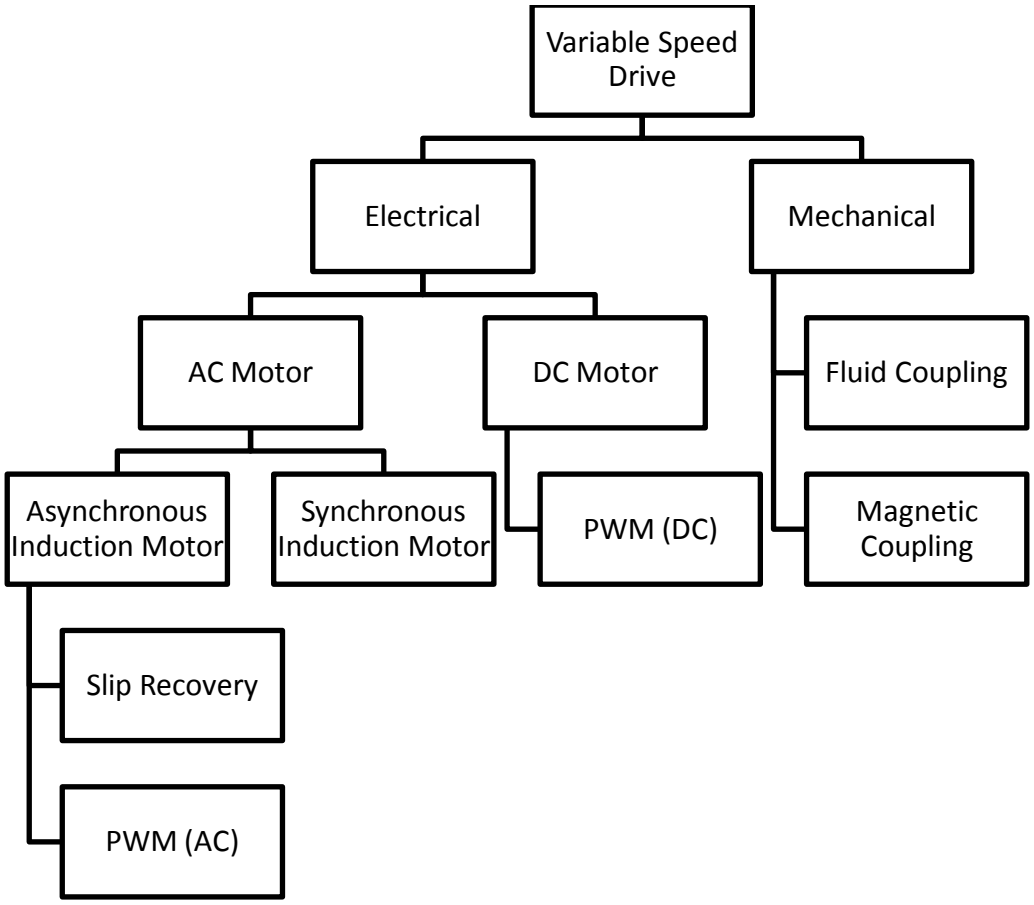

Figure 2-4 Types of Variable Speed Drives

Following EuroPump and Hydraulic Institute (2004)

There are two main methods by which the speed of an induction motor can be varied, either by varying voltage or by varying input frequency. Speed of electric motor in RPM is given by Equation 2-5.

A reduction in the supply voltage increases the slip in stator and rotor resulting in a change of rotational speed of the motor. This method of speed control significantly increases heat generation and is only practical for well cooled motors. (Europump And Hydraullic Institute, 2004)

Power supply frequency variation is the preferred method of rotational speed control. A change in RPM of the electric motor with respect to a change in input frequency can be calculated by

Equation 2-5.

$$n = 2 \times \frac{60f}{Z}(1 - s) \qquad (2\text{-}5)$$

Where, f – input frequency to electric motor

Z – number of poles in motor winding

s - % slip (the lag between rotor/shaft speed and magnetic field)

The most common type of variable frequency drive (VFD) used in practice is the voltage pulse width modulated drives. Figure 2-5 shows various stages in PWM drive.

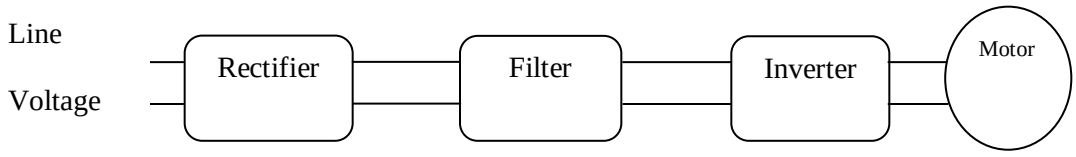

Figure 2-5 Basic stages in PWM drive

Input AC voltage is converted in to pulsated DC voltage by the rectifier. The pulsated DC voltage is smoothed, and the AC component is completely removed by the filter. This DC voltage is then modulated by semiconductor switches.

A PWM control signal is generated using a comparator to which a reference signal (sine wave) is given as an input. This reference signal is then compared with a triangular (or sawtooth waveform).

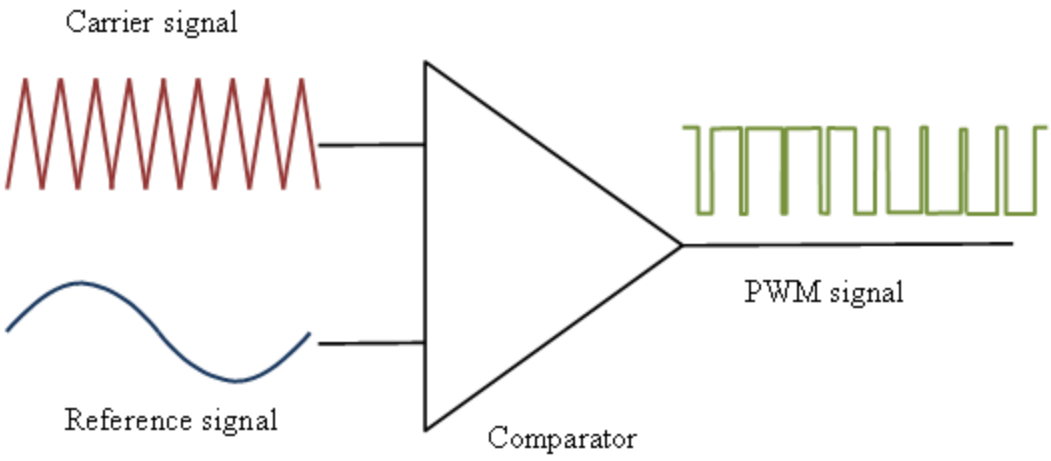

Figure 2-6 PWM Inputs and Output

Following The Fab Lab program (2000)

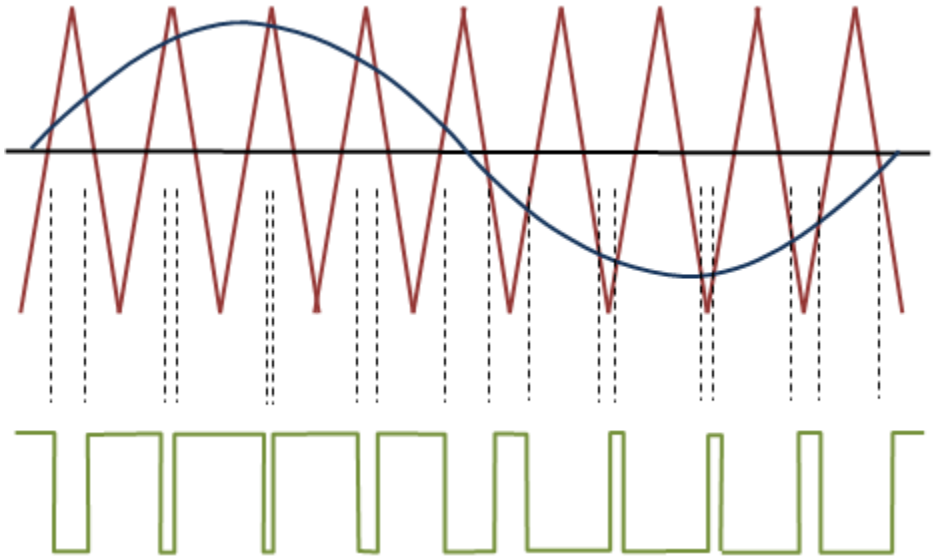

Figure 2-7 PWM working - Intersective Method (Comparator Output Waveform)

Following The Fab Lab program (2000)

Figure 2-6 shows PWM block diagram for a comparator and Figure 2-7 shows a simple way to generate a PWM wave form using the intersective method. The frequency of the sine wave is known as the control or reference frequency, while the frequency of the triangular (or sawtooth) wave is known as the carrier or switching frequency. As a rule of thumb the carrier frequency should be more than ten times the control frequency. In practice carrier frequency is about 4 kHz

to 16 kHz while the control frequency is about 60 Hz (line frequency).

It's the reference frequency which determines RPM of motor and not the carrier frequency. The coil inside the motor acts as a filter or energy storage component. During an 'on' cycle the coil stores energy and uses it over the period of the carrier wave cycle. The Pulse width of the output waveform determines the actual energy transferred to the motor.

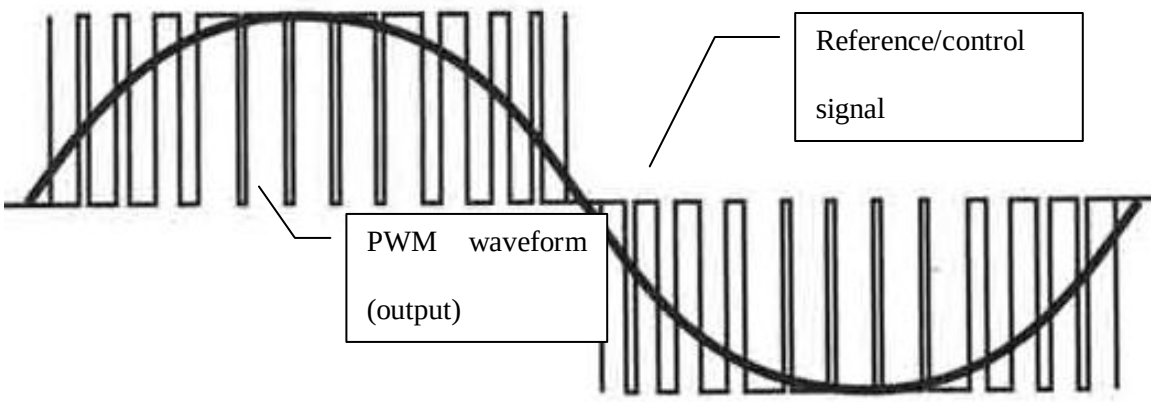

Figure 2-8 Reference and PWM signal (Courtesy of Rockwell Automation, Inc.) (www.industrial-electronics.com)

Pulse width modulation has the least amount of harmonics back to power supply and it also works well with light to heavy duty electrical motors. Intermittent power supply provides better control over pump speed and eventually the power delivered to the fluid.

Induction motors draw very high initial current during starting. Thus, they need current protection device like motor starter to avoid high fluctuation in line voltage. VFDs start the motor with very low supply frequency. This avoids high inrush current and need of separate starter. Thus, for better control over motor operation and to reduce overall pumping energy cost, VFDs are widely preferred in industries.

2.3 Pumping-Piping System Controls

There are three basic flow control methods for continuous flow single pump systems: valve

control, bypass control and speed (VFD) control (EuroPump and Hydraulic Institute, 2004).Valve control and bypass control can be used simultaneously to achieve the desired performance of the system.

On-off control system is implemented where intermittent flow is allowed. Such systems require storage facility. In multi-pump system flow rate can be controlled by turning on or off pumps in parallel or series.

In direct throttle / valve control (Figure 2-9); the valve is attached in series with the system and the system flow rate is varied by increasing the resistance of the system. As an inline valve is closed, the overall system resistance increases thereby making the system curve steeper. The operating point shifts to the left and flow reduction is achieved.

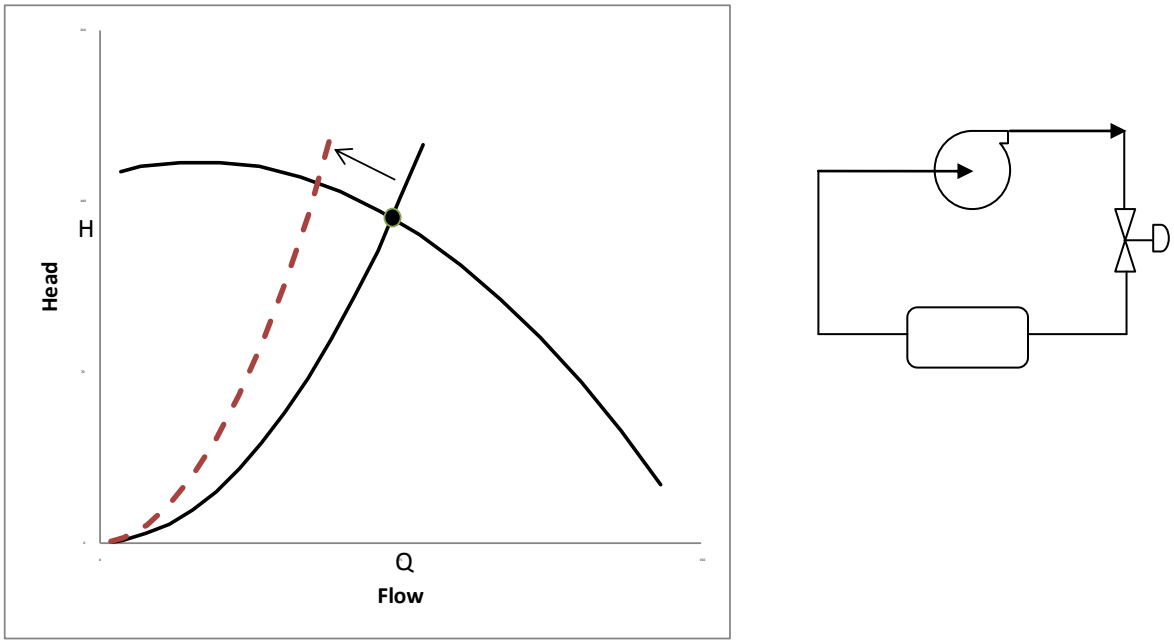

Figure 2-9 Valve (Direct Throttle) Control

In bypass control (Figure 2-10) a bypass branch is connected across the pump or a component (or a group component) depending upon where flow control is desired. Due to the addition of a branch in parallel, the overall system flow resistance decreases. This shifts the operating the point

to the right and flow increase is achieved.

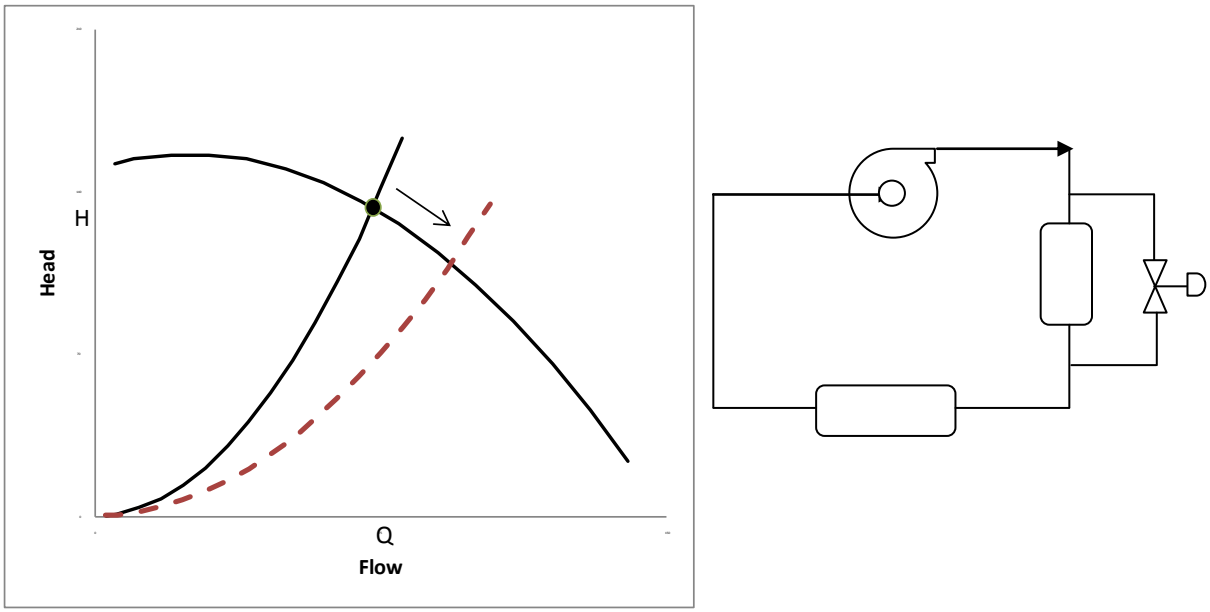

Figure 2-10 Bypass Control

Control methods can also be classified according to the types of HVAC systems which employ them. As we are concerned with control methods in HVAC systems only, the following discussion is limited to closed loop control only.

2.3.1 Differential Pressure Control

In this type of system, a differential pressure range is defined for operation. A differential pressure transducer is connected across the pump which feeds input to the controller. Then, based on entered logic, the controller moves the system operating point between A and B as shown in Figure 2-11. For intelligent VFD products (which have a provision to enter control logic) the output of the pressure transducer can be directly given to the VFD which then adjusts the flow rate between points C and D.

In this type of control the pump will operate within the pressure range specified by points A and B as shown in Figure 2-11.

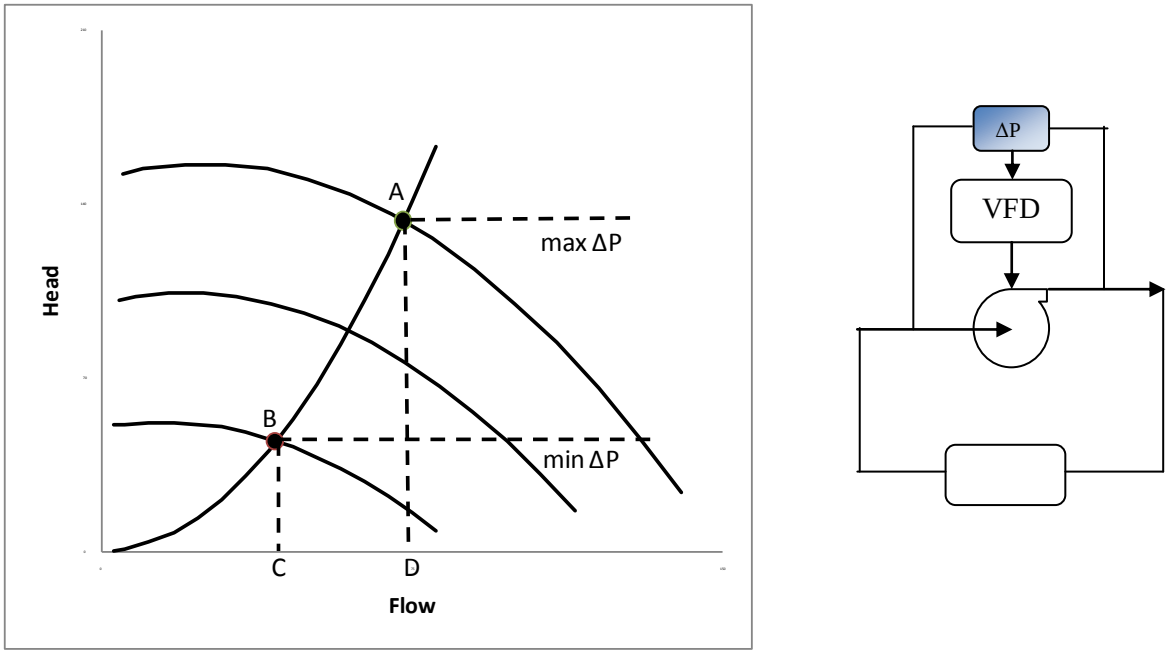

Figure 2-11 Differential Pressure Control

This type of control is most widely used in HVAC and closed loop systems (EuroPump and Hydraulic Institute, 2004). Same logic is been implemented in EnergyPlus with RPM range.

2.3.2 Variable Pressure Fixed Mass Flow Rate Control

The VFD system is considered the optimum system for maintaining constant system mass flow rate through the system components even if, valve positions are varied, or components in parallel branches are turned off. Some chiller, cooling, spraying and washing applications need a constant flow rate regardless of current conditions on that particular component (load, heat to reject or suction, delivery condition etc.). In HVAC systems when constant flow rate is required by chillers a bypass (often called a common pipe) is attached between the demand and supply sides[4]. This common pipe takes care of excess flow rate at part load conditions. Flow through the common pipe is controlled by a valve. This changes the overall system resistance and thereby the pressure-drop across the system. To maintain constant flow with changed system characteristics,

[4] In the schematic (Figure 2-12) supply and demand side are not shown separately, they are combined together and considered as single load on pump. Variation due to common pipe is shown by variable load symbol.

the VFD changes the motor input frequency which scales the pump curve.

For example in Figure 2-12 when the system curve 1 shifts to system curve 2 due to a change in valve position the same pump speed will tend to increase the flow rate through the system. A Flow-meter will sense this increase in flow rate and will send a signal to the VFD. To maintain a constant flow rate, the VFD will reduce RPM such that the pump curve 1 will scale down to pump curve 2, and the new operating point B is attained maintaining constant flow rate.

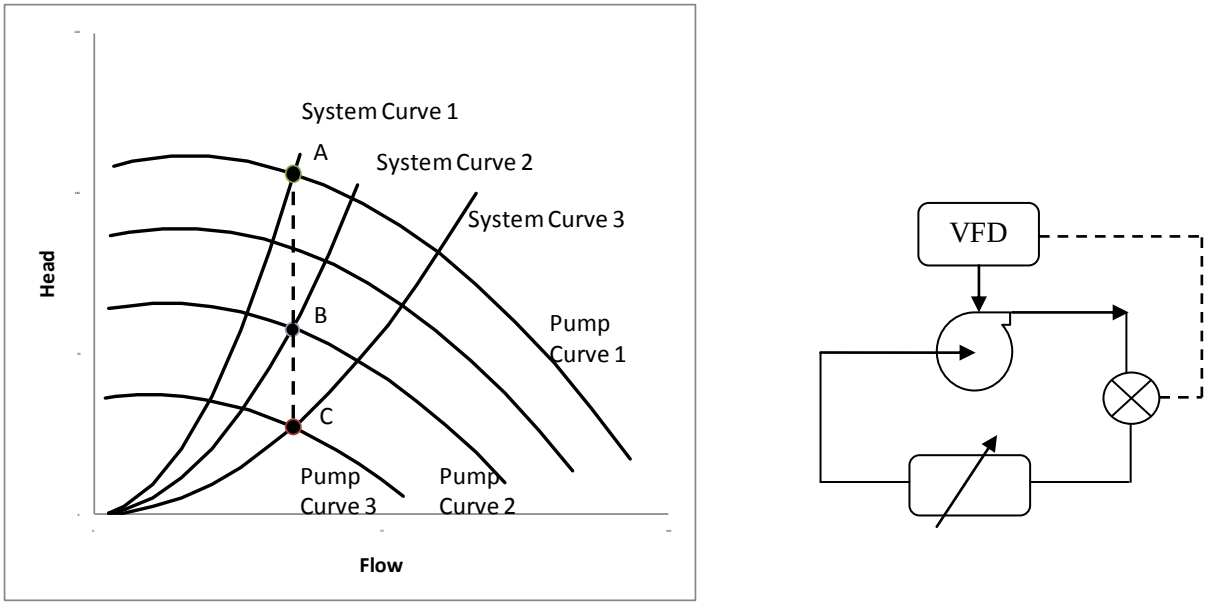

Figure 2-12 Variable Pressure Fixed Mass Flow Rate Control

2.3.3 Variable Flow Fixed Temperature Control

Sometimes in HVAC systems and process industries VFDs are used to maintain a specific temperature at a particular point in the system. Depending upon the load on the system and the required difference between attained temperature and set-point temperature, the mass flow rate is calculated.

Figure 2-13 shows a fixed temperature control implemented in a heating load application. A thermocouple placed after the heating coil reports the current temperature to the VFD and based on this temperature difference the VFD increases or decreases the flow.

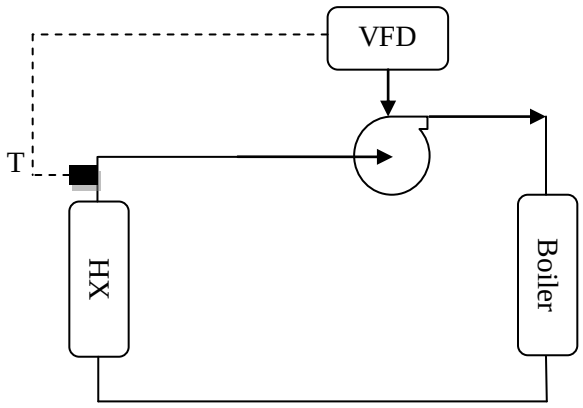

Figure 2-13 Varying Flow Fixed Temperature Control

2.3.4 VFD Manual Control

VFDs have manual mode of operation in practice. In this mode its output frequency can be adjusted (thus RPM of electric motor) manually. This mode doesn't require an additional controller which will be governed by pressure drops or flow rates recorded by sensors. The operator should have an approximate idea about change in flow rates with respect to change in frequency.

2.3.5 Pressure Range Based Control

Pressure based control is a pump control method which uses differential or single point pressure to operate the pump within a desired or safe range. This differential pressure is often measured across the system which is equal to pressure rise across the pump.

Pressure limits are applied to control pump operation for stable, efficient and safe operation of the pumping system.

Mechanical design of hydronic components (heat exchangers, piping, fittings, valves etc) is based on the maximum pressure that can be developed in the system. Excessive pressure rise can damage the system components. The upper pressure limit is based on the maximum design pressure of the system.

Often minimum flow is required to pass through the system components in order to keep the working fluid above its freezing point. Sometimes the pump manufacturer specifies minimum flow required for stable and efficient working of pumping system. (For instability due to low flow rate refer section 2.1.3) The lower pressure limit is decided from the minimum flow that is required by system components (or the pump itself).

High rotational speed in large pumps leads to very high impeller tip speed. This causes high fluid velocity and low pressure on the concave side of the impeller blades and leads to cavitation in the pump. Thus there is an upper limit for pump rotational speed.

VFDs generally have a lower limit for output frequency which naturally provides a minimum limit value for the rotational speed of the pump.

2.4 EnergyPlus Hydronic System Simulation

EnergyPlus is a modular energy simulation program written in FORTRAN. It calculates energy required for heating and cooling by buildings and equipments associated with the HVAC systems when subjected to different environmental and operating conditions. The core of the EnergyPlus model is based on fundamental heat balance principles. EnergyPlus calculates heating and cooling loads necessary to maintain thermal control set-points, conditions throughout plant and condenser loop. Simultaneous integration of building, primary and secondary HVAC system loops allows simulating as a real building would perform. It also allows sub-hourly, user defined time-steps (while maintaining numerical stability) for interaction between thermal zones and environment.

2.4.1 EnergyPlus Loop Structure

EnergyPlus models both air and hydronic systems as ‘fluid loops’ as shown in Figure 2-14.

The plant loop supplies or rejects the heat transferred from the air loop through coils, baseboards

or radiant systems depending on the heating or cooling load. The load demand placed by the air loop is satisfied by equipment in the plant loop such as chillers and boilers. The plant loop is connected to the condenser loop which transfers heat between the environment and equipment like cooling towers or ground loop heat exchangers.

Plant and condenser loops are further divided into “demand side” and “supply side” half loop. Chilled and hot water demand is met by supply side energy conversion equipment. Dividing the main loops in sub loops allows for implementation of a successive substitution solution technique.

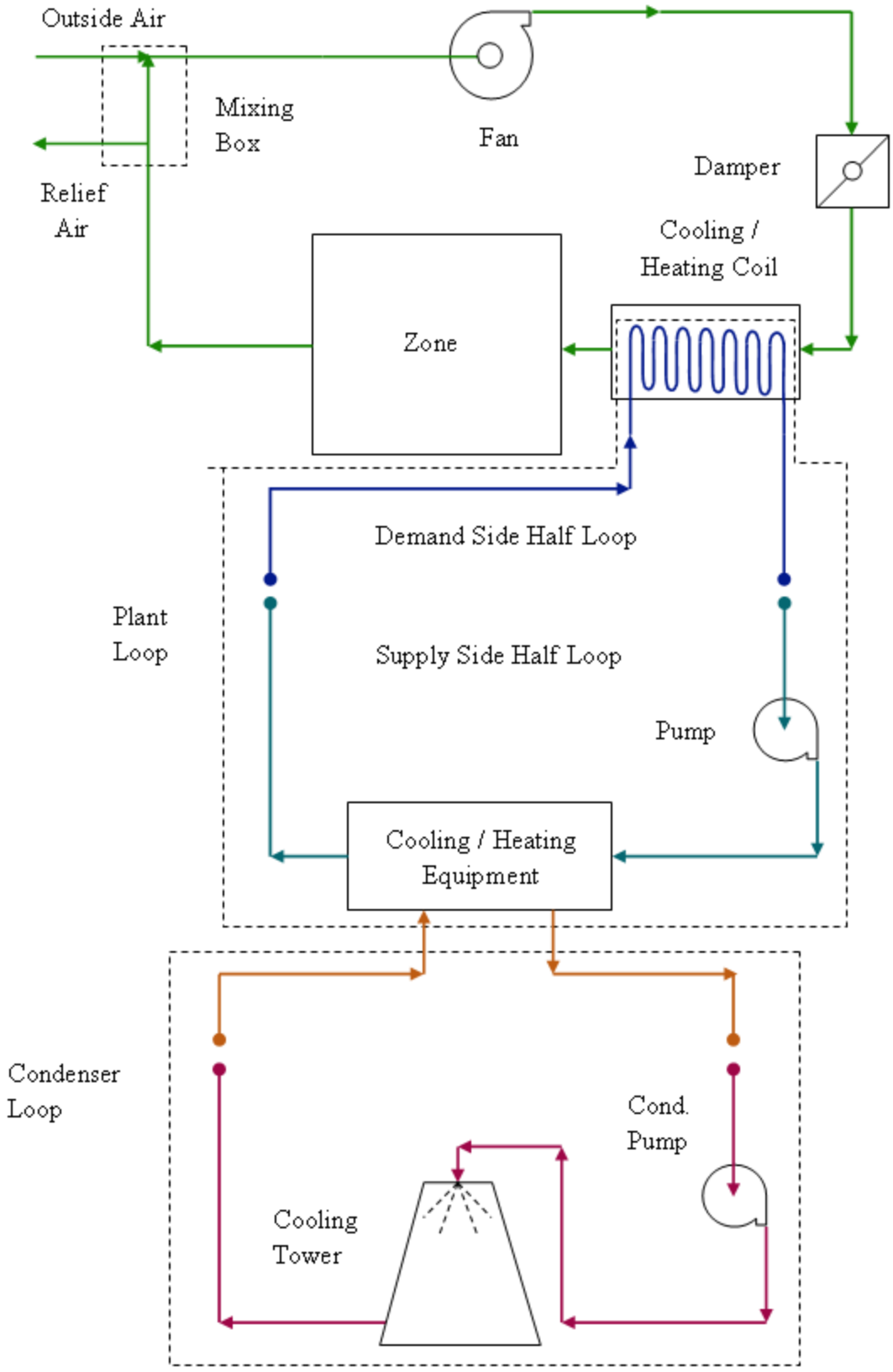

Figure 2-14 EnergyPlus Loop Structure

2.4.2 Pumps in EnergyPlus

There are basically two variables which decide EnergyPlus pump operation. First, the pump is classified as constant or variable speed. Second, pump operation is specified as continuous or intermittent.

For the constant speed pump, the user specifies the maximum flow rate. When the pump is turned on, it supplies the specified flow and consumes full load power. Maximum and minimum flow rates are defined for variable speed pumps; they satisfy the flow demand between these specified limits. The flow supplied by the pump is based on the request made by the demand side. A part load performance curve can be specified for a variable speed pump. This cubic curve is basically the fractional power consumption for the part load the pump is running at and transfer pump heat to the loop.

If continuous operation mode is selected, the pump will run regardless of the flow demand. For the cooling load case this will add heat to the loop even if the chillers are turned off and there is no demand on the loop. If intermittent operation mode is selected, the pump will run only when there is demand on the loop.

Chapter 3. Analytical Pump Performance Curve Model

The basic function of the pump is to convert rotational kinetic energy to potential (or pressure) energy. With sufficient pump design data, it is possible to predict both the energy conversion and losses occurring in pump using a rigorous thermodynamic and flow analysis. The procedure is to calculate the theoretical head and all the losses occurring in the pump in order to get output head for a given flow rate.

Analytical performance prediction can play an important role in pump design. Using this method one can roughly guess pump performance before design and construction. This can also be helpful in carrying out parametric studies to demonstrate the effect of geometrical and dynamic variables on pump performance.

3.1 Objectives

The basic objective of this chapter is to perform a detailed study of the fluid mechanics in a pump in order to get a better idea of the effect of geometrical and operational variables on pump performance. This will help in deciding the exact relationship between variables like pump head, flow rate and impeller diameter, rotational speed etc.

One of the objectives behind the study was to determine how well pump performance can be predicted using a minimum number of variables. The basic idea was to develop a detailed pump model, carry out a parametric study and eliminate the variables which do not significantly affect the pump performance. If the variables affecting pump performance are readily available or measureable, then an approximate pump curve can be generated. This will be helpful where pump curves are not available. If such an algorithm can be developed, one can calculate pump curve coefficients for use in simulation programs with limited inputs.

For existing pumping system, this type of model would allow a pump curve to be generated with just few inputs such as impeller diameter and width.

3.2 Literature Review

An expression for the theoretical head generated by the pump is derived from the angular momentum conservation equation. Hodge & Taylor (1999) provide a derivation of the theoretical head from Euler's Pump Equation. The derivation assumes that fluid enters the impeller with a zero tangential velocity component (i.e. only the radial component is present at the inlet of the pump). From the derived equation for theoretical head, the general head-flow characteristics of pumps with forward, radial and backward curved exit blades are explained. This describes the effect of exit blade angle on pump characteristics.

There are analytical performance prediction methods discussed in many books and papers. One of the earliest models is proposed by Spannhake (1934). He estimates theoretical head and then subtracts losses from it. According to the author local losses in pumps are proportional to the square of the fluid velocity at each location. And every such velocity can be expressed in terms of flow (Q) and rotational speed (N). Thus, the effective pump head can be expressed in terms of Q and N. Head losses occurring due to shock at the entrance to the impeller, friction within the impeller, and shock losses due to flow transition from the impeller to the volute are considered in calculation. Shock losses are due to the loss of velocity head when flow direction is changed.

This calculation assumes that the coefficient (ζ) representing the term $f\,{}^{L}/_{D}$, in the friction loss equation is constant even though cross-sectional areas are changing. The final equation obtained by Spannhake (1934), term for effective head is a second order equation in Q, which results in a parabolic pump curve.

Tuzson (Tuzson & Iseppon, 1997), (Tuzson J. , 2000) uses a similar method. His model

calculation can be used for radial and mixed flow pumps with dimensionless specific speeds[5] of 0.2 to 2 (500 to 5000 in English units[6]) and flow rates of 100 to 5000 gpm (0.006 to 0.3 m^3/s).

Tuzson (2000), includes FORTRAN code for performance prediction. In this code, flow equations are applied at the average streamline. In this design various loss coefficients are determined for a simple pump design. Loss coefficients depend on existing manufacturing processes. According to the reference, to get satisfactory results, calibration of the model is required. This means adjusting the loss coefficients in order to get the exact pump curve. Once the calibration is done the model can be used for geometrical similar pumps. Geometrical similarity is discussed further in section 4.4.

Tuzson (2000), states that the effect of some variables like the number of impeller blades, inlet diameter and impeller exit width on pump performance is often complex and contradictory. The program can be used to observe the combined effect of the input variables.

According to Manivannam (2010) impeller geometric features have a great effect on pump performance. The shape of the blade and the resulting flow pattern in the impeller determines final effective head and how much of the input energy is transferred to the fluid. A Computational Fluid Dynamics (CFD) analysis is carried out by Manivannam (2010) using the Star CCM+ software tool. This reference basically studies the effect of inlet and exit blade angles on pump performance. The study starts with blade angles from empirical calculations and suggests another set of blade angles which might improve pump performance. The effect of blade angles on pump head, efficiency and power is been displayed in Manivannam (2010). This reference is used to get a rough idea of the values of blade angles and to verify the results obtained from the VBA models

[5] Dimensionless specific speed (N_s) of pump is given by,

$$N_s = \frac{NQ^{1/2}}{g^{3/4}H^{3/4}}$$

[6] Value of specific speed is affected by the units used in the calculations. Conversion factor of 0.00037 is used to convert specific speed from English unit to metric system.

discussed in Section 3.4 and 3.5. In the results Manivannam (2010) states that increase in exit blade angle results in smooth flow in exit region thereby reducing the flow losses whereas reduction in inlet blade angle results in low flow separation loss and high effective head. The article also states that exit blade angle has more control over pump performance as compared to inlet blade angle.

3.3 Theoretical Head and Euler's Equation

Following Hodge & Taylor (1999), Figure 3-1 is a schematic of pump impeller showing entering and exiting fluid velocities. 'U' is the impeller tangential velocity, 'W' is the velocity of the fluid relative to the impeller and 'C' is the absolute velocity which is resultant of the impeller tangential velocity and fluid relative velocity. Subscript 1 stands for impeller inlet parameters, 2 for impeller exit and 3 for volute. Alphabetical subscripts like t stand for tangential component, m for meridian (radial) and CS for cross-sectional.

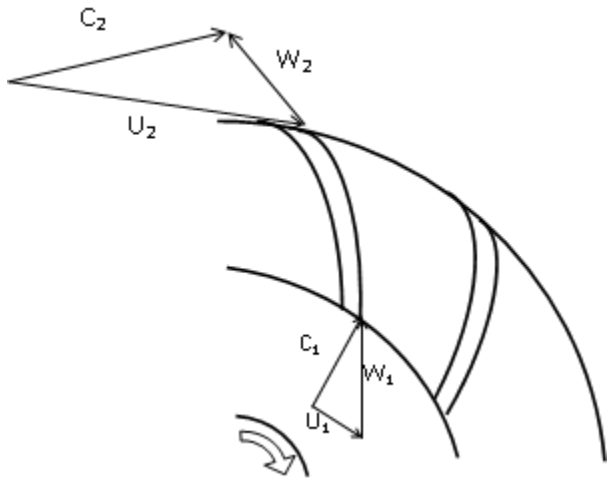

Figure 3-1 Velocity Diagrams at Inlet and Outlet of Impeller (Hodge & Taylor, 1999)

Thus vectorially these velocities can be written as,

$$\bar{C} = \bar{W} + \bar{U} \qquad (3\text{-}1)$$

Figure 3-2 shows the components of the impeller tangential velocity U, and fluid relative velocity W.

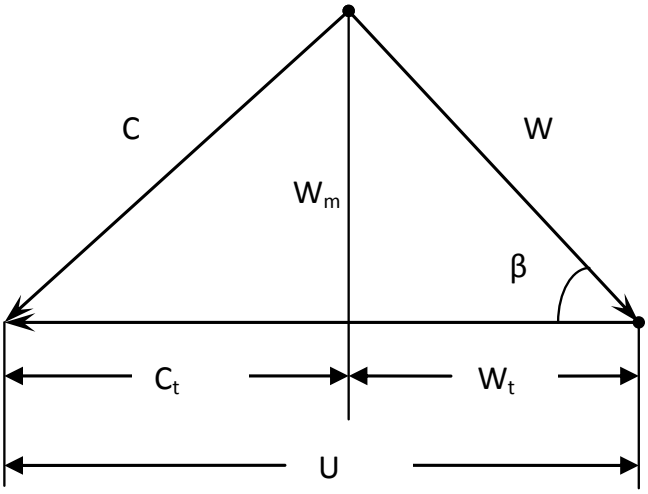

Figure 3-2 Velocity Traingle Nomenclature (Hodge & Taylor, 1999)

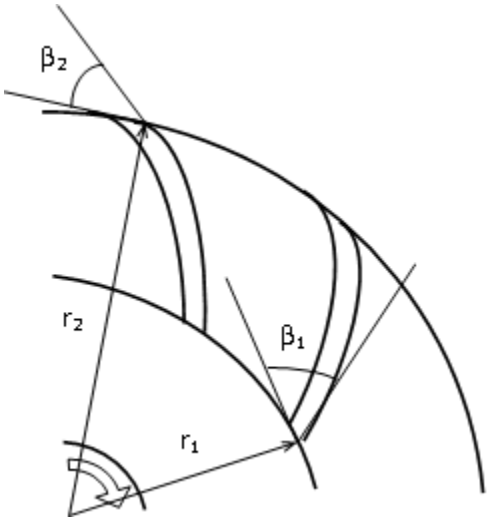

Figure 3-3 Impeller Angles and Radius

Following Hodge & Taylor (1999)

The energy transfer takes place from the pump impeller to fluid as a result of the change in angular momentum. If angular momentum conservation is applied to the pump impeller we can say that the rate of change of angular momentum is equal to the input torque to the pump.

$$\tau = \frac{\dot{m}}{g}\left(r_2 C_{t_2} - r_1 C_{t_1}\right)$$

Power transferred to the shaft is,

$$P = \tau\omega = \frac{\dot{m}}{g}\{(r_2\omega)C_{t_2} - (r_1\omega)C_{t_1}\}$$

Where $r\omega$ is impeller tangential velocity, U:

$$\Rightarrow P = \frac{\dot{m}}{g}\{U_2C_{t_2} - U_1C_{t_1}\}$$

Thus the theoretical head H_{th} at pump exit should be,

$$H_{th} = \frac{P}{\dot{m}} = \frac{1}{g}\{U_2C_{t_2} - U_1C_{t_1}\} \qquad (3\text{-}2)$$

Equation 3-2 is considered one of the most fundamental equations in turbo-machinery analysis. Velocity vector nomenclature followed henceforth in the chapter is explained in Figure 3-2.

At inlet of impeller, zero prewhirl condition is assumed i.e. fluid absolute velocity has only radial component. $\Rightarrow C_{t_1} = 0$

Thus Equation 3-2 will be reduced to,

$$H_{th} = \frac{U_2C_{t_2}}{g} \qquad (3\text{-}3)$$

Tangential velocity at the exit of the impeller cannot be measured thus, it has to be expressed in terms of other parameters which are measurable or can be calculated from measurable quantities. From Figure 3-2 and Equation 3-1,

$$C_{t_2} = U_2 - W_{t_2}$$

Since relative velocity at the exit of the impeller (W_2) is along the exit blade angle (β_2) we can write,

$$\cot\beta_2 = \frac{W_{t_2}}{W_{m_2}}$$

$$\Rightarrow C_{t_2} = U_2 - W_{m_2}\cot\beta_2 \qquad (3\text{-}4)$$

Using Equation 3-3 and Equation 3-4,

$$H_{th} = \frac{U_2\left(U_2 - W_{m_2}\cot\beta_2\right)}{g}$$

Mass flow rate through impeller of width 'w' is

$$Q = (\pi D_2 w)W_{m_2}$$

where $\pi D_2 w$ is the fluid exit area of the impeller

$$\Rightarrow H_{th} = \frac{{U_2}^2}{g} - \frac{U_2}{\pi D_2 w g}Q\cot\beta_2 \qquad (3\text{-}5)$$

For constant speed of rotation (i.e. $U_2 = constant$), theoretical head can be written as linear function of the flow rate,

$$K_1 = \frac{{U_2}^2}{g}$$

$$K_2 = \frac{U_2}{\pi D_2 w g}\cot\beta_2$$

$$\Rightarrow H_{th} = K_1 - K_2 Q$$

For constant speed of rotation, K_1 and K_2 are functions of pump geometry. Depending upon the value of the exit blade angle, the slope of the H-Q curve will vary.

For forward curved blades:

$$\beta_2 > 90^0 \quad \Rightarrow \cot\beta_2 < 0 \qquad \Rightarrow K_2 < 0$$

Theoretical head will be linear function of flow with a positive slope.

For radial blades:

$$\beta_2 = 90^0 \quad \Rightarrow \cot\beta_2 = 0 \qquad \Rightarrow K_2 = 0$$

Theoretical head will be a straight line passing through H = K_1 parallel to x the axis.

For backward curved blades:

$$\beta_2 < 90^0 \quad \Rightarrow \cot\beta_2 > 0 \qquad \Rightarrow K_2 > 0$$

Theoretical head will be a linear function of the flow with a negative slope.

The solid lines in the Figure 3-4 show theoretical head curve for forward, radial and backward curved blades. The dashed lines show actual pump curve which are obtained after pressure head losses are subtracted from theoretical head.

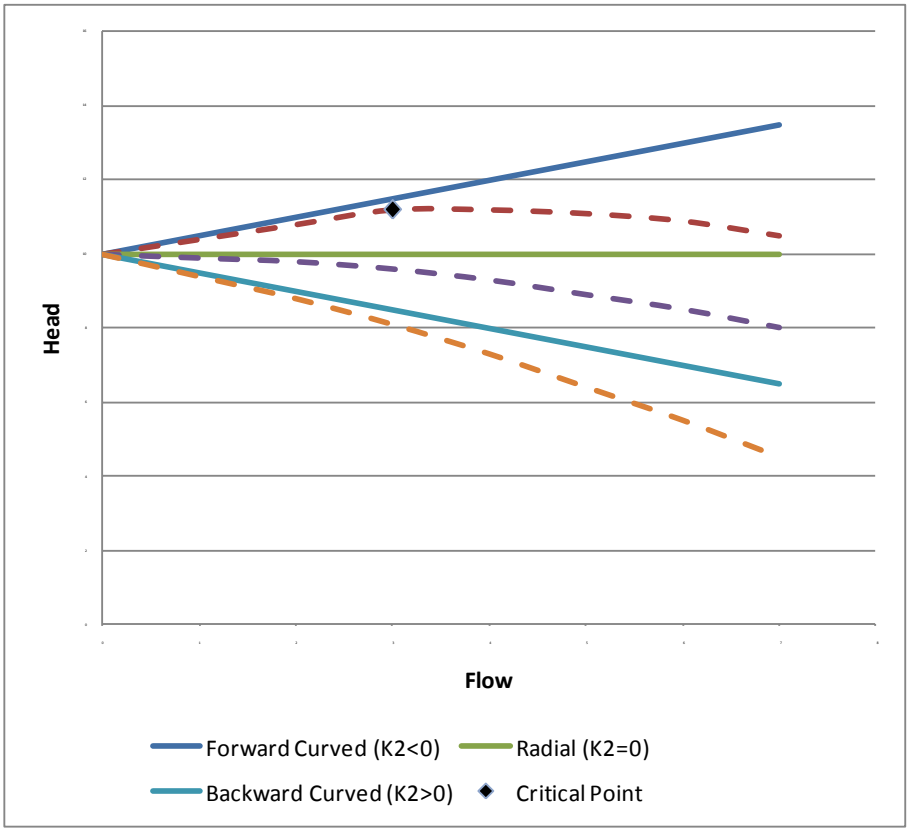

Figure 3-4 Effect of Exit Blade Angle on Shape of Pump Curve

Following Hodge & Taylor (1999)

For most of the HVAC applications, radial and backward curved blades are preferred for stability of operation. As shown in Figure 3-4 forward curved blades result in critical point at flow rate greater than zero this leads to unstable operating region as explained by Figure 2-3 in Section 2.1.3.

3.4 Tuzson Model

For a pump with U_2 and W_{m2} as impeller tip speed and radial flow velocity at outer periphery of impeller respectively, theoretical head calculated from following formula:

$$H_{th} = \frac{U_2 C_{t2}}{g} = \frac{{U_2}^2 \sigma - U_2 W_{m2} tan\beta_2}{g} \qquad (3\text{-}6)$$

The starting point for the Tuzson model (Tuzson J. , 2000) is slightly different from Equation 3-5

derived in Section 3.3. A slip factor σ, is introduced in the equation. Slip (σ) is introduced in the equation because fluid flow does not follow the impeller blades exactly. The direction of the relative fluid exit velocity[7] vector is slightly inclined opposite to the direction of rotation. Thus, slip is not exactly an energy loss phenomenon; it's part of the impeller energy which does not get converted into potential energy (i.e. pressure head). There are several empirical relations suggested to measure the slip coefficient for different cases, but the most widely used is suggested by Wiesner (1967).

$$\sigma = 1 - \frac{\sqrt{\sin(90 - \beta_2)}}{Z^{0.7}}$$

where Z is the number of blades.

The impeller blade angle (β) in Equation 3-6 Theoretical Head is also defined differently by Tuzson (2000) as shown in Figure 3-5. Tuzson's (2000) definition of β_2 results in a "tan β_2" in Equation 3-6 compared to "cot β_2" term in Equation 3-5.

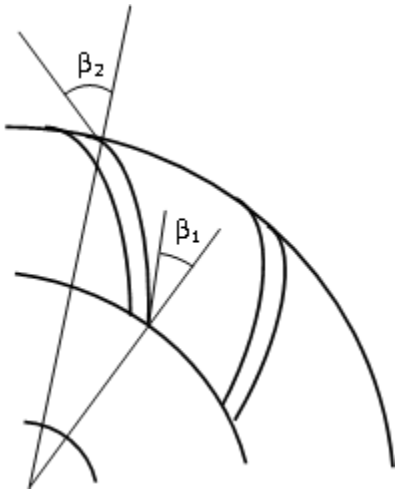

Figure 3-5 Impeller Blade Inlet and Exit Angles

The assumption that $C_{t_1} = 0$ in Equation 3-3 requires no flow separation at impeller blade. This

[7] Relative velocities of fluid are the velocities with respect to impeller direction of rotation whereas; absolute velocities are considered in non-rotating frame of reference.

in fact is not the case. Flow separation at impeller blade produces a low pressure region with reverse flow towards the impeller. Due to this leading edge flow separation and sudden expansion (after mixing of separated flow with main stream) there is an energy loss which is called the incidence loss.

Incidence loss is a loss in kinetic energy which will be proportional to the difference in the tangential component of the inlet velocity (C_{t1}) and blade inlet edge velocity (U_1)[8].

$$h_{in12} = \frac{(U_1 - C_{t1})^2}{2g} = \frac{(U_1 - C_1 \tan \beta_1)^2}{2g} \qquad (3\text{-}7)$$

Where, $U_1 = \pi D_i N$ and,

$$C_1 = \frac{Q}{\frac{\pi}{4}\left({D_1}^2 - {D_h}^2\right)}$$

where D_i is the hydraulic diameter based on the hub diameter, D_h and the impeller inlet diameter, D_1 and N is the rotational speed in rps.

Pressure head loss also occurs due to surface friction as the fluid flows through impeller, diffuser and volute. Since the flow sections are irregular in shape, the surface friction defined in terms of hydraulic diameter, blade passage length and average velocities. Hydraulic diameter of the impeller cross-section is calculated using impeller width (w), impeller outer diameter (D_2), outlet blade angle (β_2) and the number of blades (Z). An average friction coefficient of 0.005 is suggested by Tuzson (2000).

The impeller cross-sectional area, A_{CS}, perimeter, P_{CS} and hydraulic diameter, D_{EQ}, are calculated as follows:

[8] It is a simplified form of the incidence loss equation provided by Tuzson (2000) which gives similar results.

$$A_{CS_{impeller}} = W\left(\frac{\pi D_2}{Z}\right)\cos\beta_2 \tag{3-8}$$

$$P_{CS_{impeller}} = 2\left[W + \left(\frac{\pi D_2}{Z}\right)\cos\beta_2\right] \tag{3-9}$$

$$D_{EQ} = 2\left(\frac{A_{CS_{impeller}}}{P_{CS_{impeller}}}\right) \tag{3-10}$$

$$l = \frac{D_2 - D_1}{2\cos\beta_2} \tag{3-11}$$

$$h_{sf12} = f\frac{l}{D_{EQ}}\frac{\left(\frac{W_1+W_2}{2}\right)^2}{2g} \tag{3-12}$$

The model assumes that the diffusion loss occurs in impeller only if $W_1/W_2 > 1.4$. For this case Tuzson (2000) defines the diffusion loss as:

$$h_{diff} = \frac{\left(W_1/2\right)^2}{2g}$$

The fluid velocity approaching the volute is generally greater than fluid velocity in the volute. This velocity mismatch causes velocity head loss. The model assumes 0.8 as volute head loss coefficient.

$$h_{in23} = 0.8\frac{({C_2}^2 - {C_3}^2)}{2g}$$

where C_2 is the velocity leaving thee impeller and C_3 is the average volute velocity calculated from the overall flow-rate (Q);

$$C_3 = \frac{Q}{A_{Volute\ CS}} \tag{3-13}$$

Skin friction in the volute is calculated in similar way as for the impeller. The approximate hydraulic diameter, D_{hyd_volute}, is calculated from the volute cross-section area and perimeter. The

equivalent length, l_{eq_volute}, is calculated from the impeller diameter.

$$h_{sf23} = f \frac{l_{eq\_volute}}{D_{hyd\_volute}} \frac{{C_{Q3}}^2}{2g}$$

All the head losses are then subtracted from the theoretical head and the effective pump head is calculated as follows:

$$H_{effective} = H_{th} - (h_{in12} + h_{sf12} + h_{diff} + h_{in23} + h_{sf23}) \qquad (3\text{-}14)$$

3.5 Spannhake Model

The Spannhake model (Spannhake, 1934) is similar to the Tuzson model, but it expresses all the terms involved in the calculation in terms of flow rate (Q) and revolutions per second (N) of the impeller.

The gross lift i.e. theoretical head is given by[9],

$$H_{th} = \frac{1}{g}\left\{(\pi D_2 N)^2 + \pi D_2 \frac{\cot \beta_2}{A_2} NQ\right\}$$

where Spannhake defines β_2 as shown in Figure 3-6.

[9] To maintain the consistency in notations subscripts are numbered in similar way as that of (Tuzson J. , 2000) i.e. subscripts 12 and 23 indicate inner and outer peripheries of impeller; r-impeller and sp-impeller. Most of the other notations are followed from (Spannhake, 1934) to maintain similarity of equations.

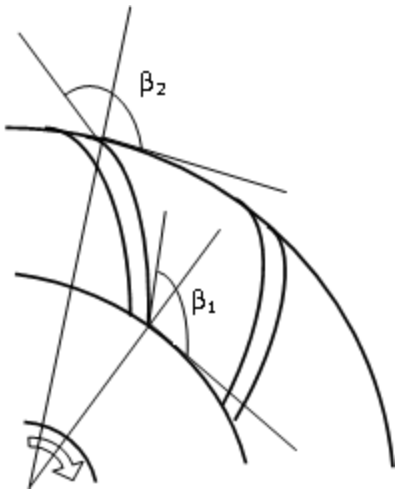

Figure 3-6 Inlet and Exit Angles(Spannhake, 1934)

It is assumed that at the entrance of the impeller, the shock velocity head is lost. This loss is similar to the incidence head loss as shown in Equation 3-7. The shock velocity at the entrance of the impeller is,

$$C_{s1} = \left(\frac{\cot\beta_1}{A_1}Q + \pi D_1 N\right)$$

The loss due to shock at the entrance is $h_{in12} = {C_{s1}}^2 \Big/ 2g$,

which can be expanded as:

$$\Rightarrow h_{in12} = \frac{1}{2g}\left\{(\pi D_1 N)^2 + 2\pi D_1 \frac{\cot\beta_1}{A_1} NQ + \frac{\cot^2\beta_1}{{A_1}^2}Q^2\right\}$$

Friction loss in the impeller is calculated using:

$$h_{sf_{12}} = \frac{1}{2g}\frac{\zeta_r}{{A_2}^2 \sin^2\beta_2}Q^2$$

where $\zeta = f\, L/D$

This equation is similar to Equation 3-12 with the average radial velocity expressed in terms of

flow-rate (Q). The velocity approaching the volute and the velocity from the impeller are not equal, due to the transition shock loss. This shock loss can be calculated from the shock velocity which is the difference between the tangential velocity of flow from the impeller, C_{t2}, and velocity of the flow in the volute.

The tangential velocity of the flow leaving the impeller is defined as,

$$C_{t2} = \frac{\cot \beta_2}{A_2} Q + \pi D_2 N$$

And the velocity of the flow in the volute calculated as[10]:

$$C_{t2}{}' = \frac{\cot \alpha_{sp}}{A_2} Q$$

where α_{sp} is the angle between the tangent to the volute and volute entering fluid streamline (relative velocity vector) at the exit of the impeller.

Thus, shock velocity is,

$$C_{s2} = \frac{\cot \beta_2 - \cot \alpha_{sp}}{A_2} Q + \pi D_2 N$$

The velocity head due to the shock velocity is not completely lost (unlike the shock loss at the entrance of the impeller); part of it is utilized in increasing the pressure head. The loss is proportional to ${C_{s2}}^2 \Big/ 2g$ with proportionality constant ζ_2 less than one.

$$\Rightarrow h_{in23} = \frac{\zeta_2}{2g} \left\{ \left(\frac{\cot \beta_2 - \cot \alpha_{sp}}{A_2} \right)^2 Q^2 + (\pi D_2 N)^2 + 2 \left(\frac{\cot \beta_2 - \cot \alpha_{sp}}{A_2} \right) (\pi D_2 N) Q \right\}$$

Friction loss in volute is given by

[10] According to (Spannhake, 1934)α_{sp} determined from dimensions of spiral and it is the angle at which flow approaches the periphery of the wheel.

$$h_{sf_{23}} = \frac{\zeta_v}{2g}\left(\frac{\cot^2 \alpha_{sp}}{{A_2}^2} - \frac{1}{{A_{sp}}^2}\right)Q^2$$

The loss coefficient ζ_v is assumed to vary from 0.15 to 0.2.

The actual available head at exit of pump is then calculated by subtracting the losses from theoretical head.

$$H_{effective} = H_{th} - (\, h_{in12} + h_{sf12} + h_{sf_{23}} + h_{in23} + h_{sf_{23}})$$

$$2gH_{effective} = AN^2 + 2BNQ - CQ^2 \tag{3-15}$$

Where,

$$A = (\pi D_2)^2(2 - \zeta_2) - (\pi D_1)^2$$

$$B = (\pi D_2)\frac{\cot \beta_2}{A_2} - (\pi D_1)\frac{\cot \beta_1}{A_1} - \zeta_2\left(\frac{\cot \beta_2 - \cot \alpha_{sp}}{A_2}\right)(\pi D_2)$$

$$C = \frac{\zeta_s}{{A_1}^2} + \frac{\cot^2 \beta_1}{{A_1}^2} + \frac{\zeta_r}{{A_2}^2 \sin^2 \beta_2} + \zeta_2\left(\frac{\cot \beta_2 - \cot \alpha_{sp}}{A_2}\right)^2 + \zeta_v\left(\frac{\cot^2 \alpha_{sp}}{{A_2}^2} - \frac{1}{{A_{sp}}^2}\right)$$

The bracketed terms are constants for given pump and the coefficient ζ can be assumed as constant. Then for constant RPM pump head characteristic is a parabola with Q as a variable. It can be observed that effective head is not simplistic function of impeller diameter.

3.6 Results and Discussion

A VBA program was written to study the performance of the models discussed above. All of the required inputs are not provided in pump catalogs. These inputs are either approximated from the available design data or are selected from the generalized ranges suggested in literature.

3.6.1 Literature Review for Pump Blade Angles

Inlet and exit blade angles are usually not available in the manufacturer's datasheets. Thus,

typical values of inlet and exit blade angles as reported in the literature are used. A number of schemes are used to specify impeller inlet and exit blade angles. Before using these values from a reference, they need to be converted to the way the angles are specified in the models discussed in Section 3.4.

Manivannam (2010) started the modeling of the impeller, with optimum inlet and outlet impeller angles calculated by using empirical relations. The inlet and outlet impeller angles suggested in the reference are β_1= 75° and β_2 = 55°. The angle measurement method in Manivannam (2010) is same as Tuzson (2000), thus the values suggested can be directly used in his model. For Spannhake (1934) model, the values will be β_1= 165° and β_2 = 145°. The reference also provides the approximate value of blade thickness as t = 0.05" (~1.25 mm). The blade thickness is used in the impeller outlet area calculation.

Sherstyuk, et al.(2002) provide experimental data to compare with recommendations made for exit blade angles. A graph provides values of β_2 where experimental data and analytical results are compared. The approximate range for β_2 in experimental results is β_2 = 23° to 33°. For Tuzson J. (2000) and Spannhake (1934) the range will be β_2 = (57° to 67°) and β_2 = (147° to 157°) respectively.

3.6.2 Comparison of Spannhake and Tuzson Models

To demonstrate the performance of the model geometrical inputs and performance curves of Goulds Pumps model 3642/3742 size 1 x 1 1/4 -5 is used. The same values of impeller blade angles, impeller inlet diameter, impeller diameter, casing width are used for both models to compare the results.

After calculation of theoretical head, losses are subtracted from it and the results from Spannhake and Tuzson models are compared in Figure 3-7. Dashed curves represent the the Tuzson model. Theoretical head is almost constant with respect to flow rate in the models. The slight decline in it

indicates that the impeller blades are backward curved. Significant difference is observed in the theoretical head calculated by the models. The lower value of theoretical head in the Tuzson models is due to consideration of the slip factor. In the program with Tuzson model, if the slip factor is fixed at unity; the values of theoretical head from both models match.

Considerable difference is also observed in casing shock loss. This difference is due to the formula used in the calculation of this loss. In the Tuzson model it is assumed that part of the difference between the impeller exit and the volute kinetic energy is lost; while the Spannhake models calculates this loss using the shock velocity. The shock velocity calculated in the model incorporates the difference in the direction of the fluid velocity vector and the tangent to the impeller blade using the factor $\left(\cot\beta_2 - \cot\alpha_{sp}\right)$. This is similar to the concept of slip factor; which is not considered in the theoretical head calculation of Spannhake model.

Impeller incidence loss in both models is almost the same and goes on increasing exponentially with increasing flow rate.

From Figure 3-7 it is clear that the incidence and shock losses are the major losses occurring in the pump and friction losses hardly affect performance curve.

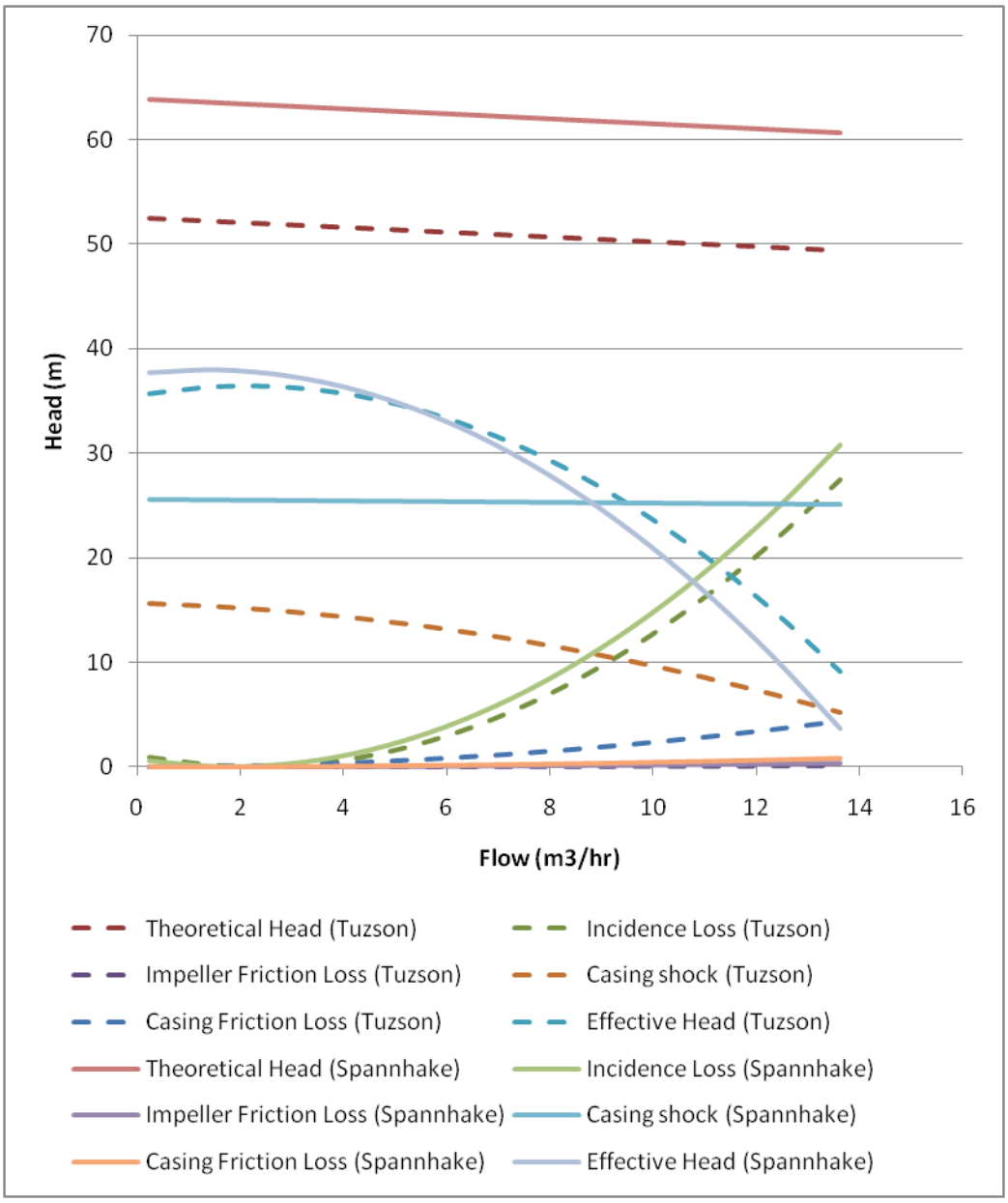

Figure 3-7 Comparison of Theoretical Head and Pump Losses

From the above discussion we can conclude that skin friction hardly affects the pump performance. Very high surface finish will not help in improving pump performance. Pump material and surface finish should be decided according to application, environmental conditions and cost.

The results obtained from the models are compared with manufacturer's data in Figure 3-8. It can

be observed that for the same input data the Tuzson model provides performance curve with results close to manufacturers' data.

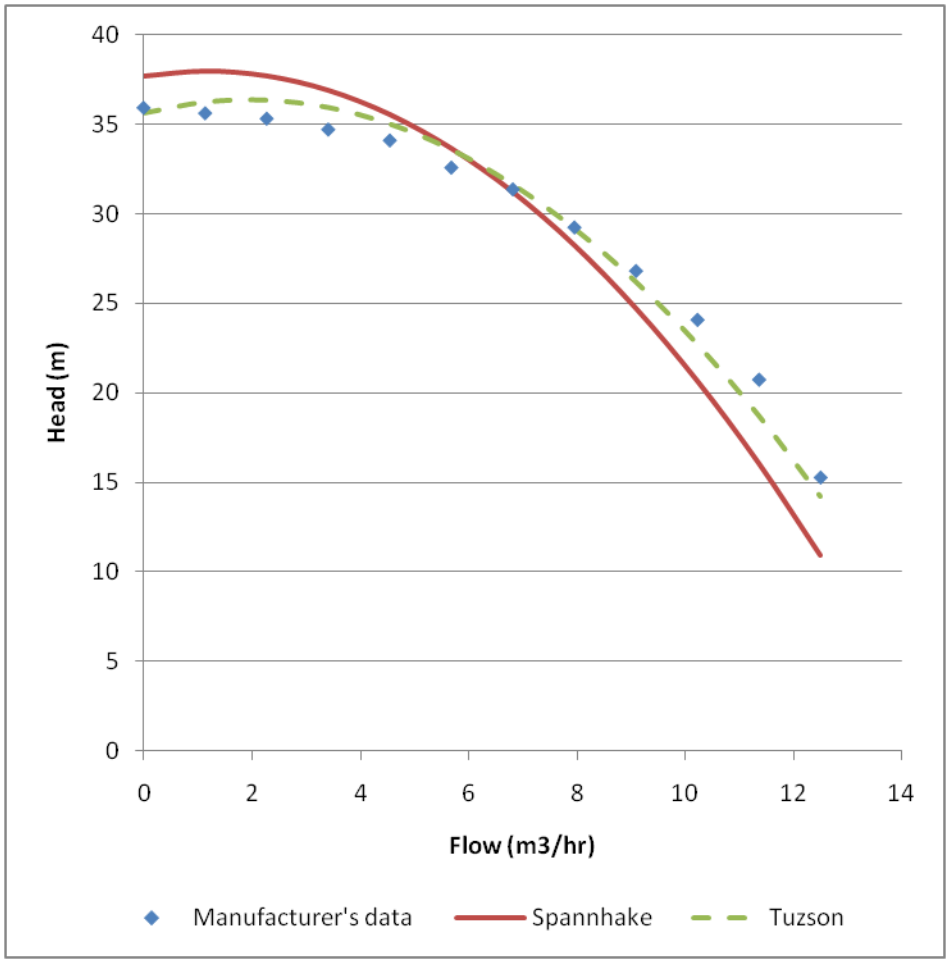

Figure 3-8 Comparison of Spannhake and Tuzson Model with Manufacturers' data

Comparison and error in the model values for this case can be observed in Figure 3-9. For Spannhake model the error ranges from -28% to 7% while for Tuzson it is -10% to 4%.

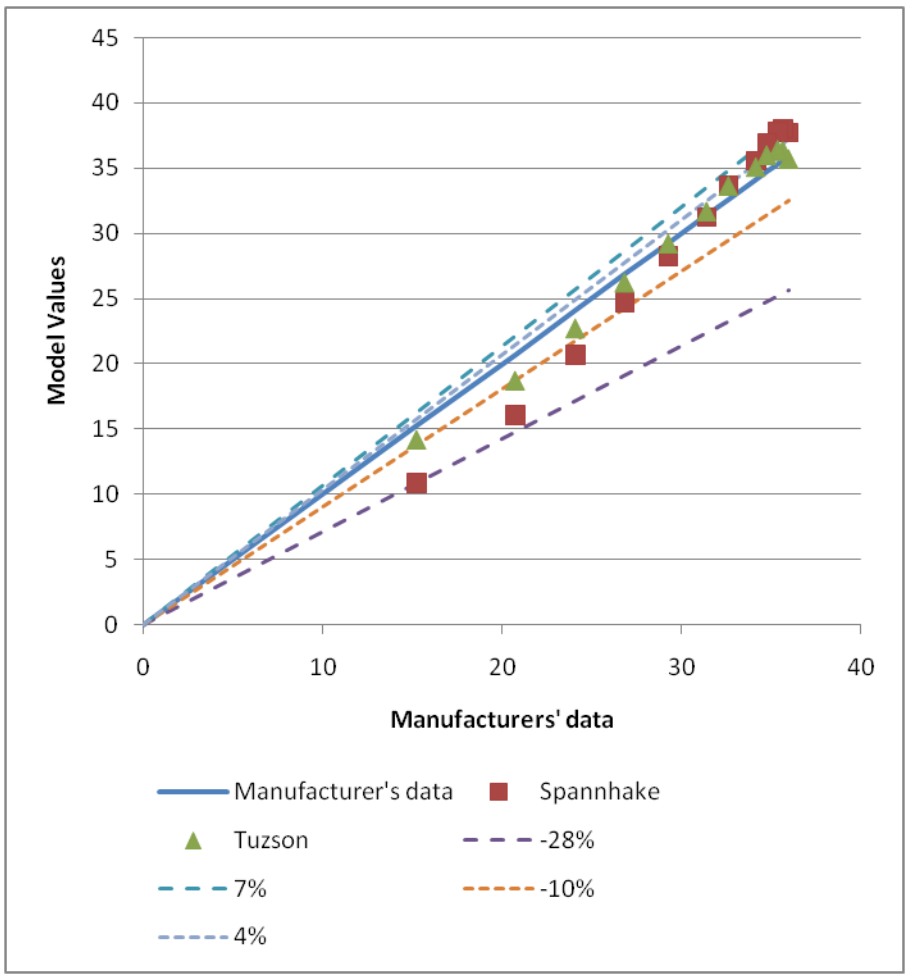

Figure 3-9 Comparison between manufacturer's data and model values

Results obtained from the Spannhake model are compared with manufacturers' pump curves for reduced impeller diameters in Figure 3-10.

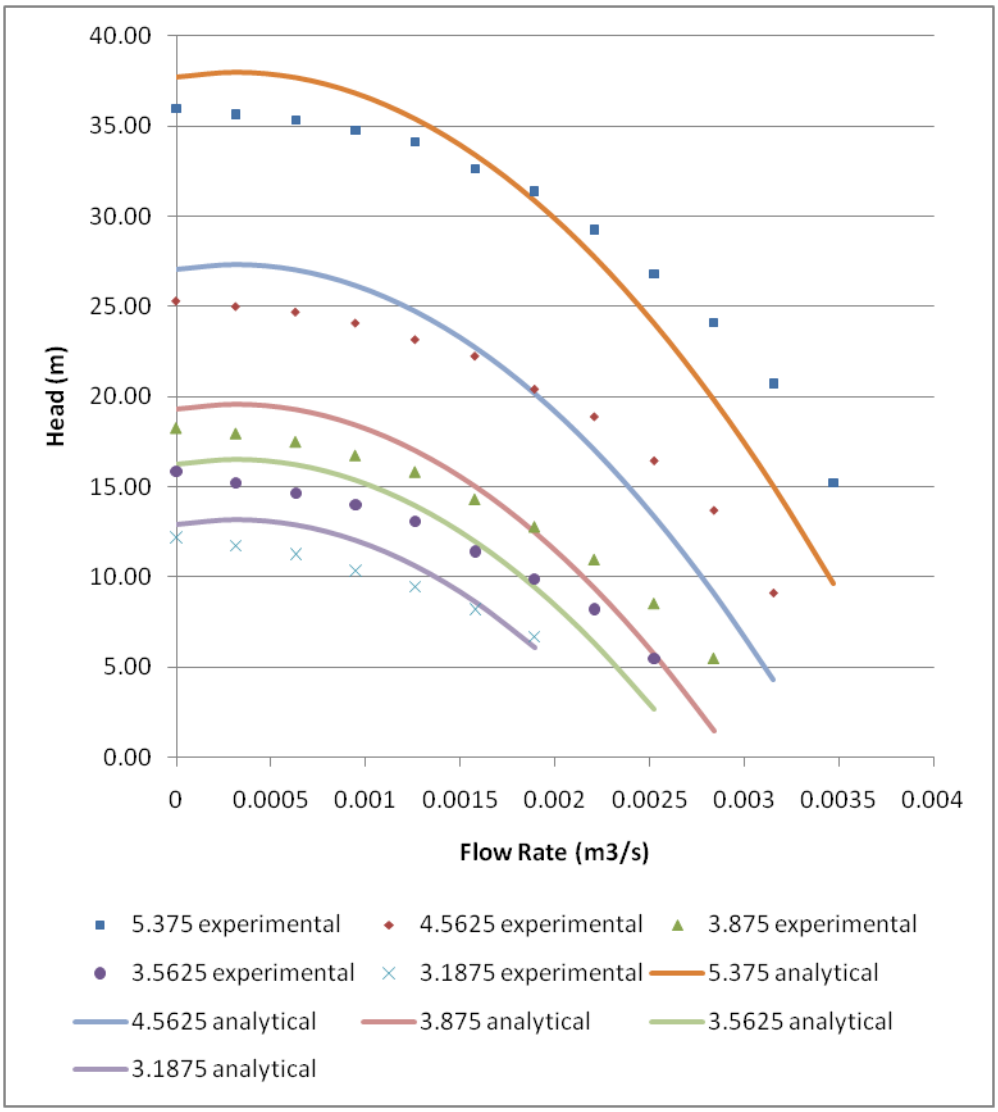

Figure 3-10 Comparison of Spannhake Model and Manufacturers data

Results obtained from the Tuzson model are compared with manufacturers' pump curves for reduced impeller diameters in Figure 3-11.

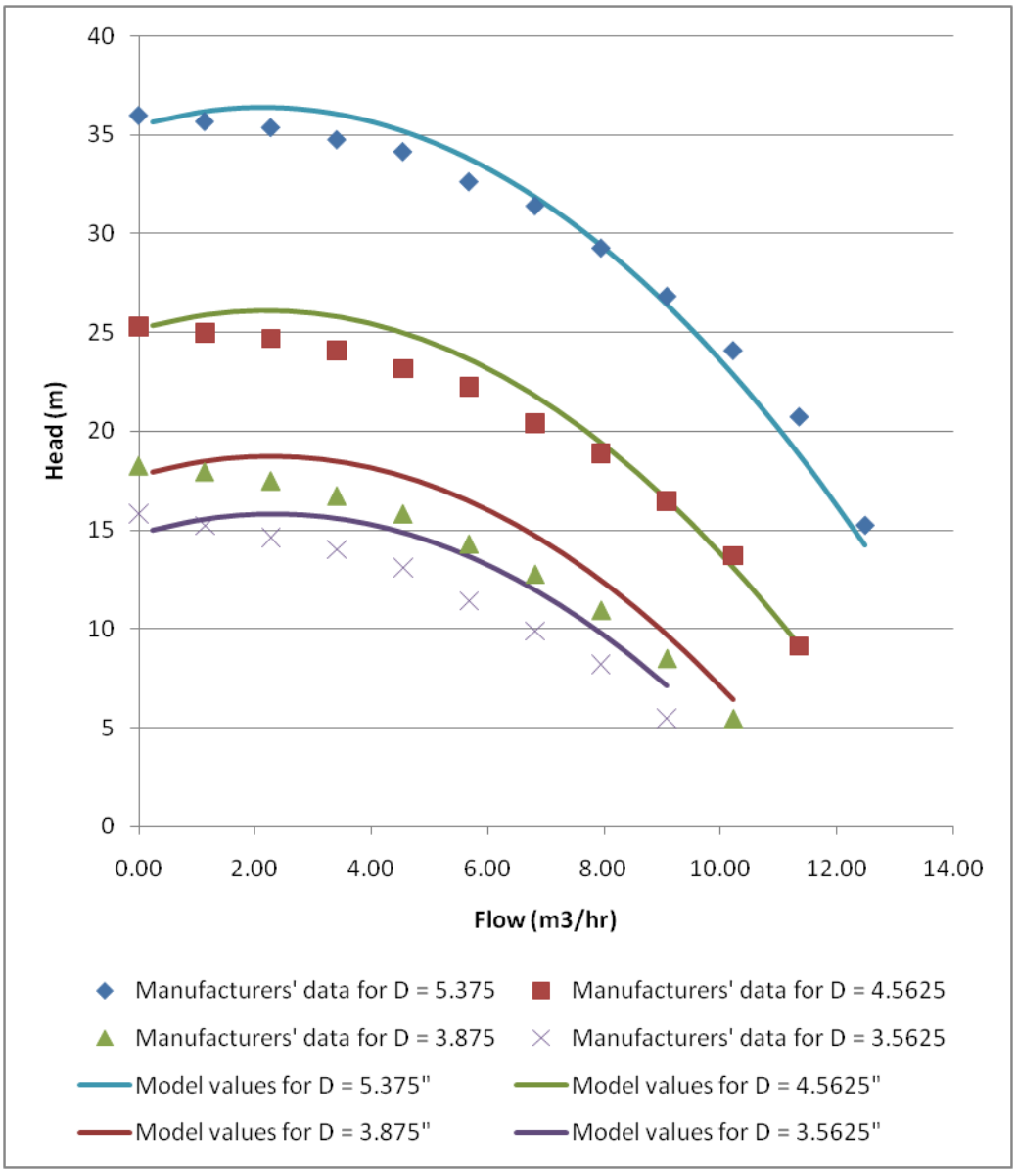

Figure 3-11 Comparison of Tuzson Model and Manufacturers data

Results obtained from the model match closely with manufacturers data but for the results values such as loss coefficient, casing incidence angle, and impeller width are assumed (but are coherent with other geometrical values). Since exact values of blade angles are not available the average values from the ranges specified in literature are used.

3.6.3 Effects of Pump Parameters on Performance Curve

From the developed model we can study the effect of several pump parameters that can affect the

pump performance curve. It provides a rough idea of the trend that can be observed. The effect of impeller rotational speed and flow on pump head can be observed from the derived equation (Equation 3-15). Further discussion is concerned with other pump parameters such as impeller width and impeller inlet diameter.

Figure 3-12 shows the effect of a decrease in impeller width on pump pressure rise. With a decrease in impeller width the curve shifts downwards. A decrease in the impeller width reduces the passage area for the flow this leads to an increase in frictional losses, but an increase in impeller frictional losses is not the major reason behind the rise in steepness of the curve. The major factor affecting the shape of the curve is an increase in the slope of theoretical head curve. As the impeller width decreases the value of $K_2 = {U_2 \cot \beta_2}/{\pi D_2 w g}$ (which is the negative slope of the theoretical curve) increases considerably in Equation 3-5. In another words, decrease in impeller width leads to increase in impeller exit velocity; whose tangential component acts against the impeller tangential velocity; thereby reducing the overall velocity head for same value of flow rate.

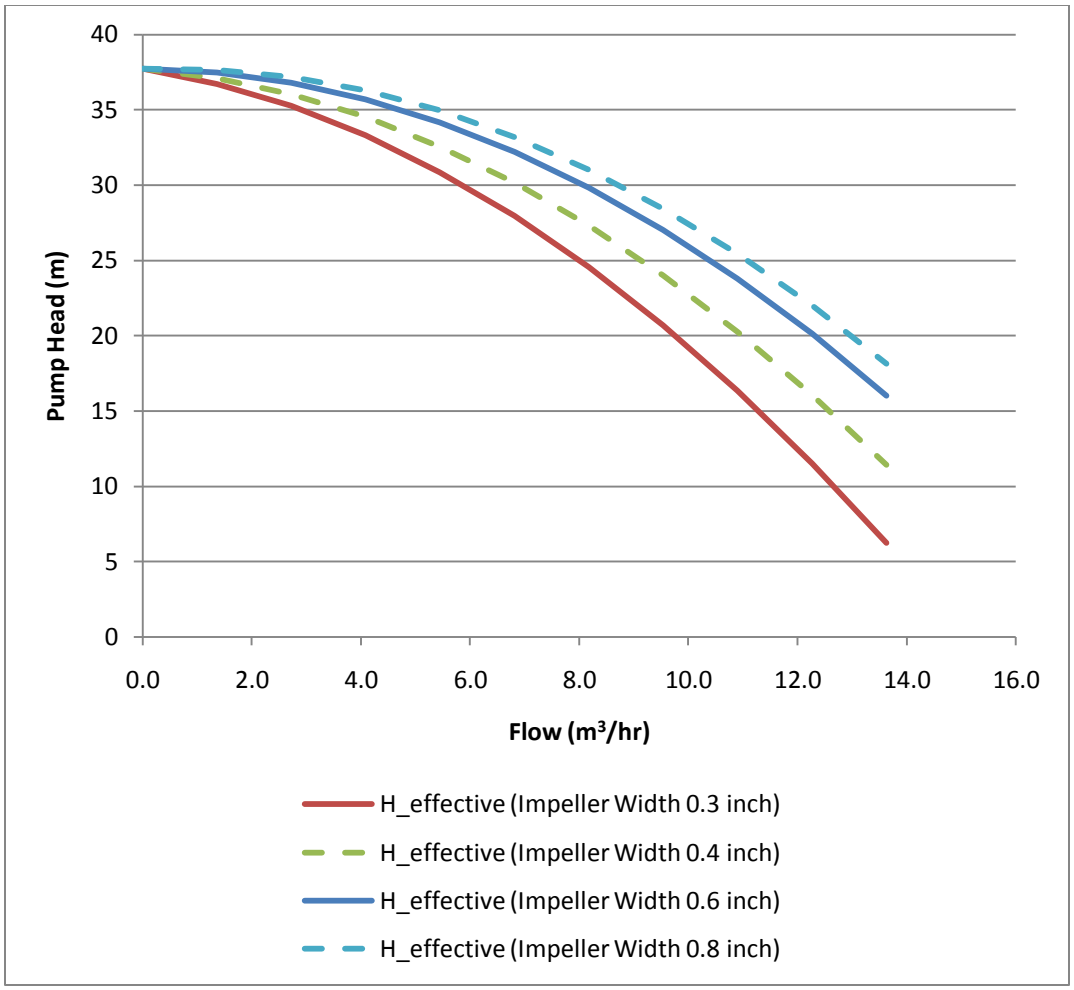

Figure 3-12 Effect of Impeller Width on Pump Curve

Figure 3-13 demonstrates the effect of impeller inlet diameter on the pump curve[11]. With an increase in inlet diameter, the overall discharge of the pump for the same pressure rise increases significantly. This increase in flow is due to a drop in shock loss at the entrance of the impeller. From the entrance shock loss, $h_{in12} = {C_{s1}}^2 / 2g$ and $C_{s1} = \left(\frac{\cot\beta_1}{A_1} Q + \frac{\pi D_1}{60} n\right)$ it might appear that with an increase in inlet diameter (D_1) the shock loss should increase which is contrary to the obtained result. An increase in inlet diameter causes increase in inlet flow area thereby reducing the shock velocity for the same flow rate. This leads to a significant reduction in inlet shock loss.

[11] The results obtained here are from Tuzson model.

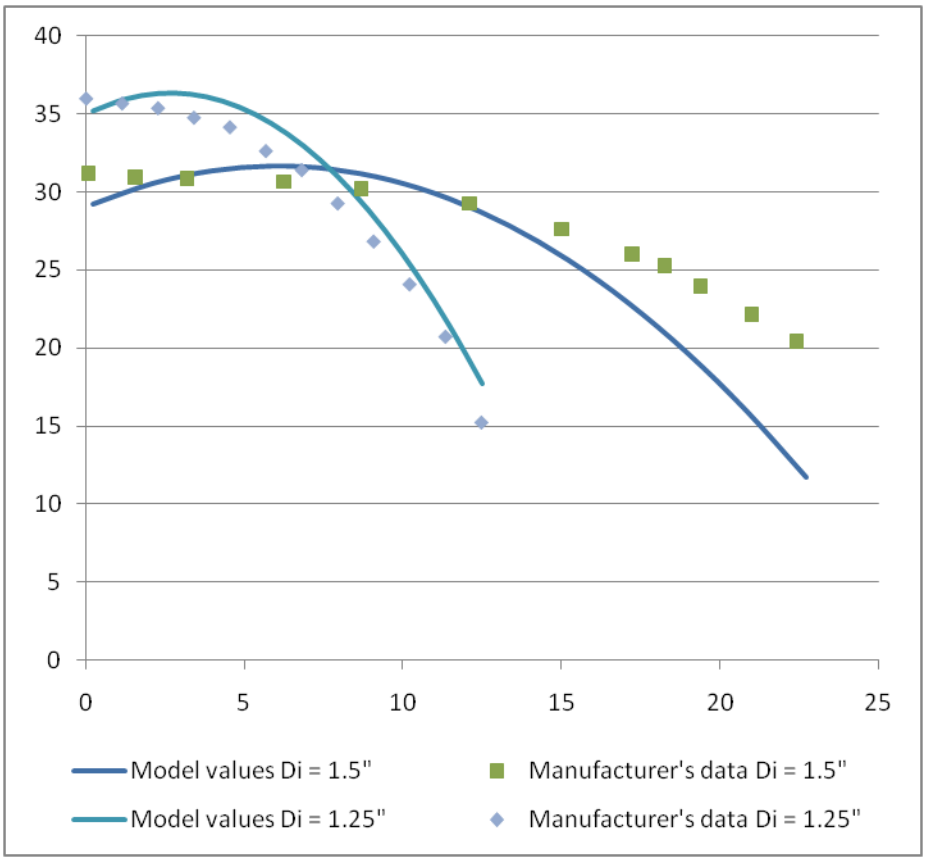

Figure 3-13 Effect of Impeller Inlet Diameter on Pump Curve

A similar trend is observed in the manufacturer's catalogues for the same family of pumps with variation in inlet diameter. Figure 3-13 shows pump curves for Goulds 3642/3742 close-coupled centrifugal pumps of sizes 1 x 1¼ - 5 and 1¼ x 1½ - 5. The first number in the size specification indicates outlet pump diameter while the second number is inlet impeller diameter in inches. Average values were used in the model. The deviation of the model results from the manufacturer's data could be reduced by parameter estimation. Model results and manufacturer's data show a similar effect on pump performance curve due to variation in inlet diameter.

3.6.4 Observations

The effect of impeller diameter and impeller inlet diameter on pump characteristics is observed in Section 3.6.3. Broadly it can be stated that the impeller diameter can shift the pump curve vertically (along the y-axis) while the impeller inlet diameter can reduce the steepness of the

pump curve (i.e. increase in impeller inlet diameter will stretch the pump curve along the x-axis).

An increase in impeller diameter leads to an increase in momentum imparted to the fluid by the impeller, thereby increasing the pressure head at the outlet of the pump. The more time the fluid spends in the impeller; the more energy is transferred to the fluid. Thus, an increase in inlet impeller diameter also leads to a slight decrease in developed pressure head.

An increase in impeller diameter has an effect that is similar to that of adding pumps in series. In both cases the fluid spends more time in the impeller.

An increase in the impeller inlet diameter and the impeller width leads to higher flow passage area. Increased flow area increases the flow through the impeller. Thus, an increase in the impeller width and inlet diameter pumps results in higher flow. An increase in the impeller width has a limited effect on pump flow and there are restrictions on increasing the impeller width due to pump casing limitations. But impeller inlet diameter has a significant effect on the pump flow. While investigating use of this model in sizing applications, it was found that the design flow rate of the pump (flow rate with maximum pump efficiency) is directly proportional to the square of impeller inlet diameter. This observation is justified because flow is directly proportional to impeller inlet flow area and flow area, is proportional to the square of the impeller inlet diameter.

An increase in impeller inlet diameter has an effect that is similar to adding pumps in parallel. In both cases flow area is increased.

3.6.5 Use of the Results for Sizing in Simulation Programs

This chapter mainly discusses predicting head-flow characteristics from pump parameters. From observations of the results of this study, correlation between some important parameters and pump performance can be drawn. These correlations can be helpful in pump sizing (i.e. with known required pump head and flow-rate a simulation program can suggest geometrical specifications for the pump).

It can be observed that apart from impeller inlet and exit angles[12]; impeller diameter, impeller inlet diameter and rotational speed affect the pump performance significantly. Also while selecting or sizing the pump from a particular pump family these parameters play important role.

To reduce the number of factors required for sizing, the shutoff head (no flow) condition is selected. Losses in the pump are proportional to the flow. At the no flow condition several pump parameters will not affect the performance significantly. At the no flow condition theoretical head is given by,

$$H_{th} = \frac{{U_2}^2}{g}$$

$$\Rightarrow H_{th} = \frac{(2\pi N D_2)^2}{g}$$

Parameters involved in the calculation of the theoretical pump head at no the flow condition are readily available. These same parameters are required in pump sizing. The theoretical pump head at the no flow condition was calculated for different pump diameters and speeds. These theoretical values were compared with the manufacturer's shutoff pump head from pump curves. It was found that the shutoff head from the manufacturer's data is 30% of the calculated theoretical head. Comparison of that shutoff head to theoretical head ratio for 22 pumps from Bell and Gossett Series 60, Series 80 and Series 1510 are shown in Figure 3-14.

[12] The correlations in the derivations of pump performance discussed in this chapter, involve tangent function of these angles. Thus, these models are highly sensitive to the impeller angles.

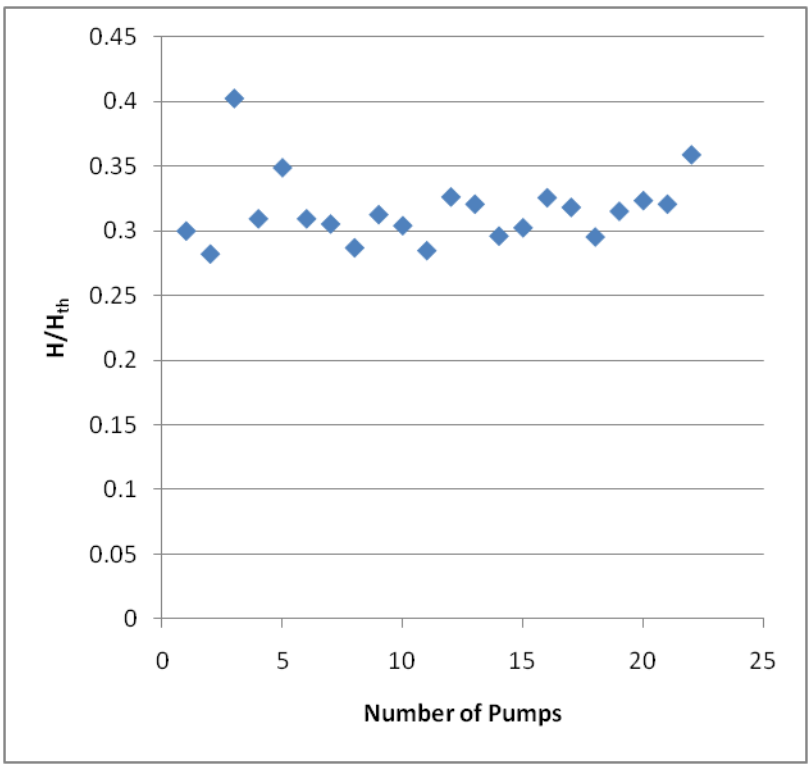

Figure 3-14 Comparison of Pump Shutoff Head from Theoretical Calculations and Manufacturers' Data

Thus, we can say that,

$$\frac{H}{H_{th}} \approx 0.3$$

$$\Rightarrow \frac{Hg}{(2\pi N D_2)^2} \approx 0.3$$

$$\Rightarrow N D_2 \approx \frac{1}{2\pi}\sqrt{\frac{Hg}{0.3}}$$

Pressure head can be substituted as:

$$H = \frac{P}{\rho g}$$

Where P is pressure in Pa, ρ is water density:

$$\Rightarrow ND_2 \approx \frac{1}{2\pi}\sqrt{\frac{P}{0.3\rho}} \tag{3-16}$$

In Equation 3-16 N is in rps while D_2 is in meters. In practice rotational speed and impeller diameters are specified in terms of rpm and inches thus:

$$\Rightarrow \left(\frac{n}{60}\right)\left(\frac{d_2}{0.0254}\right) \approx \frac{1}{2\pi}\sqrt{\frac{P}{0.3\rho}}$$

Where d_2 is impeller diameter in inches and n in rpm:

$$\Rightarrow nd_2 \approx 60 \times 0.0254 \times \frac{1}{2\pi}\sqrt{\frac{P}{0.3\rho}} \tag{3-17}$$

$$\Rightarrow d_2 \approx \frac{1.524}{n} \times \frac{1}{2\pi}\sqrt{\frac{P}{0.3\rho}} \tag{3-18}$$

In most of the cases pump curves are available for 1150, 1750 and 3500 rpm. Thus, with the calculated value of pressure drop in the loop we can get combinations of pump diameter and pump speed from Equation 3-18.

Equation 3-18 can be generalized as:

$$\Rightarrow d_2 \approx \frac{1.524}{n} \times \frac{1}{2\pi}\sqrt{\frac{P}{C\rho}} \tag{3-19}$$

Where C is constant which can be set as default value (0.3 for the pumps investigated) or can be taken as input from the user.

A similar study was carried out for flow rate, but the minimum pressure equivalent to pump shutoff head (which is maximum pressure head a pump can provide) does not exist since there is no maximum flow rate value specified. This is because, pumps curves are not extended much

beyond the design flow rate value and pumps are not expected to be operated in that region. Thus, flow rate corresponding to the best efficiency point is selected for analysis. From observations in section 3.6.4 it is clear that pump flow rate is dependent on impeller inlet diameter, impeller diameter and the rotational speed of the pump i.e. $Q \propto N$, $Q \propto D_2$ and $Q \propto {D_1}^2$. Since N, D_2 and D_1 are independent variables we can write:

$$Q_{BEP} \propto N D_2 {D_1}^2$$

$$\Rightarrow k = \frac{N D_2 {D_1}^2}{Q_{BEP}} \tag{3-20}$$

Where k is a non-dimensional constant of the equation

A study was carried out to determine the value of k. It was found that k remains constant for a family of pumps. With change in the pump family k varies. Values of k for about 50 pumps in Bell & Gossett Series 80 pumps are shown in Figure 3-15. Value of this constant for the series is about 0.04.

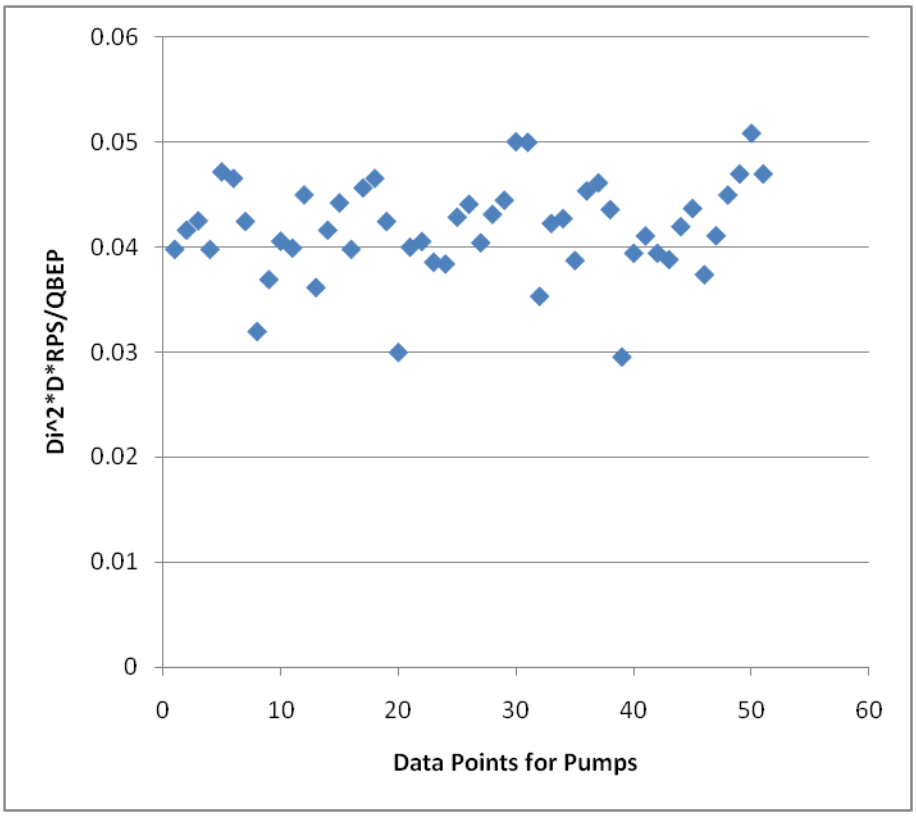

Figure 3-15 Calculation of proportionality constant for Bell & Gossett Series 80 Pumps

The value of k is a function of the overall configuration of the pump. This change in value of k was expected as the point under consideration is the best efficiency point, where several pump parameters come into consideration. It was found that the value of k varied from 0.02 to 0.05. This range is too high for the exact determination of any pump parameter. But, here the point under consideration is the best efficiency point. Thus, with a conservative value of the proportionality constant we may not get the pump with operation exactly at the best efficiency point but we will get a pump which can satisfy the given flow requirement.

Equation 3-20 can be written as,

$$D_1{}^2 = \frac{kQ_{BEP}}{ND_2}$$

$$\Rightarrow {D_1}^2 = \frac{k\ \frac{q_{BEP}}{15852}}{\left(\frac{n}{60}\right)\left(\frac{d_2}{0.0254}\right)}$$

$$\Rightarrow {D_1}^2 = 0.0058\frac{kq_{BEP}}{nd_2}$$

$$\Rightarrow \frac{d_1}{0.0254} = 0.076\sqrt{\frac{kq_{BEP}}{nd_2}}$$

$$\Rightarrow d_1 = 0.002\sqrt{\frac{kq_{BEP}}{nd_2}} \qquad (3\text{-}21)$$

With known value of nd_2 from Equation 3-17 and required flow rate value an approximate value of inlet impeller diameter can be calculated by a sizing subroutine. Thus, for a given rotational speed, the impeller inlet and outlet diameters can be sized using a detailed pump model in simulation program.

3.7 Limitations of Theoretical Model

Theoretical models are sufficiently accurate for sizing calculations as discussed in the previous sections, but they have several limitations which make them inconvenient for general use in simulation programs. These limitations are discussed in the following sections. For applications requiring high accuracy, there are several CFD based simulation programs which can predict the pump performance characteristics with great accuracy. They demand large number of inputs but results obtained are highly accurate.

3.7.1 Model Simplifications and Assumptions

It can be observed that in pump head loss calculations several geometrical generalizations are made. For example both model assume fluid entry along the impeller axis and exit tangential to impeller. Manufacturers have their own set of geometric configurations, which might change the loss coefficients and cross-section area calculations in the models.

From the results of the study it is observed that pump geometry plays an important role in major losses i.e. incidence and shock losses. And these losses significantly affect pump performance characteristics.

Both models discussed in this chapter assume a 2-D impeller geometry for calculations purpose. This neglects the 3-dimensional nature of the flow and adds uncertainty to the head loss calculation.

In addition, both models assume an average flow cross-sectional area. In actual practice the impeller fluid passage area and casing cross-sectional area is not uniform. Finally, when fluid passes through the impeller and casing it has a velocity profile across the cross-section. Due to the varying cross-sectional area of the impeller passage and the volute, the velocity varies along this path. For simplification the average velocity is considered which leads to added uncertainty in the calculation of losses.

3.7.2 Input Availability and Approximations

Even after a number of assumptions all of the inputs required for the calculations are not readily available in pump catalogs. These inputs can be approximated with reasonable results as previously demonstrated; however, if the type of pump is known a-priori, it is more convenient and accurate to simply specify the pump curve as input to the simulation.

3.8 Summary

It was observed that performance predicted by the Tuzson model was a better match with manufacturer's data compared to the Spannhake model. But, neither of these models is convenient to use in a HVAC simulation program when the pump has been specified and pump curves are available. For this situation, the models can be used to determine the effect of each individual parameter on the performance curve.

When the size of the pump is unknown, such as in a hydronic system sizing calculation, these models can be used to predict the inlet and outlet diameters of the pump impeller, assisting the designer in sizing the pump for the system. These diameters can be calculated explicitly using the equations developed in this study.

Chapter 4. Non-Dimensional Pump Model

The models presented in Chapter 3 provide sufficient accuracy for sizing calculations in simulation programs. However, the detailed analytical models have their limitations and need a number of inputs that are difficult to obtain. For these reasons, a non-dimensional pump models are often used in simulation programs.

According to Lazarkiewicz & Troskolanski (1965) 'In view of the wealth of the experimental material, which pump manufacturers have at their disposal, the problem of theoretically establishing head-discharge curves has lost its importance.' Thus, instead of using performance prediction model for simulation purposes a simplified model with fewer inputs that are readily available in pump catalogs is useful. The model should have sufficient accuracy to predict the performance of the pump over its entire range of operation. For many simulation applications, the user has selected the pump but wants to adjust the impeller diameter or the speed to reduce power consumption. A non-dimensional model which has a limited number of inputs is promising for this in whole building simulation applications.

The well known affinity laws are one such non-dimensional model. The main limitation of the affinity laws is that they do not account for changes in fluid properties. In this chapter significance of fluid properties is evaluated and a new non-dimensional model that account for fluid properties is proposed.

4.1 Need for Non-dimensional Pump Models

4.1.1 Prototype development

If geometric, kinematic and dynamic similarity is achieved by the model then development of

new pump prototypes is simplified. One such application is the development of the artificial heart using a miniature centrifugal pump with suspended impeller (Chua & Akamatsu, 2000). In their research a detailed study of fluid dynamics between the impeller and the casing was required. In the actual blood pump, the gap between the impeller and the casing is about 0.2 mm, and it was impossible to measure shear stress within the gap. An enlarged model (5:1) was created, and the measurements were taken. They used their non-dimensional pump model to scale the experimental prototype down to the actual size required for the artificial heart pump.

4.1.2 HVAC Simulation Programs

Pump head flow characteristics are often presented graphically in feet-gpm (or m-m^3/hr) by pump manufacturers. To use this data in a flow network simulation, polynomial curve-fits are generated and their coefficients are used. These curves are specific for a particular pump rotational speed, impeller diameter and fluid density. Using curve-fit coefficients generated directly from the manufacturer's plots works fine for constant speed pumping applications. However for variable speed pumping applications a non-dimensional model is preferred. Using a non-dimensional model the pump curves can be easily scaled up or down at each time step. One characteristic curve can be used for all possible operating speeds of the pump.

Pump affinity laws are widely used in industry to predict pump performance with respect to changes in impeller diameter and rotational speed.

For a fixed diameter (and other dimensional parameters) flow is directly proportional to speed; the pressure rise (head) across pump is proportional to the square of the speed, and the power transferred to the fluid is proportional to the cube of speed as shown in the Equation 4-1 through Equation 4-3.

$$\frac{Q_1}{Q_2} = \frac{N_1}{N_2} \tag{4-1}$$

$$\frac{H_1}{H_2} = \left(\frac{N_1}{N_2}\right)^2 \quad (4\text{-}2)$$

$$\frac{P_1}{P_2} = \left(\frac{N_1}{N_2}\right)^3 \quad (4\text{-}3)$$

For a particular pump with constant speed, flow is directly proportional to the impeller diameter; pressure rise across pump is proportional to the square of the impeller diameter, and power transferred to the fluid is proportional to the cube of impeller diameter as shown in Equation 4-4 through Equation 4-6.

$$\frac{Q_1}{Q_2} = \frac{D_1}{D_2} \quad (4\text{-}4)$$

$$\frac{H_1}{H_2} = \left(\frac{D_1}{D_2}\right)^2 \quad (4\text{-}5)$$

$$\frac{P_1}{P_2} = \left(\frac{D_1}{D_2}\right)^3 \quad (4\text{-}6)$$

A user can implement variable flow in a piping network without non-dimensionalization of pump characteristics by varying valve positions/pressure constants or by using affinity laws. Varying the valve position in the simulation will move the system curve to attain the required flow in the loop. Using affinity laws will approximate the non-dimensional model but will not incorporate variations in the fluid properties.

Pump performance curves are generally concerned with water at standard conditions as the working fluid. In HVAC operations, water temperature may vary from 4°C to 90°C depending upon the load requirement, and often mixture of Ethylene glycol and water is used in order to achieve a higher boiling point and a lower freezing point. This causes variation in fluid properties. In HVAC simulations fluid density will continuously vary according to fluid temperature ad mixture. These variations can easily be incorporated in pump performance curves using a non-dimensional model.

4.2 Literature Review

4.2.1 BEP (Best efficiency point) Model

This model is one of the non-dimensional models suggested by Bernier & Lemire (1999) for calculation of required pumping power. Pump curves are re-constructed from values corresponding to best efficiency points (BEPs). At this *best efficiency point*, the pump achieves maximum efficiency, and the flow and pressure head corresponding to the point are noted as rated flow and pressure head for the pump. At BEP, non-dimensional pressure head (H_{nd}) and non-dimensional flow rate (Q_{nd}) are both assumed to be unity. Values at each point on the pump curve are calculated using,

$$H_{nd} = {}^{H}/_{H_{BEP}}$$

$$Q_{nd} = {}^{Q}/_{Q_{BEP}}$$

This model is specifically used for calculation of pumping power in a procedure suggested by Bernier & Lemire (1999). But, this model does not provide a generalized curve for a set of pump curves and is therefore not suitable for use in HVAC simulation programs.

4.2.2 Previous work in Dimensional Analysis

Every book that discusses dimensional analysis of turbo-machinery has its own set of similar non-dimensional numbers.

Lazarkiewicz & Troskolanski (1965) consider fluid density (ρ), fluid viscosity (ν), Output energy per unit mass (gH) (instead of discharge head), impeller diameter (D), volumetric flow-rate (Q) and rotational speed (N). There are six variables under consideration thus three non-dimensional numbers are generated:

$$Characteristic\ head: \pi_1 = {}^{gH}/_{D^2N^2} \tag{4-7}$$

$$Characteristic\ flow: \pi_2 = {}^{Q}/_{D^3N} \tag{4-8}$$

$$Characteristic\ discharge\ number: \ \pi_3 = {}^{\nu}/_{D^2N} = {}^{\mu}/_{\rho D^2N} \tag{4-9}$$

From these numbers further similarity numbers are generated. For example from the product of π_1 and π_2 an expression for characteristic power can be generated.

Timar (2005) uses a matrix method to generate similar dimensionless products and shows from experimental results the effect of the Reynolds number on the head and the characteristic flow.

Hodge (1999) considers power (P) and efficiency (η) along with the terms considered by Lazarkiewicz & Troskolanski (1965). Since efficiency itself is a dimensionless number it becomes one of the non-dimensional numbers along with characteristic power (π_4) and π_1, π_2 and π_3:

$\pi_1 = {}^{gH}/_{D^2N^2}$ $\qquad$ $\pi_2 = {}^{Q}/_{D^3N}$

$\pi_3 = {}^{\mu}/_{\rho D^2N}$ $\qquad$ $\pi_4 = {}^{P}/_{\rho D^5N^3}$

$\pi_5 = \eta$

Depending upon the number of variables considered every reference has a different set of non-dimensional numbers. Pressure head, volumetric fluid discharge/mass flow rate, rotational speed, characteristic length/impeller diameter, fluid density and fluid viscosity are some of the commonly used variable in all references. Along with above variables a few books also consider fluid elasticity and pump efficiency for non-dimensionalization. All of the above variables can be expressed in terms of the basic independent variables mass (M), length (L) and time (T). Thus the

number of non-dimensional numbers generated will be three less than the number of variables under consideration. (Following further discussion in Appendix we will be using six variables.)

While carrying out a detailed dimensional analysis of a centrifugal pump, several variables can be taken into consideration. These variables can be broadly classified into three basic types (Shepherd, 1956).

The first category is geometrical variables which include physical dimensions of pumps such as volute cross-section area, impeller width, impeller diameter etc. In most of the references impeller diameter represents the characteristic dimension of the pump. The effect of other dimensional parameters is discussed in Section 3.6.

The second category is kinematic variables which include radial and tangential fluid velocities in the impeller, volumetric and mass flow rate, and the rotational speed of the impeller.

The third group consists of dynamic variables which can be further divided into fluid properties[13] and performance characteristics. Density, viscosity, elasticity and surface tension affect the flow. A careful investigation is required to omit extraneous parameters. Performance characteristics include pressure rise, power and torque.

4.3 Non-dimensionalization

For whole building simulation programs, the energy balance is the fundamental calculation. For this reason, mass flow rate, rather than volumetric flow rate is typically the state variable. For this reason we are interested in developing a non-dimensional pump model based on pressure rise, mass flow rate and power along with fluid properties, impeller diameter and rotational speed. The objective is to develop a non-dimensional model and eliminate variables which do not affect pump performance significantly.

[13] Fluid properties are included in dynamic variables because they affect forces and energy loss inside turbo-machinery.

Volumetric flow rate can be represented by mass flow rate and density. Tip velocity of the impeller can be replaced by impeller diameter and rotational speed. Thus the volumetric flow and velocities inside the pump are extraneous parameters that need not be considered in the model.

Dimensionless groups selected to develop a pump model for whole building energy simulation programs is stated in Equation 4-10, Equation 4-11 and Equation 4-12:

Lazarkiewicz & Troskolanski (1965) suggest following functional relationship:

$$\pi_2 = f(\pi_1, \pi_3)$$

For the new model this results in:

$$\Rightarrow {}^{\Delta p}\!/_{\rho N^2 D^2} = f\left({}^{\dot{m}}\!/_{\rho N D^3}, {}^{\mu}\!/_{\rho N D^2}\right)$$

The order of magnitude of the variables in the above equation is as follows;

Table 4-1 Variables in Non-Dimensionalization

Variable	Symbol	Range	Order	Dimension
Mass flow rate	m	2-12 kg/s (30-200 gpm)	10	M^1T^{-1}
Rotational speed	N	20-30 rps	10	T^{-1}
Dynamic Viscosity	μ	0.0017-0.0002 Ns/m^2	10^{-3}	$M^1L^{-1}T^{-1}$
Density	ρ	900-1200 kg/s	10^3	M^1L^{-3}
Impeller diameter	D	0.1-0.2 m	10^{-1}	L
Pressure	Δp	10^5-10^7 N/m^2	10^6	$M^1L^{-1}T^{-2}$

$$\Rightarrow \frac{\Delta p}{\rho N^2 D^2} = f\left(\frac{10^1}{10^3 10^1 (10^{-1})^3}, \frac{10^{-3}}{10^3 10^1 (10^{-1})^2}\right)$$

$$\Rightarrow \frac{\Delta p}{\rho N^2 D^2} = f(10^0, 10^{-5})$$

It can be observed that the order of magnitude of the term involving viscosity is very low compared to the characteristic flow number (basically this term is the inverse of the Reynolds number, which implies that flow in the impeller is mostly turbulent). Thus, pump head is a weak function of viscosity.

This is to be expected, since it is the inverse of the Reynolds number for the impeller with outer diameter as the characteristic length. In the turbulent region of the Moody chart, the Reynolds number hardly affects the value of the friction factor (i.e. the friction factor is independent of viscosity change in this region). Thus we can conclude that in the turbulent region, viscosity does not significantly affect pump performance.

Experimentally it has been confirmed that for turbulent flow through the impeller the effect of viscosity is negligible (Lazarkiewicz & Troskolanski, 1965).

Timar (2005) performed experiments relating head and flow coefficients and found that for different values of the inverse Reynolds number, the generated curves matched. He also concludes that the third dimensionless parameter does not affect the pump curves significantly, thus confirming our dimensional analysis.

There are six basic variables which are concerned with pump performance and their dimensions are shown in Table 4-1:

The non-dimensionalization procedure which is shown in Appendix C results in the following dimensionless groups:

$$\Rightarrow \pi_1 = \dot{m}/\rho N D^3 \qquad (4\text{-}10)$$

$$\Rightarrow \pi_2 = {\Delta p}/{\rho N^2 D^2} \tag{4-11}$$

$$\Rightarrow \pi_3 = {\mu}/{\rho N D^2} \tag{4-12}$$

If we multiply Equation 4-10 and Equation 4-11 we will get power coefficient;

$$\pi_4 = \left({\dot{m}}/{\rho N D^3} \times {\Delta p}/{\rho N^2 D^2} \right)$$

$$\Rightarrow \pi_4 = \left({\dot{m} \times \Delta p}/{\rho} \right) \times {1}/{\rho N^3 D^5}$$

$$\Rightarrow \left({\dot{m}}/{\rho} \right) \times {\Delta p}/{\rho N^3 D^5} = Q \times {\Delta p}/{\rho N^3 D^5}$$

Using, $Power\ (P) = \Delta p \times Q$

$$\Rightarrow \pi_4 = {P}/{\rho N^3 D^5} \tag{4-13}$$

4.3.1 Significance of Non-dimensional Numbers

The first non-dimensional number π_1 (Equation 4-10) can be written in terms of the volumetric flow rate, Q:

$$Q = {\dot{m}}/{\rho} \tag{4-14}$$

$$\Rightarrow \pi_1 = {Q}/{N D^3} \tag{4-15}$$

Noting that Q can be represented in terms of fluid velocity, V, and flow area, A.

$$Q = Velocity * flow\ area \propto V * A$$

Noting also that impeller tip velocity, U, can be represented in terms of rotational speed, N, and impeller diameter, D.

$$U = ND \tag{4-16}$$

$$\pi_1 = \frac{A}{D^2}\left(\frac{V}{U}\right)$$

Thus, if the geometrical similarity is maintained (i.e. A/D^2 = constant), π_1 is equivalent to (V/U) i.e. ratio of fluid velocity and blade speed. The same value of π_1 basically represents geometrically similar pump velocity triangles which may have different rotational speed (N), mass flow rate (m) of density (ρ). This term represents kinematic similarity.

For the second non-dimensional number π_2 (Equation 4-11) pressure rise, p (in Pa) can be expressed in terms Pressure head (H) of as:

$$\Delta p = \rho g H$$

$$\Rightarrow \pi_2 = {gH}/{N^2D^2}$$

The impeller tip velocity can be expressed in terms of rotational speed and impeller diameter as:

$$U^2 = N^2D^2 \propto Kinetic\ Energy$$

$$\Rightarrow \pi_2 = {gH}/{U^2}$$

Thus π_2 (head coefficient) represents the ratio of the pressure head to the kinetic energy of the impeller. This term represents dynamic similarity.

Using Equation 4-16, the third non-dimensional number π_3 (Equation 4-12) can be written as:

$$\pi_3 = {\mu}/{\rho UD}$$

This is similar to the inverse of the Reynolds number with the impeller diameter as the characteristic length.

These non-dimensional π-groups are derived assuming impeller diameter as a single dimensional shape parameter. Although this is dimensionally correct, the impeller diameter it is not necessarily an appropriate length scale for the non-dimensional pump model.

4.4 Development of the Non-Dimensional Model

Pump manufacturers often provide pump curves for the same pump with different impeller diameters and different rotational speeds. The non-dimensional model allows a user to input a single curve and simulate the whole family of pumps.

In non-dimensionalization, the variables that affect the pump performance are considered and used in the π-theorem to get non-dimensional numbers. Variables used in this method can be representative terms. For example instead of various physical dimensions of pump (which are mostly not available in data sheet) just a single parameter i.e. impeller diameter is considered. In the derivation of π-terms geometric similarity is assumed i.e. it is assumed that other physical dimensions that might affect the performance will change in proportion to impeller diameter (which may not be the case every time). A non-dimensional model is used to predict performance of a pump when one or more parameters are changed. In such cases the approximation to use a single representative term may cause significant errors in prediction of performance. The π_1 term derived from the simple non-dimensionalization process is inconsistent with flow/geometry relationship predicted by the affinity laws. The affinity laws predict that the volumetric flow rate, Q, is directly proportional to the impeller diameter, D.

From $\pi_1 = {\dot{m}}/{\rho N D^3}$ it appears that the mass flow rate is proportional to cube of the impeller diameter, whereas from the pump affinity laws it is stated that flow is directly proportional to the impeller diameter.

This difference is observed in the formula for the mass flow rate, and is propagated to the power coefficient. The power coefficient is the product of the flow and the head coefficients. From

$\pi_4 = {}^{P}/_{\rho N^3 D^5}$ it can be inferred that the power is proportional to the fifth power of diameter, and according to the affinity laws, power is proportional to the cube of the impeller diameter.

The basic assumption behind the non-dimensional model is that variation in pump parameters maintains geometric similarity. The effect of geometric similarity on the π-terms is explained in (Shepherd, 1956). If we assume that there are three linear dimensions B, C and D selected to represent three-dimensional shape of pump then two more π-terms B/C and C/D (or B/D) would have to be added. This will provide options for flow coefficient such as, ${}^{\dot{m}}/_{\rho NBCD}$, ${}^{\dot{m}}/_{\rho NB^2 D}$ or ${}^{\dot{m}}/_{\rho NC^2 D}$ and so on (not affecting other π terms except the power coefficient).

As explained in section 4.3.1 the term ND^3 in $\pi_1 = {}^{Q}/_{ND^3}$ can be separated as follows,

$$ND^3 = ND * D^2$$

In non-dimensionalization the impeller diameter is taken as a physical dimension to represent geometrical parameter. The term D^2 in above equation represents the flow area (A). Thus we can rewrite $\pi_1 = {}^{Q}/_{ND^3}$ as:

$$\phi = {}^{Q}/_{NDA} \qquad (4\text{-}17)$$

To distinguish the non-dimensional flow and head from non-dimensional π-groups separate notation is used. Where φ represents non-dimensional flow, and ψ non-dimensional head:

$$\Rightarrow \phi = {}^{\dot{m}}/_{\rho NDA}$$

And,

$$\psi = {}^{\Delta p}/_{\rho N^2 D^2}$$

Similarly $\pi_4 = {}^{P}/_{\rho N^3 D^5}$ can be written as:

$$\Rightarrow \pi_4 = {}^{P}/_{\rho N^3 D^3 A} \qquad (4\text{-}18)$$

Now in (Equation 4-17 Modified flow coeffcient) and (Equation 4-18: Modified power coeffcient) the non-dimensional terms are in accordance with pump affinity laws.

HVAC 2 Toolkit (Brandemuhl, 1993) and HVACSIM+ Reference Manual (Clark, 1985) specify non-dimensional flow coefficient and dimensionless pressure head coefficient as:

$$\Rightarrow \phi = {}^{\dot{m}}/_{\rho N D^3}$$

And,

$$\psi = {}^{\Delta p}/_{\rho N^2 D^2}$$

Which are exactly similar to the non-dimensional π-groups. Non-dimensional curves plotted using non-dimensional π-groups [non-dimensional coefficients mentioned in HVAC 2 Toolkit (Brandemuhl, 1993) and HVACSIM+ Reference Manual (Clark, 1985)] and the non-dimensional model developed in above discussion is compared in Section 4.5.

4.5 Evaluation of Non-Dimensional Model and π-groups

When the non-dimensional π-groups are used to generate non-dimensional pump curve for different rotational speeds it is observed that, for the same pump, these curve match. Figure 4-1 shows non-dimensional curves when for Bell & Gossett Series 80SC 1.5x1.5x7B centrifugal pump operated at 1150, 1750 and 3500 rpm.

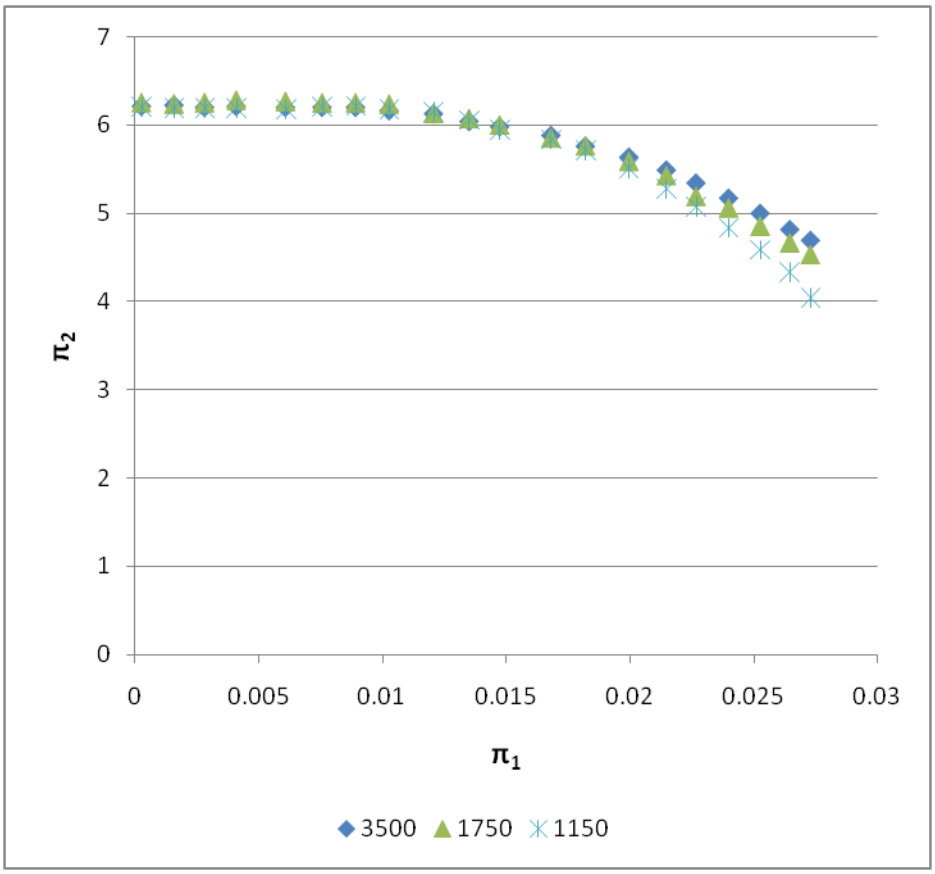

Figure 4-1 Non-dimensional pump curves when pump operated at various rotational speeds

It can be observed that the non-dimensional π-groups give good results for different rotational speeds. Thus, if a single non-dimensional pump curve is available, pump curves for different rotational speeds can be generated from the model.

In order to assess the performance of the non-dimensional model for changed in impeller diameter, pump curves for Goulds 3642/3742 1 X 1.25 - 5 are non-dimensionalized using the modified π-groups discussed in the previous section. These curves are shown in Figure 4-2.

In order to apply the non-dimensional model with $\phi = \dot{m}/\rho NDA$ and $\psi = p/\rho N^2 D^2$, the area, A, must be specified. However, if the dimensions used to calculate the area are related only to the pump housing geometry and not to the impeller geometry, then A will be a constant and will be retained in the phi equation only to maintain the non-dimensional form of the equation. This is

in fact the case as demonstrated in Figure 4-2 where A=1. This explains the form of the Affinity Laws and yields a simplified non-dimensional model with $\phi = \dot{m}/_{\rho N D}$.

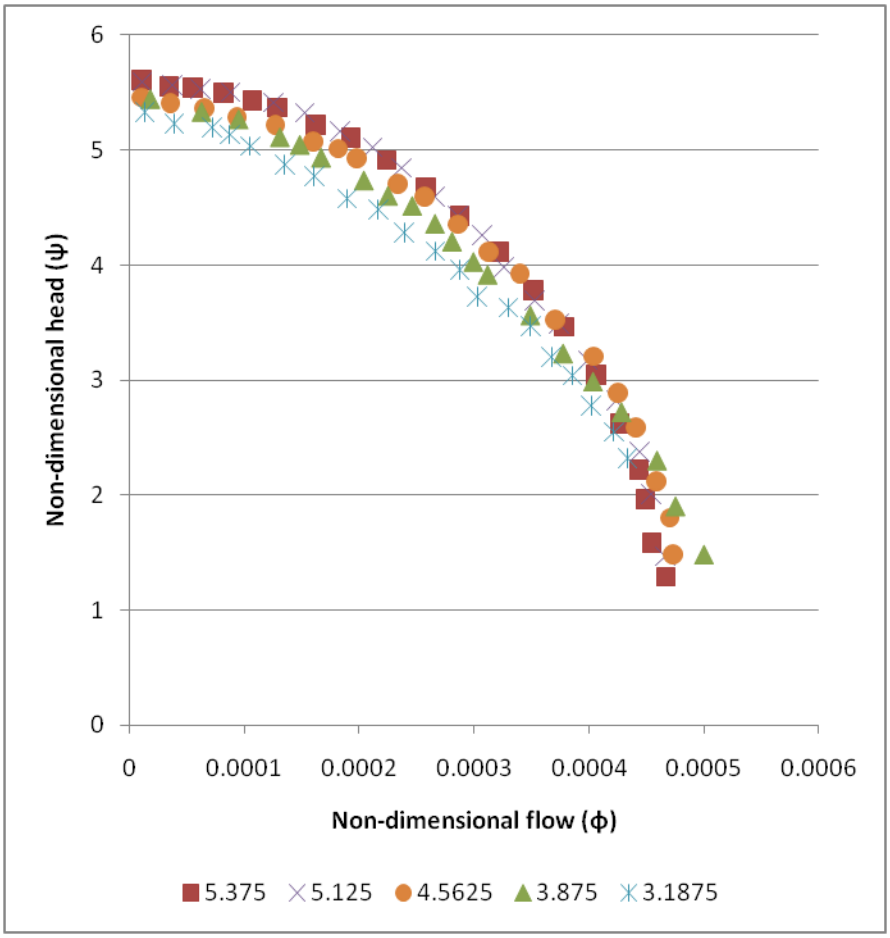

Figure 4-2 Non-dimensionalized pump curves using modified flow coefficient

On the other hand when same pump curves are plotted using the original π_1 group with mass flow rate proportional to D^3 five separate equations are needed to model the five curves as shown in Figure 4-3. This confirms that the scaling suggested by the affinity laws and incorporated in the π groups in the previous section is correct.

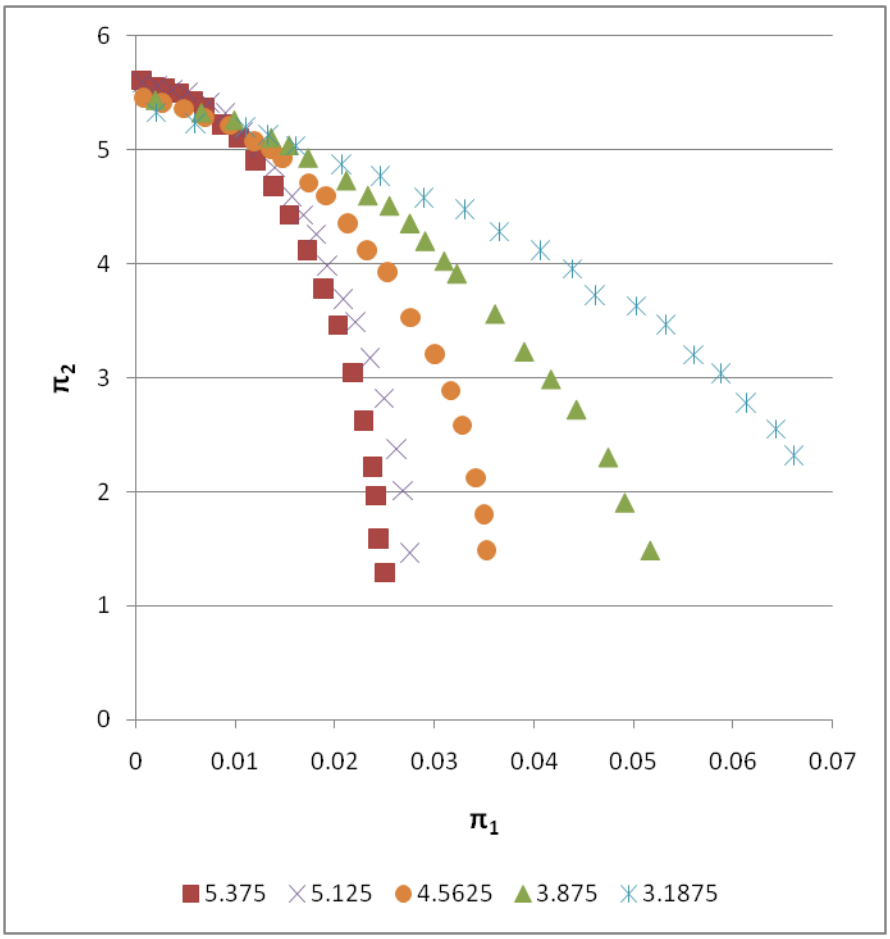

Figure 4-3 Non-dimensional pump curves for variation in impeller diameter

It is important to measure the deviation of the non-dimensional curves from the main curve (non-dimensional curve with maximum impeller diameter) before using for simulation purpose. For determination of the deviation pump curves with different RPM, flow rate (35 GPM to 1600 GPM) and shape (steep and flat from same pump family) are selected. Figure 4-4 and Figure 4-5 shows the comparison between model values and curves obtained from manufacturers' data.

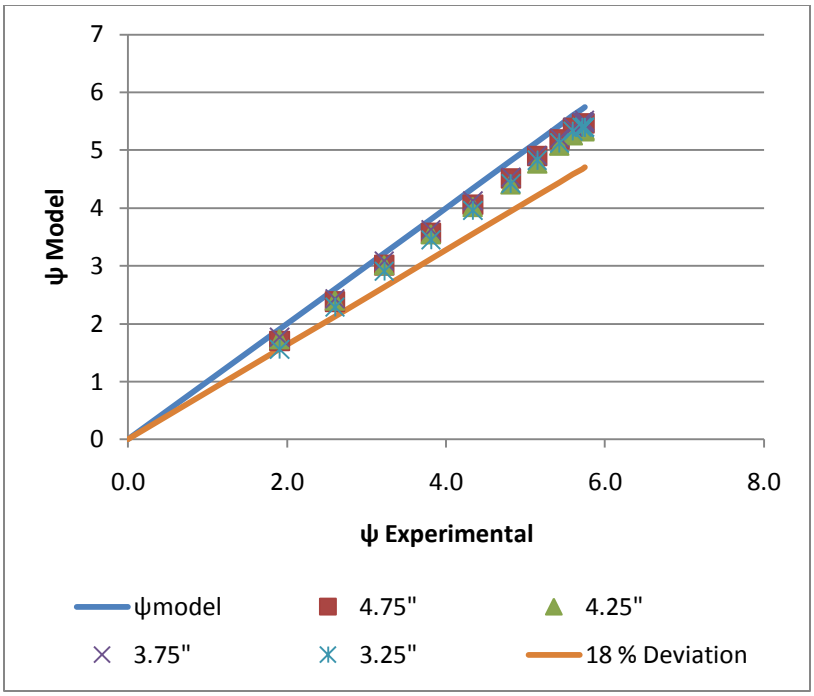

Figure 4-4 Deviation of Non-Dimensional Curve (Bell & Gossett SERIES 60 1x1x5.25)

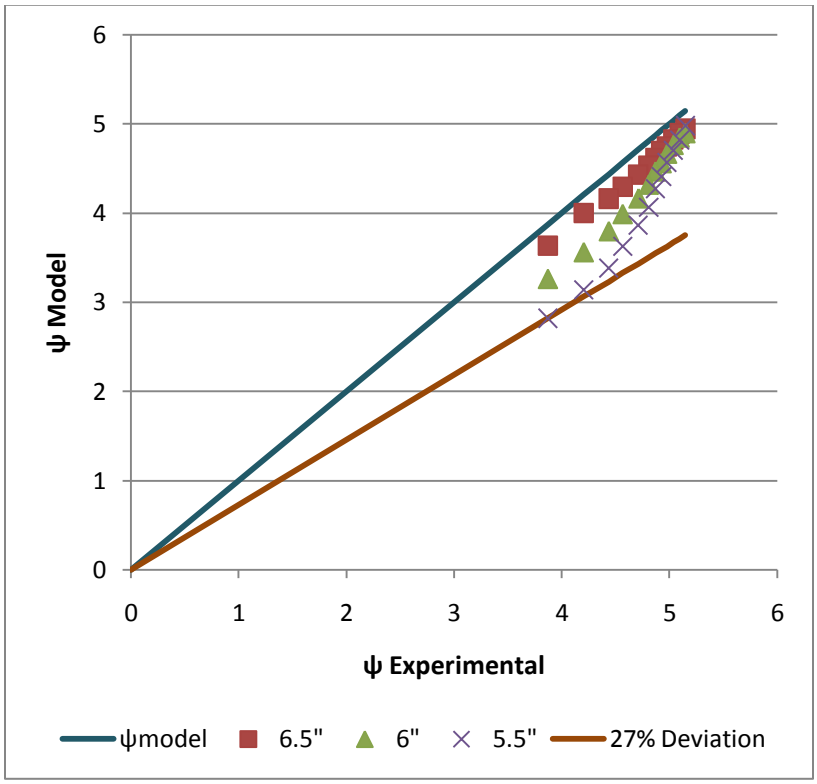

Figure 4-5 Deviation of Non-Dimensional Curve (Bell & Gossett Series 80 6x6x7B)

From Figure 4-4 Figure 4-5 it can be observed that with a reduction in diameter the deviation from the main curve goes on increasing. Thus, the non-dimensional model does not completely eliminate the effect of the diameter.

Table 4-2 shows the % deviations of the manufacturer's data from the model values for different pump curves. It can be observed that for an impeller diameter reduction of 15 to 32%, a deviation of 18% to 30% is observed. No specific trend is observed in the results. For example for a 32% reduction in impeller diameter a maximum deviation of 18% is observed for the Series 60 - 1 x 1 x 5.25 pump; whereas in the case of the Series 80 - 6 x 6 x 7 pump, for a 15% reduction in diameter results in a 27% deviation from the manufacturer's data.

Table 4-2 Deviation for various Pump Curves

B&G Series	Specification	Rotational Speed	Maximum Flow rate (GPM)	% Reduction from maximum impeller diameter	% Deviation from model values
Series 60	1x1x5.25	1750RPM	60	32	18
Series 60	2x2x5.25	1750RPM	180	32	30
Series 80	1.5x1.5x7B	3500RPM	140	23	28
Series 80	6x6x7	3500RPM	1600	15	27
Series 90	1AA	1725RPM	35	27	30
Series 90	2AA	1725RPM	105	29	26

4.6 Conclusions

Evaluation of the non-dimensional model showed that both the model and affinity laws can give error up to 30% for diameter variation. This error increases with reduction in impeller diameter from actual design size. Maximum error is observed at higher flow rates and it is minimum near the pump shutoff head. Even with parameter estimation to get the unknown inputs, the Tuzson

and Spannhake model are within -30% to 10% error range. Non-dimensional model provides comparable accuracy with fewer inputs.

The dimensional analysis shown in this chapter demonstrated that the non-dimensional model first presented by Clark (1985) is only appropriate if the geometrical similarity of the pump is maintained. It is incorrect for use with a single pump housing and trimmed impellers. For this case, the modified model presented in this chapter should be used.

Chapter 5. Experimental Validation of Non-Dimensional Model

From the discussion in Chapter 3 it is clear that various pump geometric factors can affect pump performance significantly. Manufacturers have their own set of geometric configurations, which can change the loss coefficients and cross-sectional area calculations in the detailed models. Thus, it is very difficult to find a generalized correlation which will predict pump performance precisely. Furthermore, the accuracy of the pump manufacturer's data is not known. Many manufacturers measure only a few points and then use their own models to generate the rest of the data set. This leads to the conclusion that experimental validation of the pump model and manufacturer's data is necessary.

Even though according to Singh & Mitchell (1998) impeller trimming is relatively easy to implement and has a short payback period (compared to VFD setup), a large experimental setup is required to experimentally determine a generalized correlation between pump performance and impeller diameter. Since the experimental facility and budget is limited, the experimental results reported in this chapter only consider changes in the speed of the pump.

An existing VFD pumping piping system was used with few modifications to verify the effect of pump speed on performance. Equation 3-15 suggests linear relation between flow and rotational speed and a second order relation between pump head and rotational speed. This analytical finding can be verified on a VFD setup.

5.1 Objectives

In addition to the experimentally validating the pump model and the checking the accuracy of the manufacturer's data two additional objectives are discussed in the following sections.

5.1.1 Verification of Energy Savings

Non-dimensional model especially the affinity laws are widely used to estimate energy savings from variable frequency drives. From affinity laws it can be easily inferred that a 50% reduction in pump rotational speed (or flow rate) will lead to 88% reduction in power due to the cubic nature of relation between pump power and pump rpm.

$$P_2 = P_1\left(\frac{N_2}{N_1}\right)^3 \Rightarrow P_2 = P_1\left(\frac{1}{2}\right)^3 \Rightarrow \frac{P_2}{P_1} = \frac{1}{8} \Rightarrow P_2\ is\ 12.5\%\ of\ P_1$$

This suggests huge power savings due to VFD installation. The objective of the experiments is to verify the power savings estimated by the affinity laws.

5.1.2 Verification of Affinity Laws at Low Pump Speed

A second objective is to verify the applicability of the affinity laws at low pump speeds. Pump curves in manufacturer's data-sheet are provided for standard RPMs (i.e. 1150 RPM, 1750 RPM and 3500 RPM). However, simulation models assume that pumps can run at much lower rpms. The experimental test matrix will confirm that the following correlations:

$$Q \propto N$$

$$H \propto N^2$$

still hold good at sub 1200 RPM.

5.2 Literature Review

In order to estimate the overall energy savings, the value of all component efficiencies over the operating range of the pump are required. According to Gao (2008), a variable speed drive can achieve significant reduction in input energy but it is not possible to achieve all energy savings potential predicted by affinity laws. Gao (2008) addressed the issue of energy savings estimated by affinity laws by studying overall system efficiency of a 15 HP variable speed pumping system.

In the experiment efficiency at each stage was found and overall efficiency was calculated. The experiment was repeated for different values of motor control frequency, and mass flow rate was varied by throttling. It was found that at fixed motor control frequency (constant pump speed) the overall efficiency decreases with decreasing flow rate. The combined efficiency of variable speed pumping system also decreases when the flow rate is held constant and motor speed is reduced by decreasing control frequency.

Based on Gao's results (Gao, Mclnerny, & Kavanaugh, 2008) a correlation between non-dimensional system efficiency and non-dimensional flow rate was confirmed. The test results indicate significant energy savings by variable speed pumping system at partial load conditions but the 'wire to water efficiency' (overall efficiency based on electric input to the VFD) drops drastically for flow rates less than 60% of full load flow rate. The experiments conclude that for an accurate value of power savings, the value of the overall system efficiency is required over the entire operational range.

Bourret & Bernier (1999) experimentally determined the difference between theoretical power variation and actual power variation for three motors: a properly sized motor and 50% and 100% oversized motors over the range of rotational speeds. The reason for the difference is that the affinity law neglect the effect of speed on inefficiencies.

Timar (2005) checked the effect of Reynolds number on non-dimensional curves. An experiment is performed on a pump with 220 mm impeller diameter. Reynolds number of the flow is changed by varying the pump rotational speed. In the experiment the speed of the pump is varied from 1200 RPM to 2000 RPM and for corresponding variation in Reynolds number it was found that non-dimensional pump curve superimpose. This led to conclusion that for given variation in pump speed, the correlations $Q \propto N$ and $H \propto N^2$ are applicable.

5.3 Description of Experimental Facility

5.3.1 Existing Facility

The VFD controlled pump located in Hybrid Ground Source Heat Pump Lab at Oklahoma State University was used to experimentally verify the pump model and estimate overall pump efficiency at low flow rates. This facility was developed for a previous research project by Shawn Hern. The source side of the facility consists of three environmental heat exchangers namely a Ground Loop Heat Exchanger (GLHE), a Plate Heat Exchanger[14] (PHE) and a Pond Heat Exchanger (currently disconnected) along with two Heat Pumps (HP) and a water circulating pump. Figure 5-1 is not a complete representation of source side of experimental facility, but it shows the components used in this experimental verification[15].

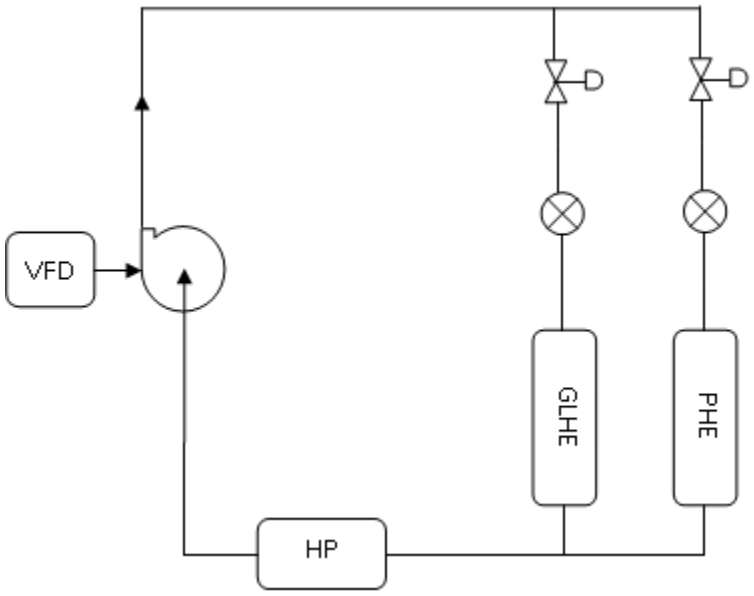

Figure 5-1Source Side Schematic

The ground loop heat exchanger, plate heat exchanger and heat pump act as fixed load on the pumping system. Pumping load can be reduced by allowing flow through both branches and can be increased by partially closing the valves or completely turning off one of the branches.

[14] The other side of PHE is connected to cooling tower setup in the facility.
[15] Complete description of the facility is available in (Hern, 2002)

A Bell & Gossett Series 80 1-1/2 X 1-1/2 X 7B inline centrifugal pump with 6.5" impeller diameter is installed in the source side loop. The pump is shown in Figure 5-2. Rotational speed of this pump is controlled by a Siemens SED2-1.5/22X variable frequency drive. Output frequency of the VFD can be reduced up to 10 Hz (higher values were not checked experimentally to avoid hydraulic overloading of components and piping network).

For flow and power measurement flow-meters and power transducers already installed in the system. Vortex flow-meters, which are attached in series with the GLHE and the PHE, can measure 0 to 15 GPM of flow with an accuracy of ±1% full-scale range. The flow-meters offer stable operation and accurate readings when flow is completely developed thus, some straight pipe length is required before and after the flow-meter. A straight length of 20 pipe diameters upstream and 7 pipe diameters downstream is provided. A watt transducer is attached before the VFD to measure input pumping power. This Ohio Semitronics GW5 power transducer provides accuracy of ±0.04% the full-scale.

5.3.2 Installation of Pressure Transducer

For pressure measurement, a pressure transducer from Setra as shown in Figure 5-5 was selected. Setra Model 230 is a high output, low differential pressure transducer series for wet to wet differential pressure measurements of liquids. This series has fast response and high accuracy. Analog voltage output of the transducer is linearly proportional to the differential pressure applied across it. The series has transducers with a pressure range up to 250 psig. Bell & Gossett Series 80 1-1/2 X 1-1/2 X 7B pump with 6.5" impeller diameter can provide maximum of 19 feet of water head i.e. ≈ 8.2 psi. Thus the pressure range of 0-10psi is selected from the Setra 230 series.

Figure 5-2 Pump and Pressure Transducer

To avoid sudden pressure shocks, shutoff valves and shunt valve were installed to isolate the pressure transducer as shown Figure 5-3 and Figure 5-4.Valves A and B are shutoff valves which should be closed during start up and should be opened only if the differential pressure is within the specified range of the transducer. The shunt valve C should be partially open at first and should be closed slowly while checking the output reading of the transducer. If the output voltage is above the limit then the differential pressure is higher than pressure range of the transducer. Once the shunt valve is completely closed then the transducer will provide the correct reading.

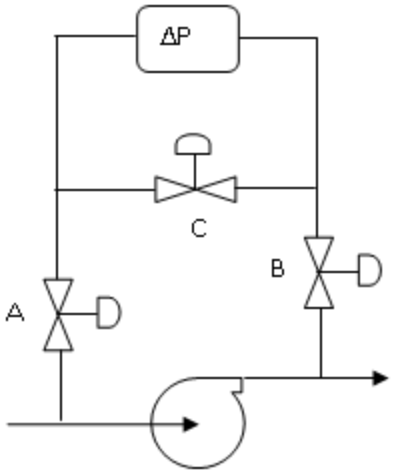

Figure 5-3 Pressure Transducer Installation Schematic

Figure 5-4 Shutoff Valves A and B at Inlet and Exit of Pump

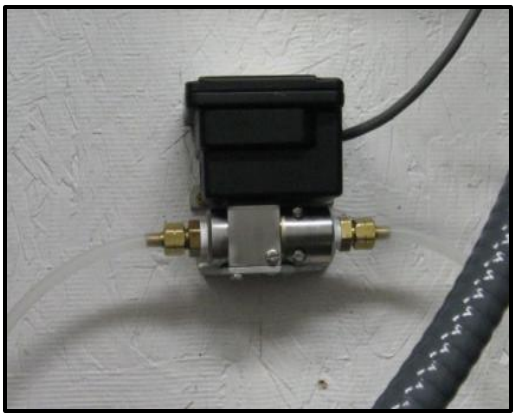

Figure 5-5 Setra Model 230 Pressure Transducer

5.3.3 Measurement of Rotational Speed

To measure rotational speed of the electric motor a digital contact tachometer was used. A slot which can be accessed by removing the safety cover from the pump is provided in electric motor shaft to measure RPM. A Cen-Tech 66400 digital contact tachometer, which can measure rotational speed from 2.5 to 19999 RPM, was used.

5.3.4 Data Acquisition Unit

Flow-meters, power transducer and pressure transducer were connected to a Fluke 2640 NetDAQ data acquisition unit to collect voltage data. NetDAQ Logger software was installed on the host computer and the data logger was connected to it. The software shows the dc voltage reading in graphical format and these readings can be exported to a .csv file.

5.4 Instrument Calibration and Uncertainty Analysis

5.4.1 Calibration

5.4.1.1 Vortex Flow-meter

The flow meters are calibrated using a purge cart, stopwatch, bucket and precision scale. The schematic for flow-meter calibration is shown in Figure 5-6. The bypass valve D, the tank and the pump in the schematic are part of one single component i.e. the purge cart. Valve E, the flow-

meter, the load (GLHE or PHE) and valve F are part of source side. Valves E and F are provided in the system for the purging operation of the piping network and the associated heat exchangers. When the valve before the heat pump and the valve after the circulation pump are closed, the environmental heat exchangers are disconnected from the network and can be operated externally by opening valves E and F. At the end of valve F, a flexible pipe is attached which can be moved from the purge tank to the bucket for flow meter calibration.

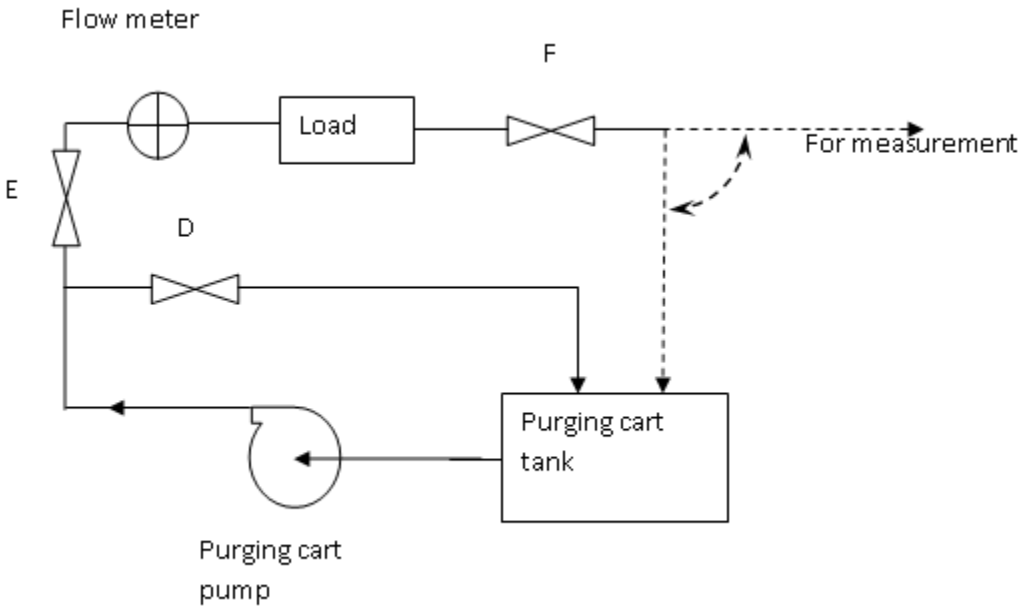

Figure 5-6 Schematic for Flow-meter Calibration

The purge cart pump is a constant speed pump. To take flow-meter readings for different values of mass flow rate, bypass valve D is used. When valve D is completely open, minimum flow rate passes through the flow-meter. As the valve is closed, the flow through the flow-meter increases. This provides a wide range of readings for calibration. Before taking the flow calibration readings, the piping network was purged of air using the purge cart at the maximum flow rate.

The data obtained from the flow meter calibration tests are shown in Table 5-1 and plotted in Figure 5-7.

Table 5-1 Calibration Data for Flow-meter

Reading	Time (sec)	kg	kg/s	GPM	VDC
1	11.7	14.88	1.267	20.09	11.08
2	12.0	15.56	1.300	20.61	11.09
3	15.0	17	1.131	17.93	10.21
4	15.4	17.42	1.129	17.90	10.06
5	20.4	17.7	0.868	13.77	8.19
6	26.2	17.77	0.679	10.76	6.86
7	39.3	17.42	0.443	7.03	5.27
8	41.7	18.7	0.449	7.11	5.25
9	59.5	11.87	0.199	3.16	3.48
10	72.1	16.45	0.228	3.62	3.69
11	97.0	11.92	0.123	1.95	2.93
12	159.5	4.33	0.027	0.43	1.99

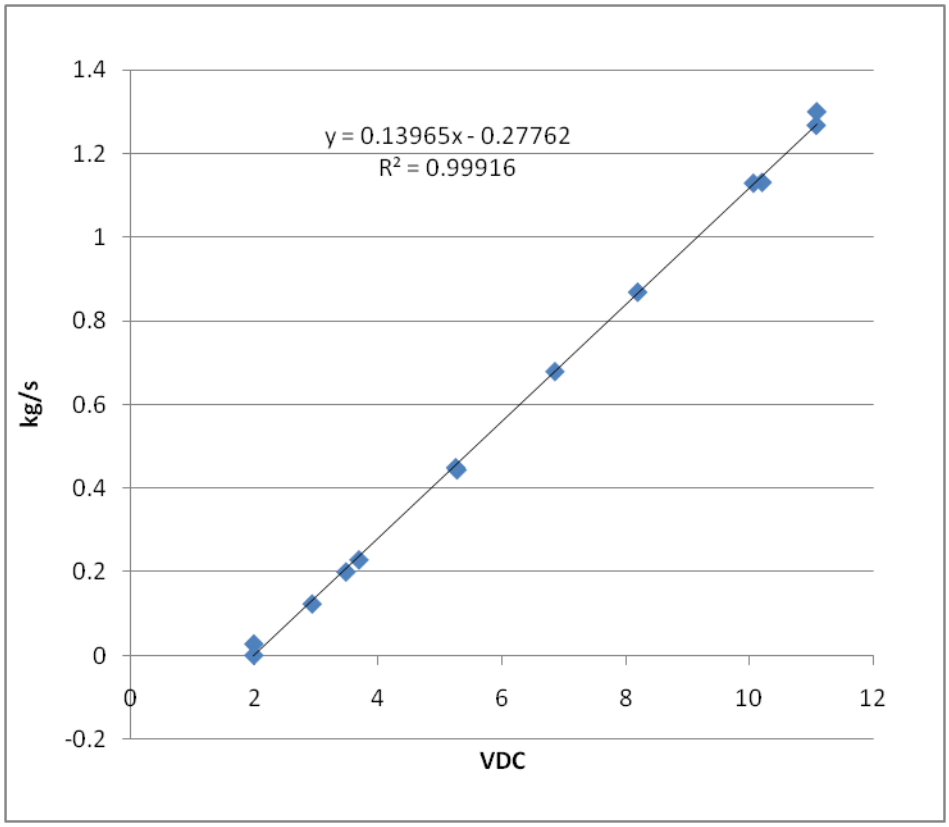

Figure 5-7 Calibration of Flow-meter

A linear correlation between mass flow rate and dc voltage is found as:

$$y = 0.14\,x - 0.277$$

Similarly, a correlation for the flow-meter, connected to PHE is found[16] as:

$$y = 0.11\,x - 0.22$$

5.4.1.2 Pressure Transducer

The Setra pressure transducer was factory calibrated. The data included with the calibration certificate was plotted and the following linear correlation between dc voltage and differential pressure was found:

$$y = 6900.5\,x - 361.9$$

5.4.1.3 Power Transducer

The Ohio Semitronics GW5 power transducer provides an output of 0-10V dc at output. According to the datasheet, the output voltage is proportional to full scale watt range i.e. 0-2000W of the transducer. This gives linear scale of,

$$y = 200\,x$$

5.4.2 Measurement of Accuracy and Uncertainty

The uncertainty analysis for all instruments except the tachometer and the differential pressure transducer was done while designing the facility. Detailed calculations for uncertainty measurement of the power transducer and the vortex flow meter are provided by Hern (2002).

According to Hern (2002), the uncertainty of the installed vortex flow-meter is given by:

$$e_V = 0.00191\,(V^2) - 0.00008\,(V) + 0.00044$$

where V is the flow rate in GPM. Since the maximum flow through the flow-meter is 10 GPM, the maximum uncertainty in flow-rate is calculated as $e_V = 0.192$ GPM.

[16] These coefficients match with those found by (Hern, 2002) when converted to find GPM values.

The total uncertainty calculated for the watt transducer is $e_W = \pm 1.807\ W$

The uncertainty of Fluke/NetDAQ logger is,

$$e_{Vfluke} = \pm\ 0.042\ \% + 0.0039\ V$$

This uncertainty of the voltage signal can be converted to an uncertainty for the pressure transducer as follows:

$$e_{Fluke} = \frac{(0.00042\ \times V_{Fluke}\ +\ 0.0039)\ \times\ \Delta Range}{\Delta V}$$

$$e_{Fluke} = \frac{(0.00042\ \times 10\ +\ 0.0039)\ \times\ 10}{10} = 0.0081\ psi$$

The transducer has an accuracy of $\pm\ 0.25\ \%\ FS$.

$$e_{PTrans} = \frac{0.25 \times 10}{100} = 0.025\ psi$$

Thus total uncertainty for the pressure measurement is,

$$e_P = \sqrt{e_{Fluke}^2 + e_{PTrans}^2} = \sqrt{0.0081^2 + 0.025^2} = 0.026\ psi$$

The tachometer is not connected to the data logger; RPM readings are directly taken from the digital display. The uncertainty for the tachometer provided by the manufacturer is:

$$e_{RPM} = 0.05\ \%\ N + 1\ RPM$$

Maximum rotational speed measured in the experiment is 1200 RPM. Thus maximum uncertainty for the rotational speed measurement is:

$$e_{RPM} = 0.0005\ \times 1200 + 1 = 1.6\ RPM$$

5.5 Experimental Procedure

Before starting the experiment appropriate valves in the piping network are opened (or closed) to obtain the required flow network. The pressure transducer shutoff valves are closed, and the shunt valve is opened. The safety cover of the pump electric motor is opened to allow to measurement of the rotational speed. The VFD is set on Manual mode and the data logger is turned on to scan the channels.

The VFD is set at a particular frequency. Rotational speed of the motor corresponding to the frequency is measured using the tachometer. Flow-meter outputs for both (PHE and GLHE) branches are checked, if they are not within the acceptable range then the valve of the corresponding branch is slightly closed to limit the flow. When all flow control valves are in an acceptable range, the pressure transducer shutoff valves are opened. Slowly the shunt valve is closed while observing the pressure transducer reading. If the data logger shows too high a pressure rise across pump then the VFD output frequency is reduced and the same operation is repeated until the output dc voltage from pressure transducer is less than 10V. When the pressure rise across the pump and the flow through the network are within the operational range of the pressure transducer and flow-meter and the network has reached steady state as determined by stable transducer readings, the data for the test is logged.

VFD output frequency was measured between 40 Hz (corresponding to rotational speed of 1150 RPM) and 10 Hz (283 RPM). 1150 RPM is the tachometer limit. Readings were taken at 1150, 1050, 901, 747, 597, 524, 453, 410, 383, 350, 319 and, 283 rpm.

Although the VFD can operate as low as 10 RPM, at such low rotational speeds, no flow is detected by the flow. Large variations in pressure readings were observed for low flow rates below 375 RPM.

Mass flow rate, pressure rise and input power were logged by the data acquisition system. The

mass flow rate and pressure rise were non-dimensionalized to get non-dimensional pump curves.

The product of the pressure rise (in Pa) and the volumetric flow rate (in m^3/s) is the power transferred to the water (i.e. output power). Using the calculated output power and the input power measure by the power transducer, the overall efficiency of the pumping system is calculated.

5.6 Results

5.6.1 Experimental Results

In centrifugal pumps an increase in mass flow rate corresponds to a decrease in the pressure rise across the pump. But, from the data collected it was observed that pressure across the pump was almost constant for all flow rates. This is because the pump was oversized and the mass flow rate through the pump was not close to the design flow rate for any rpm the pump was ran at. Thus all data, as shown in Figure 5-8 was taken in the flat part of the pump curve. To visualize the data better, the y-axis was plotted for a narrow range of rotational speed.

The non-dimensional model will be validated if the non-dimensional curves calculated from the output data for all the rotational speeds are matched.

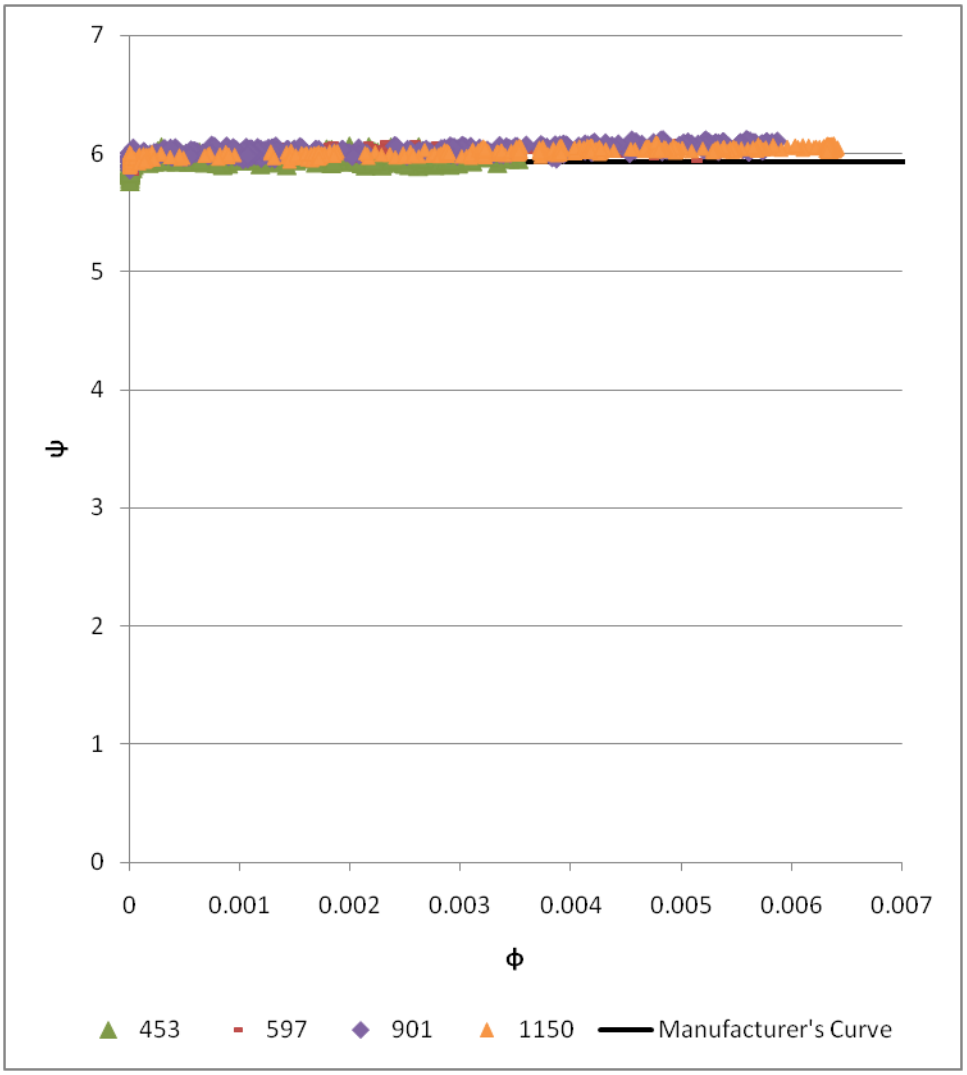

Figure 5-8 Non-dimensional curves calculated from experimental data for different rotational speeds

From Figure 5-8 it can be observed that the experimental data validates the non-dimensional model for variation in rotational speed. The experimental data also validates the manufacturers' data. Thus, Figure 5-8 shows that even at much lower rotational speeds the non-dimensional model holds well. Since the pump is not operated over complete flow rate range, for validation of non-dimensional model variation in each parameter should be considered separately with respect to change in speed.

To validate the affinity laws and the individual model parameters, variation in mass flow rate,

pressure rise, and power need to be checked with respect to changes in rotational speed. In this validation, estimated values are calculated from reading corresponding to 1150 rpm because, readings at this rotational speed can be verified using the manufacturer's data. To get the readings for this Figure 5-9, the valves are kept open (i.e. system curve is kept constant) and the rotational speed of the pump is varied.

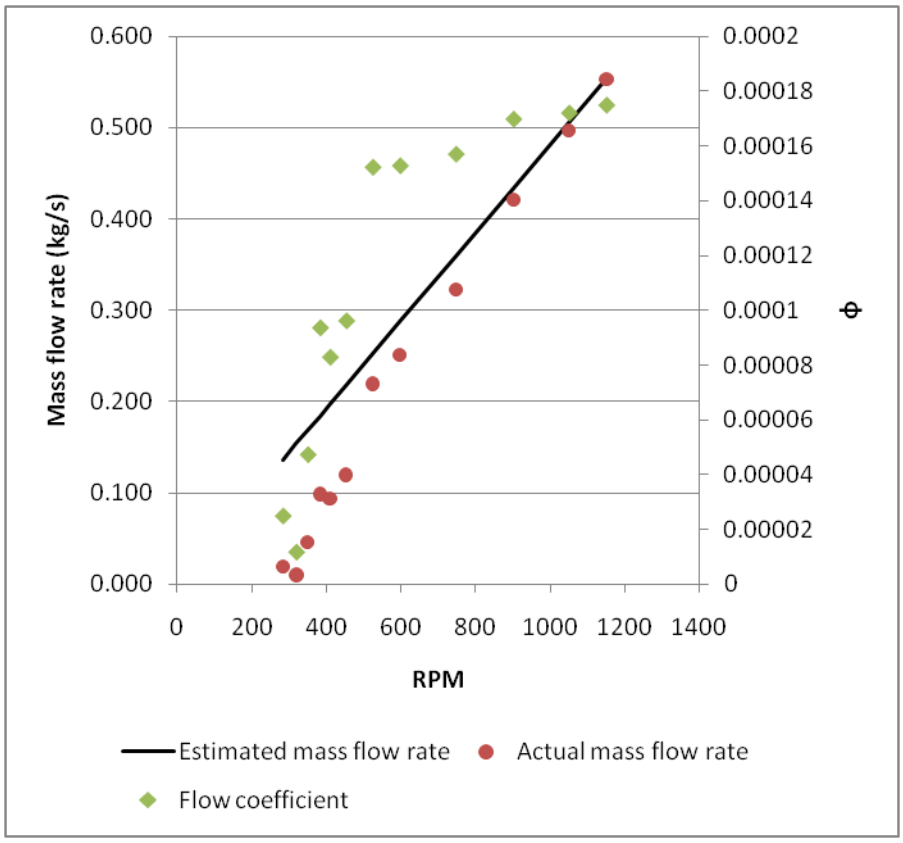

Figure 5-9 Mass flow rate vs. rotational speed

Figure 5-9 shows that mass flow rate provided by the pump is directly proportional to rotational speed up to 550 rpm. Below this rotational speed the flow rate through the system decrease drastically. This drop in the flow rate may be due to recirculation. The uncertainty of the flow meters is 0.013 kg/s (0.2 gpm) which is higher than 5% below 400 rpm.

It is expected that flow coefficient should remain constant with change in rotational speed. It can be observed that flow coefficient remains fairly constant above 550 rpm and below that value its

value drops down considerably. Thus, flow coefficient of non-dimensional model does not work effectively at low rotational speeds.

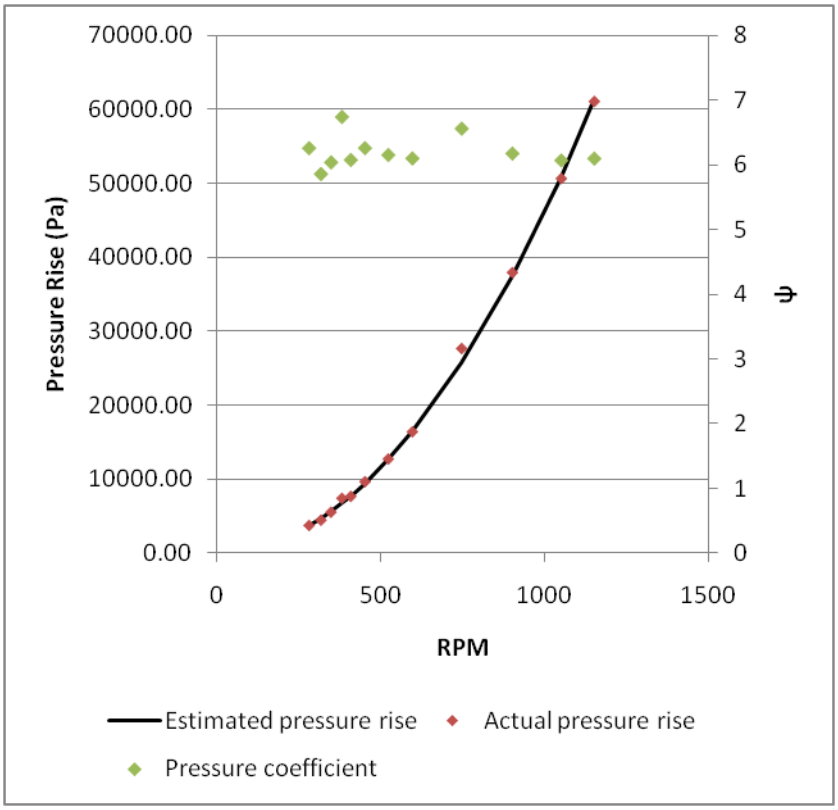

Figure 5-10 Pressure rise vs. rotational speed

From Figure 5-10 it can be observed that experimental data points match with theoretically predicted values. The pressure coefficient also remains constant over the rpm range. Thus, we can infer that the experimental results comply with the affinity law and the non-dimensional model for pressure rise across the pump. The law is perfectly obeyed even at low rotational speeds.

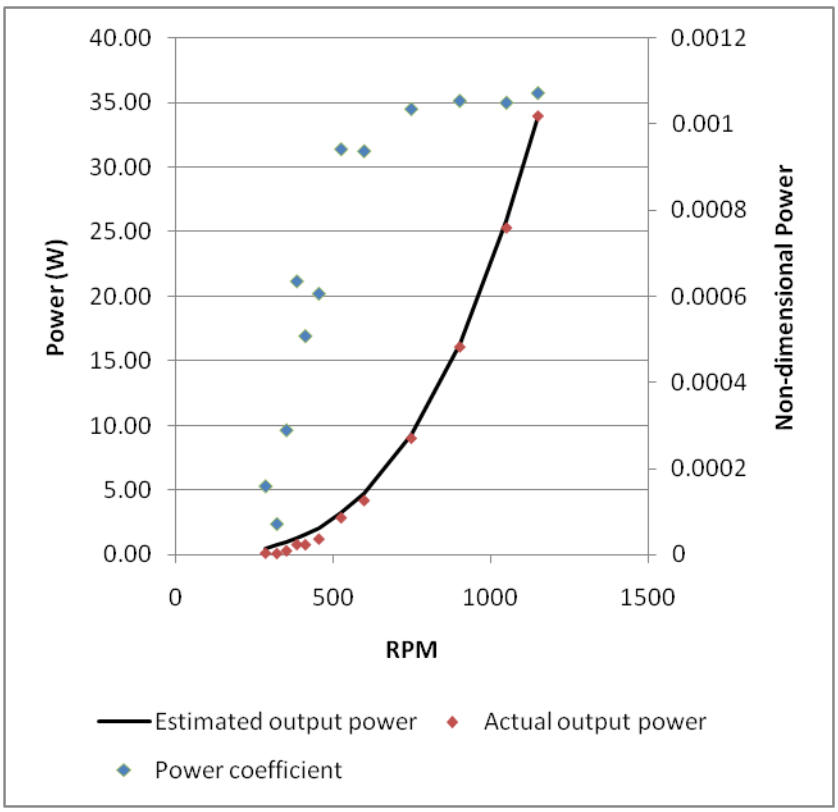

Figure 5-11 Output pump power vs. rotational speed

The pump output power is calculated from the product of the volumetric flow rate and the pressure rise. Thus, the deviation in either of these parameters will affect the value of the pump output power.

Here the deviation of experimental data points from theoretical curve is due to the mass flow rate deviation observed in Figure 5-9. This deviation can be noticed in Figure 5-11 at low rotational speeds. Percentage wise the deviation in estimated value and experimental value is high but the quantitative value of the error is negligible when compared with power consumption in regular HVAC systems. Comparing the estimated and experimental values we can conclude that the cubic relation between output power and rotational speed holds good for practical purposes.

Similar to non-dimensional flow coefficient the non-dimensional power remains constant up to 550 rpm but drops down below it. Thus, the non-dimensional model for power does not work

effectively at low rotational speeds.

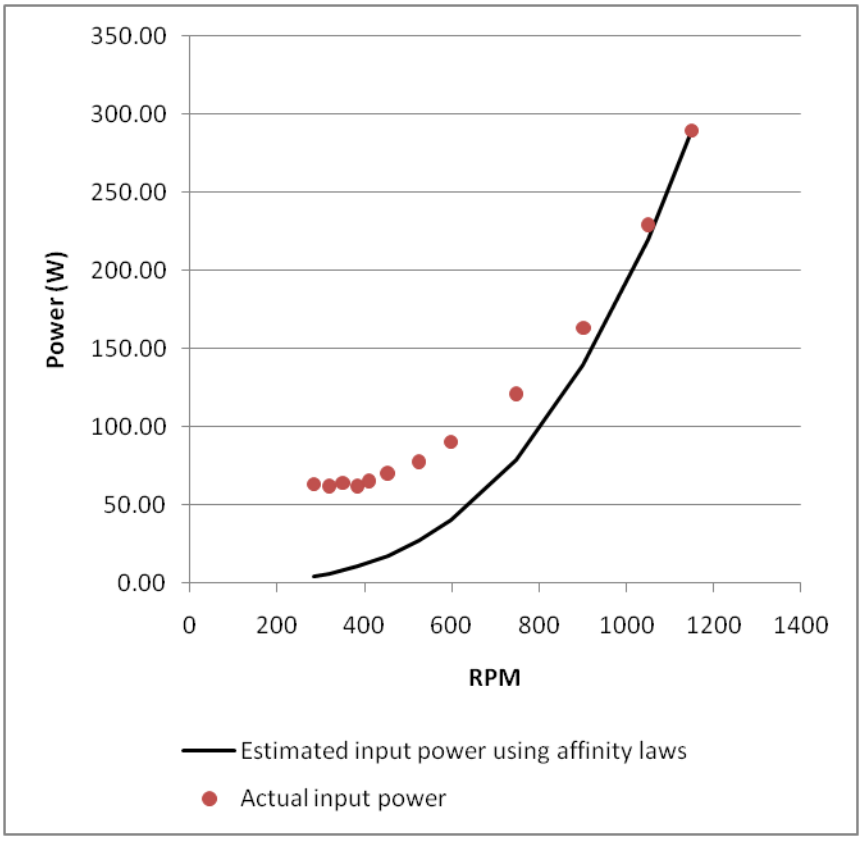

Figure 5-12 Pump input power vs. rotational speed

Pump power savings are dependent on pump input power. Figure 5-12 shows a large deviation in pump input power when input power at low rotational speeds is estimated using affinity laws. This deviation is high percentage wise and quantitatively. Thus, applying affinity laws to predict pump input power to calculate pump power savings at low rotational speeds will lead to over estimation of pump power savings.

5.6.2 Discussion

The power savings suggested by the non-dimensional model and the affinity laws were found overly optimistic. The estimated power savings in Section 5.1 were not supported by the experimental results. These findings can be explained as follows:

5.6.2.1 Application of Affinity Laws

Both the non-dimensional model and the affinity laws are intended to be used to calculate the output of the pumping system [i.e. the effects of a change in rotational speed (or diameter) as observed in the fluid flow or fluid head]. Similarly the change in power is calculated as a change in power to the fluid.

Actual power savings, however, are related to input power. 'Power to fluid' and 'input power to the pumping system' do not necessarily exhibit a linear relation thus, extending the results of the non-dimensional model and the affinity laws to power savings is not necessarily correct. Ranges for applicability of affinity laws to power savings are discussed in Section 5.6.2.2.

5.6.2.2 Component Efficiencies

In correlating input and output power individual component efficiencies play an important role. These efficiencies must be accounted to determine applicability of the non-dimensional model and the affinity laws to power savings for approximate calculations.

$$P_{VFD} = \frac{P_{in}}{\eta_{VFD}}$$

$$P_{E.\ Motor} = \frac{P_{VFD}}{\eta_{E.\ Motor}}$$

$$P_{out} = P_{Pump} = \frac{P_{E.\ Motor}}{\eta_{Pump}}$$

Between the electric motor and the pump, transmission (mechanical) losses occur. The transmission efficiency is around 98% (European Association of Pump Manufacturers, 1999) and can be assumed constant.

The output power can be calculated as,

$$P_{out} = \frac{P_{in}}{\eta_{VFD} \times \eta_{E.\ Motor} \times \eta_{Pump}} = \frac{P_{in}}{\eta_{wire\ to\ water}}$$

Behavior of these efficiency curves with respect to rotational speed (or load) will significantly affect the correlation between output and input power.

Although most VFD manufacturers provide single full load efficiency value for their drives, Bourret & Bernier (1999) show that VFD efficiency is not constant. They provide a curve for VFD efficiency vs. % speed of electrical motor compared with nominal motor speed. This curve is recommended for high efficiency VFDs. From the curve provided in Bourret & Bernier (1999), it can be observed that VFD frequency remains in the range of 87 – 96 % for 50% to 100% of nominal speed value of the motor. In experiment performed by Gao, Mclnerny, & Kavanaugh (2008) component efficiency at each stage of variable speed pumping system is measured and it was found that when motor control frequency is reduced from 60 Hz to 24 Hz, VFD efficiency was reduced from 95% to 87.1%.

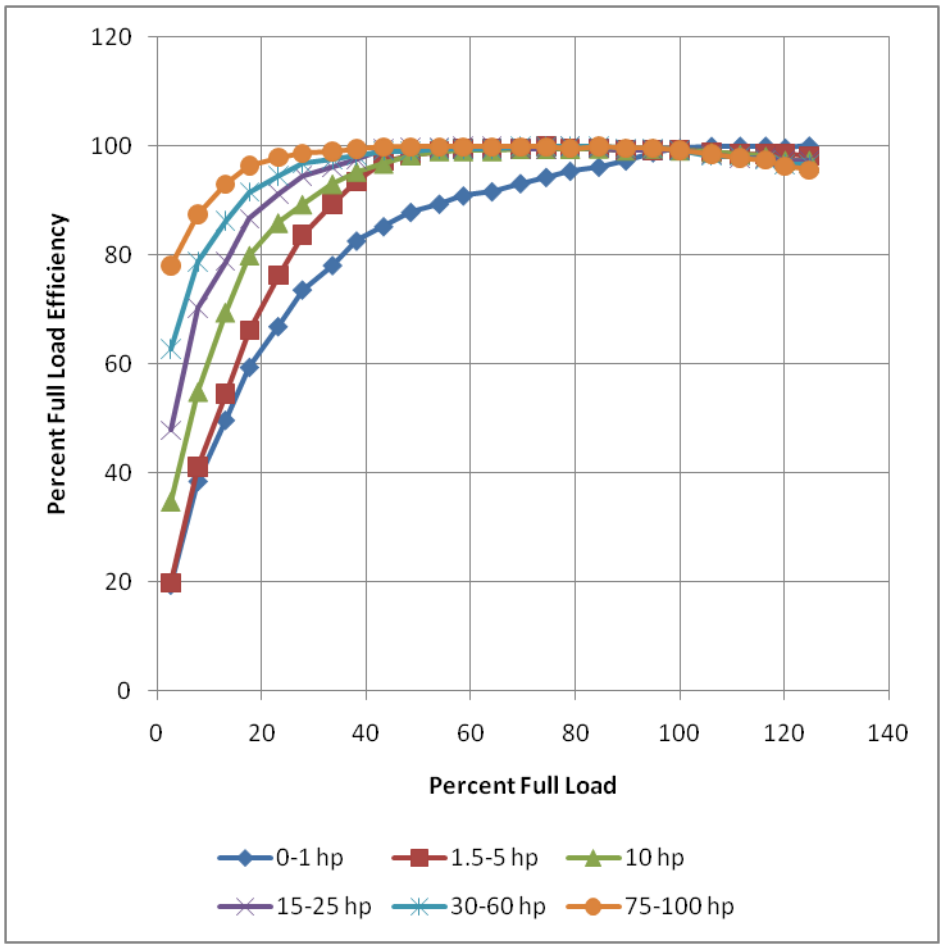

Figure 5-13 Motor part load efficiency as a function of % full load

Following McCoy, Litman, & Douglass (1993)

An efficiency curve for high efficiency motors has been provided by ASHRAE (ASHRAE Handbook, 1996). A detailed set of curves for different power rating range has been provided in McCoy, Litman, & Douglass(1993). Electric motors with high power rating have a stable efficiency curve over a wide range of part load conditions. From Figure 5-13 we can suggest a threshold load fraction below which efficiency drops drastically. Above the threshold load fraction, we can assume efficiency remains almost constant.

Pump efficiency varies with flow rate but this variation generally is not as significant as

the drop in efficiency seen in electric motors below the threshold load fraction. Thus for low load conditions we can conclude that $\eta_{\text{wire to water}}$ is a strong function of $\eta_{\text{E. Motor}}$.

As discussed in Section 5.1, a 50% reduction in pump speed will result in an 88% reduction in pump output power. Assuming a 10% reduction in pump efficiency, the electric motor load will be reduced by 80%. According to Figure 5-13, this reduction in load will result in the motor running at a very low efficiency. The non-dimensional model and the affinity laws are not applicable in the range where the electric motor efficiency varies drastically with load.

In the region where $\eta_{\text{wire\_to\_water}}$ is relatively constant, the power to fluid (i.e. output power) and the input power to pumping system will exhibit linear relationship. The region where $\eta_{\text{E. Motor}}$ remains fairly stable can be found using the Figure 5-13.

The reduction in rotational speed of motor corresponding to the reduction in load from the full load condition to the threshold load value can be found by calculating the allowable reduction in speed as follows:

$$\%\ Allowable\ Reduction\ in\ Speed = \left[1 - (\%\ threshold\ load)^{1/3}\right] \times 100 \quad (5\text{-}1)$$

Since this reduction in speed corresponds to the region where the non-dimensional model and the affinity laws are reasonably accurate the result of the calculation is referred to as allowable reduction in speed. Using Figure 5-13 and Equation 5-1, Table 5-2 can be formed which will provide values for allowable reduction in speed.

Table 5-2 Allowable Reduction in Speed

hp Motor	η Threshold	% Allowable speed reduction
0-1	65	13.4
1.5-5	45	23.4
5.5-15	30	33.1
15-25	25	37.0
30-60	18	43.5
75-100	10	53.6

Table 5-2 provides percent allowable speed reduction for various power rating zones of electric motors where affinity laws can estimate power savings with fair accuracy.

5.7 Conclusion

From the experimental results we can conclude that affinity laws work well for reasonable rotational speed range for mass flow rate and output power when rotational speed is varied. And, work perfectly for pressure rise even at low rotational speeds.

Individual component efficiency characteristics are required for exact power saving calculations. Affinity laws cannot be applied directly to input power thus, they are inadequate to predict power consumption. Power savings predicted by affinity laws are often optimistic.

Chapter 6. Implementation of Pump Model in EnergyPlus

Pumps in EnergyPlus are discussed in section 2.4.2. These pump models focus on providing the required flow with selected pump operation (continuous and intermittent), neglecting pressure-flow characteristics and eventually power consumption by the pump. It is assumed that pumps in EnergyPlus (before version 5.0) will always be able to meet the operating point.

6.1 Earlier Pump Models in EnergyPlus

Previous EnergyPlus pump models assumed that constant speed pumps provide a nominal flow rate to all the systems irrespective of pumping load on the loop. This simplified model neglected the fact that a system has its own pressure drop characteristic curve based on system components. Similarly it was assumed that the variable speed pump provides the required flow between the min-max flow range entered by the user, again, irrespective of pumping load. In actual practice the flow rate provided by the pump is dependent on both the pump head-flow characteristics and the system pressure drop characteristic curve.

Pump power consumption was calculated assuming that the pump is running at the nominal flow rate, which is not the case for all simulation conditions. Pump heat addition to the fluid was also based on the nominal power consumption by the pump. Power consumption by the pump and heat addition to the fluid varies according to the flow rate and pressure components in the loop. There is a provision in EnergyPlus for variable speed pumps, to calculate power consumption based on the part load ratio (PLR), which is defined as:

$$PLR = {}^{Q}/_{Q_{nom}}$$

Where Q_{nom} is the nominal flow rate at BEP.

Pump input data includes coefficients of a polynomial curve based on PLR, called the part load curve, which are used to calculate the power fraction. Multiplication of the power fraction and the nominal power gives the actual power consumption by the pump. The main problem with this type of model is that manufacturers generally don't provide part load data.

6.2 Plant Pressure System

In anticipation of the new pump model, a system curve was previously implemented in EnergyPlus. Pressure drop was calculated by specifying pressure drop information[17] for the piping system components such as heat exchangers and pipe segments. The pressure drop for the system is calculated using:

$$\Delta p = \frac{\rho V^2}{2g}\left[\left(f\frac{L}{D}\right) + K\right]$$

Where K is the summation of the system component pressure

Friction factor is calculated from roughness using Haaland friction factor equation (Olson, 1998), which is an approximation of the Moody chart. The user can also input a fixed friction factor.

Pressure drop in each branch is summed to obtain the loop pressure drop. If there are parallel branches in the loop, ideal control valves are assumed on each branch. These virtual control valves adjust to achieve the desired flow rate and equal pressure drop across all braches. Pump power is calculated from the product of the loop pressure drop and flow rate.

6.3 Flow Resolution Using Pump Curve

From the discussion in section 2.1.3 it is clear that the pump head-flow characteristic curve and the system curve decide the actual operating point and mass flow rate of the system.

[17] Apart from pressure drop information a generic curve can be added in which pressure drop is dependent on a single variable i.e. mass flow rate (kg/s).

The feature of calculating pressure drop in the loop, added as part of EnergyPlus version 4.0, was enhanced by the addition of the non-dimensional pump model described in Chapter 4. The model was approximated in EnergyPlus in terms of a forth order polynomial:

$$\psi = C_4\phi^4 + C_3\phi^3 + C_2\phi^2 + C_1\phi + C_0 \qquad (6\text{-}1)$$

Where ψ and φ represent non-dimensional pressure and flow respectively, $C_{1\text{-}4}$ are curve coefficients from manufacturers' data and C_0 is a non-zero constant the representing shutoff pressure head.

The non-dimensional pump curve will support implementation of VFD inputs which will permit the pump to operate at variable rotational speed in the later versions of EnergyPlus[18].

The system curve is approximated in the form of:

$$\Delta p = K\dot{m}^2 \qquad (6\text{-}2)$$

To find the system pressure constant K, initially the loop is simulated by the rated pump mass flow rate. The pressure constant K_{branch} for each branch with pressure information is calculated using:

$$K_{Branch} = \frac{\Delta P_{Branch}}{\dot{m}^2}$$

If there are parallel branches in the loop an equivalent pressure constant can be calculated by enforcing continuity and equal pressure drop across each branch. The equivalent pressure constant is then defined as:

$$\frac{1}{\sqrt{K_{ParallelEquivalent}}} = \sum \frac{1}{\sqrt{K_{Branch}}}$$

Pressure constants for all branches are added to find the loop pressure constant K. By solving

[18] Flow resolution was added in EnergyPlus version 5.0 for constant speed pump simulation.

Equation 6-1 and Equation 6-2, the operating point is calculated. The abscissa (x-co-ordinate) and ordinate (y-co-ordinate) of the operating point represent the system mass flow rate and loop pressure drop respectively.

Equation 6-1 and Equation 6-2 can be solved numerically by a Newton-Raphson or a successive substitution method. Both methods were investigated in order to select a fast and numerically stable method for this simulation.

To implement a Newton-Raphson method, initially non-dimensional form of ystem curve is calculated as:

$$\psi = K'\phi^2 \qquad (6\text{-}3)$$

Where K' is equivalent pressure constant for non-dimensional equation and can be calculated as:

$$K' = \rho K$$

Equation 6-3 is then substituted in Equation 6-1:

$$\Rightarrow g(\phi) = C_4\phi^4 + C_3\phi^3 + (C_2 - K')\phi^2 + C_1\phi + C_0 = 0$$

An iterative solution to the above equation is given by:

$$\phi_{n+1} = \phi_n - \frac{g(\phi_n)}{g'(\phi_n)}$$

Where $g'(\phi)$ is first derivative function of $g(\phi)$.

This method was verified in a VBA program and it was observed that for most of the cases this method works well. But, the presence of maxima or minima in the operating range of the equation leads to divergence. Since the entered pump curve is a 4th order approximation of the pump flow characteristics, there is a strong possibility of maxima and minima in the equation. These divergent cases can be avoided, but this makes the program lengthy and slow. Thus, this method

is discarded for flow resolution.

6.3.1 Successive Substitution

For successive substitution method, the simulation starts with the rated mass flow rate. Using this initial guess, the pressure-drop in the system is calculated. Using this pressure drop the pressure constant of the loop is calculated which will remain constant till the flow is resolved. The initial guess (or the value from the previous iteration) of the mass flow rate is used to calculate the pump pressure rise. Now, this pressure rise is equated with the system pressure drop. From the new pressure drop value and the previous pressure system constant, a new mass flow rate is calculated which is again equated to the pump mass flow rate. This process is continued until a solution within the desired accuracy is attained. The successive substitution procedure is described diagrammatically in Figure 6-1. The algorithm using dimensional flow and pressure variables is shown in Figure 6-2 using a flow chart.

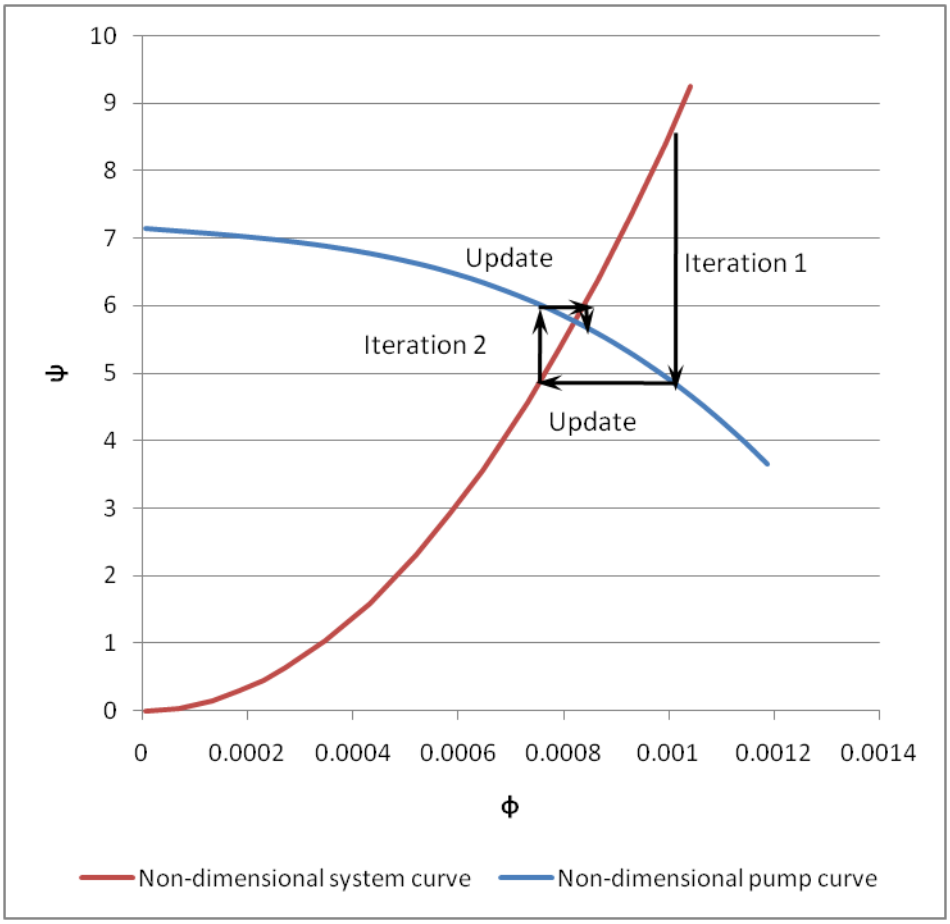

Figure 6-1 Successive substitution

In Figure 6-2 the subscripts 'sys' and 'pump' are used to describe system and pump variables, ε is the pipe roughness value, β is damping factor and D is the pipe diameter.

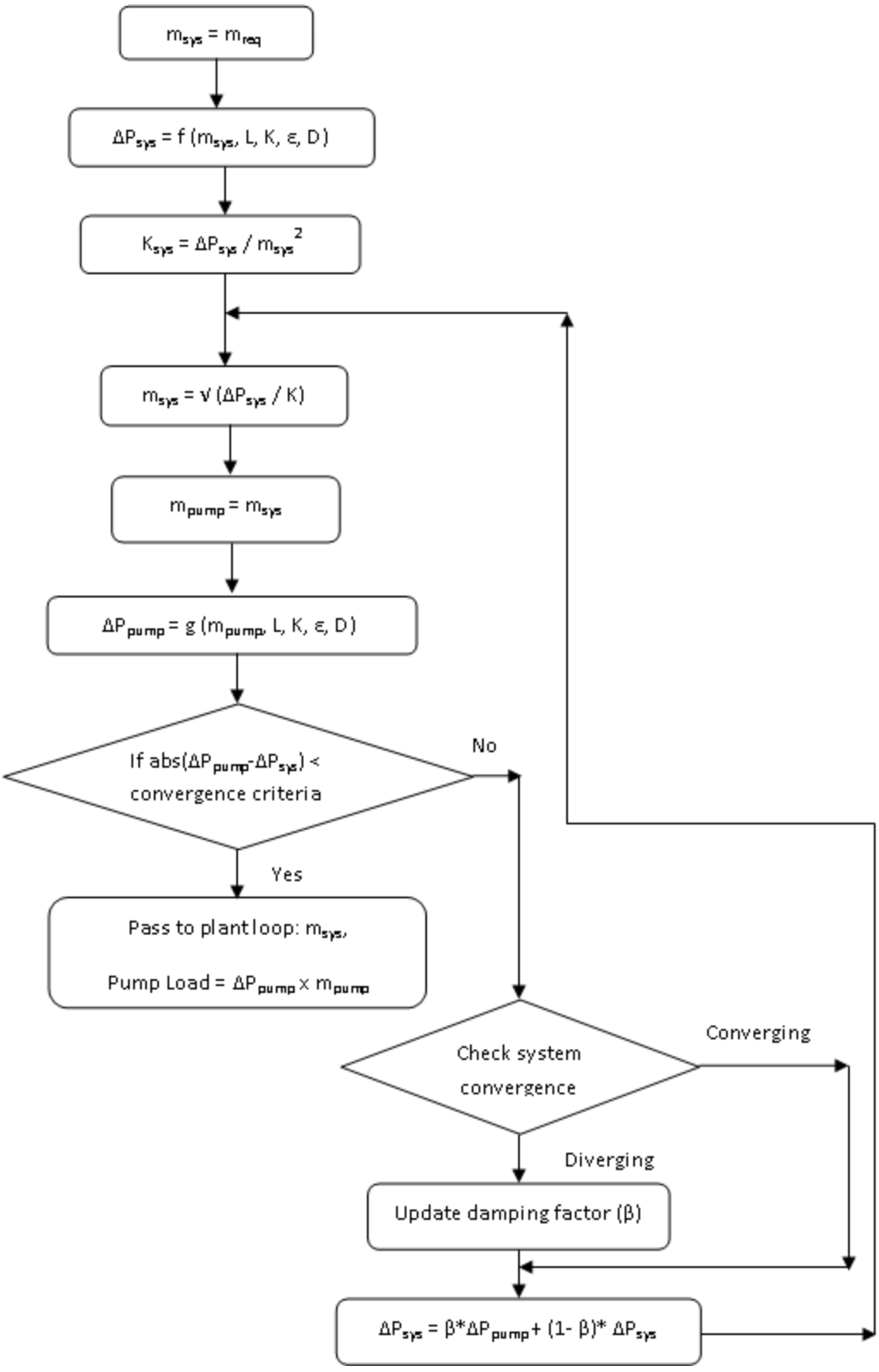

Figure 6-2 Flow chart for modified successive substitution

In successive substitution, calculating sequence and the information flow decides whether the simulation will converge or diverge. By assuming constant mass flow rate for each iteration and updating pressure for the next iteration as shown in Fig. 6.2, the iterative procedure is forced to move in the clockwise direction. When the slope of the system curve is greater than the absolute value of the slope of the pump curve, moving in the clockwise direction will always converge. However, if the slope of the system curve is less than the absolute value of the slope of the pump curve, moving in the counterclockwise direction will always converge. To solve this problem, a modified successive substitution method is proposed.

6.3.2 Modified Successive Substitution

In successive substitution, the problem of divergence is solved by partial substitution (Stoecker, 1971). In this method, the simulation always moves in the clockwise direction and a damping factor or partial substitution factor (β) is used to provide stability for unstable cases and to speed up the simulation for stable cases. The updating variable (here pressure rise) in the simulation is revised by:

$$\Delta p_{i+1} = \beta \Delta p_{i+1} * + (1 - \beta) \Delta p_i \qquad (6\text{-}4)$$

Where, subscript 'i' indicates a value from previous iteration; (i + 1)* indicates pressure rise calculated from the pump curve equation and (i + 1) indicates the revised value of the pressure rise which will be passed on to next iteration to substitute as pressure drop.

The value of the partial substitution factor varies from 0 to 1 excluding 0 (i.e. $0 < \beta \leq 1$). Substitution of $\beta = 1$ will lead to an unaltered successive substitution method and, $\beta = 0$ will put the successive substitution in an infinite non-converging loop. Inclusion of β, solves the problem of divergence even if the information flow in the simulation is reversed. And, for the converging simulation the number of iterations is reduced, speeding up the convergence.

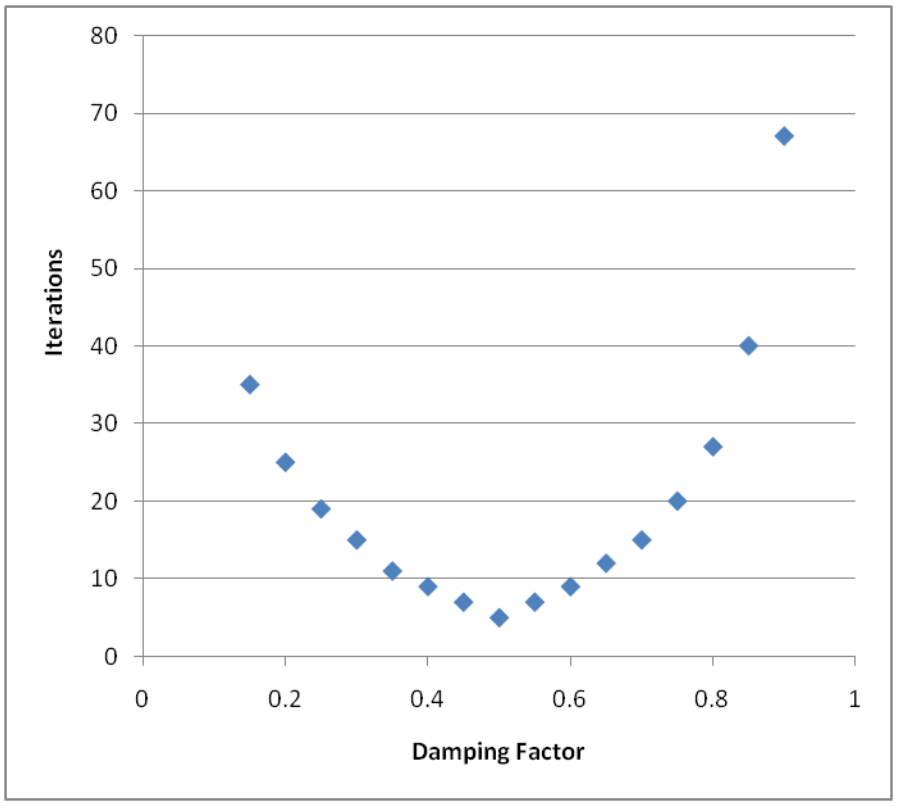

Figure 6-3 Effect of damping factor on diverging system of curves

Figure 6-3 shows that even if the system of curves are diverging for normal successive substitution (i.e. for $\beta = 1.0$) the simulation starts converging for $\beta < 1.0$.

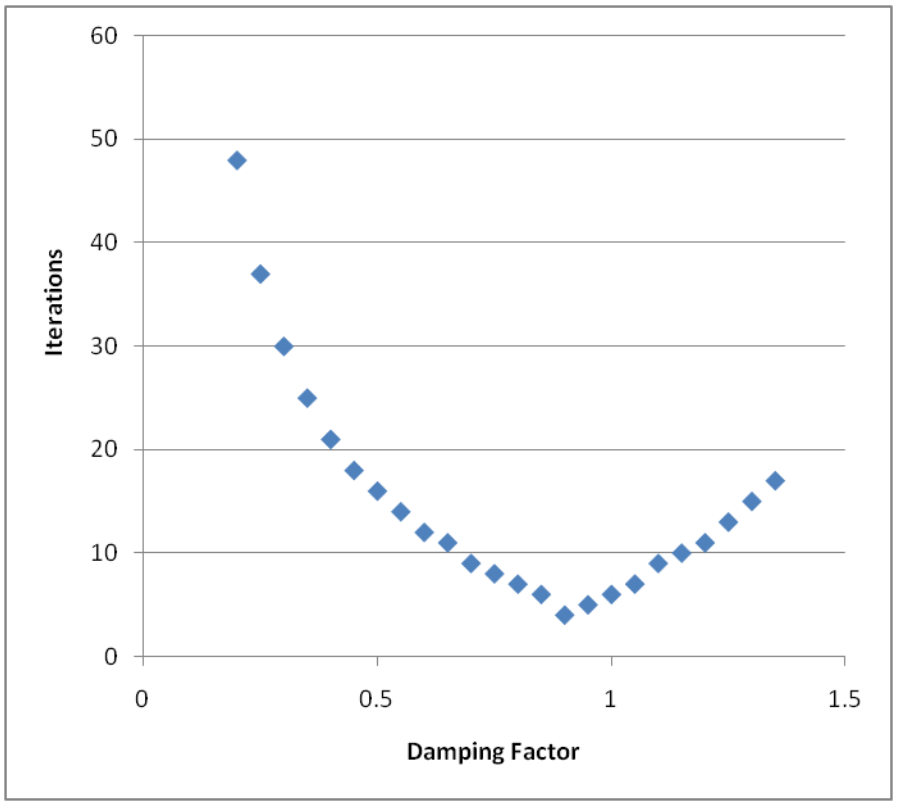

Figure 6-4 Effect of damping factor on converging system of curves

From Figure 6-4 it can be observed that for converging system of curves the convergence is achieved in fewer iterations for $\beta < 1.0$.

In the EnergyPlus subroutine a default damping factor of 0.9 is used which works for most of the pump and system curves. For other cases a variable damping factor is used as described in the following section.

6.3.3 Variable damping factor

It was observed that for most of the system and pump curves $\beta = 0.9$ works well. In rare cases where pump curve is substantially steeper than the system curve (i.e. absolute value of slope of pump curve is greater than slope of system curve at the point of intersection) the solver can diverge even for $\beta = 0.9$. In such cases, the value of the damping factor need to be reduced to ensure convergence.

To identify divergence, mass flow rates from last two iterations are stored in an array and the difference between them is checked. If 'm' is the array with three elements which stores mass low rates from the current iteration (m_3) and last two iterations (m_2 and m_1) and,

$$\Delta m_{latest} = abs(m_3 - m_2)$$

$$\Delta m_{previous} = abs(m_2 - m_1)$$

in case of divergence:

$$\Delta m_{previous} < \Delta m_{latest}$$

When this condition is identified, the value of β is reduced by 10% at each iteration until the solver starts converging.

6.4 VFD Control

The flow resolution subroutine discussed in the preceding section assumes a constant pump rotational speed and therefore can be used only for constant speed pumps.

For the simulation of variable speed pumps, VFD control logic is required in the plant pump module. As discussed in section 2.3, differential pressure control is a widely used VFD control method. Most VFDs also have a manual control mode in which the user determines the input frequency of the electric motor. Thus, a differential pressure control and a manual control method are included in EnergyPlus.

6.4.1 Additional User Inputs

To perform manual VFD control, a pump speed schedule input is required. Schedule inputs are time dependent inputs whose value for different hours and days can be specified by the user. The pump speed schedule allows the user to enter the RPM of the electric motor at different times.

To limit the rotational speed of the electric motor, the user will provide the maximum and

minimum RPM value. Requirements for these limits are explained in section 2.1.3.

6.4.2 Manual Control

VFD manual control mode is implemented in EnergyPlus with the help of the RPM schedule input. In manual control mode the user will specify the RPM at different times of the day.

For example solar collectors need variable flow depending on time of day. During the night, the solar water heater may lose heat; in this case the user may want to turn-off the pump or run the pump at minimum speed. During a low solar radiation period of the day, the thermal performance of the solar collector drops; in such a case the ratio of the heat gain due to solar collectors by pumping energy decreases. The ratio basically indicates the overall system efficiency. To improve the system efficiency the flow needs to be reduced. The user can use an RPM schedule in which rotational speed of the electric motor will go on increasing stepwise from morning to afternoon when solar radiation is maximum and then will start decreasing again and finally will drop down to a minimum value. An RPM schedule can also be used to reduce the flow rates during night time, weekends or holidays.

If manual VFD control mode has been selected the specified schedule will determine the pump rotational speed for the current time step. This RPM value will be used to scale the pump curve which is entered by the user in non-dimensional form. Once the pump curve has been fixed then the successive substitution method will use this curve with the system curve to resolve the operating point. The mass flow rate corresponding to the operating point will overwrite the rated mass flow rate value.

6.4.3 Pressure Range Based Control

In EnergyPlus, since the pump inlet pressure is always set to atmospheric pressure, a single pressure control set-point is required. Constant and variable differential pressure based control systems have been implemented in EnergyPlus as a part of this research. For variable differential

pressure based control the upper and lower limits of the pump operating range are used. This control method will maintain the differential pressure within the specified range. For constant differential pressure based control, the upper and lower limits of the VFD pressure control range are set to the same value. This will maintain a constant differential pressure across the whole system.

During the first iteration of the successive substitution solution, the pump will operate at the rated flow rate and the operating point will be located somewhere along the x-axis. During the second iteration, this rated mass flow rate will be used to calculate the pressure drop using the calculated system pressure curve. The operating point will now be located somewhere along the system curve because. During the second iteration, the type of VFD control logic will also be checked.

The pressure drop corresponding to the resolved mass flow rate will be calculated using the effective pressure constant found in the first iteration. This pressure drop will be checked against the pressure set point range. If the pressure drop is within the user specified range, then the required rotational speed of the pump will be determined. This speed will be checked against the RPM range entered by the user. If the rotational speed is also within range then it will be reported as the output variable.

While performing pressure set point control several cases may occur in which the operating point will either be out of the pressure set point range or out of the RPM range. Rules for such cases are shown in Figure 6-5. The horizontal parallel lines in the plot specify the pressure set point range. The two pump curves represent the maximum and minimum operating RPM of the pump. For the given system curve, the upper mass flow rate is limited by the maximum rotational speed while the lower mass flow rate is governed by the lower pressure set point value. Thus E-F on the x-axis shows the allowable mass flow rate range considered by the pump curves and the VFD control range.

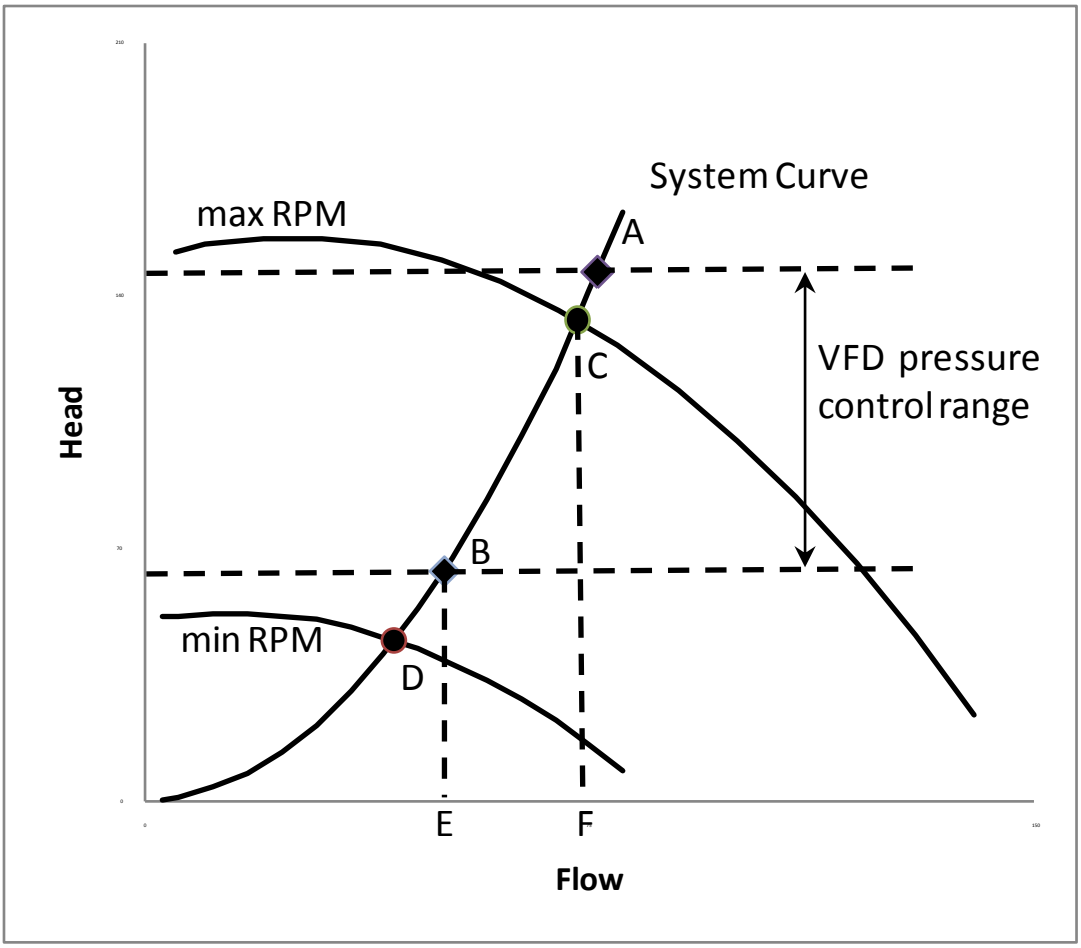

Figure 6-5 Pressure Range Based VFD Control

Points A, B, C and D locate the four constraints on the system curve and can be found by solving the system curve with corresponding limits. At points A and B, the y-coordinate (i.e. the pressure value) is already known since the points lie on the system curve. Thus, the mass flow rate is calculated from the effective pressure constant value. At points C and D, both (x and y) coordinates are unknown. Then the system curve and the pump curve corresponding to maximum and minimum rotational speed value will be solved by successive substitution and coordinates of these two points will be found. The requested flow rate then can be compared with these limiting values once coordinates of all points are known. Depending upon the location of the requested flow rate point, action will be taken to satisfy the conditions. The following table shows the cases that can occur while locating the operating point and the action that the EnergyPlus algorithm

takes.

Table 6-1 Action table for Figure 6-5

Case	Operating point location	Pressure	RPM	Action
1	Beyond point A	Too high	Too high	Points A and C will be compared and point with lower mass flow rate value will be the operating point
2	Between points C and A	Condition Satisfied	High	Pump will run at maximum RPM and point C will be the operating point
3	Between points B and C	Condition Satisfied	Within range	Requested flow rate will be provided by the pump. From operating point coordinates required RPM will be calculated and reported
4	Between points D and B	Low	Within range	Pump will run to maintain minimum pressure drop. From coordinates of point B RPM will be calculated
5	Below point D	Too low	Too low	Points B and D will be compared and point with higher mass flow rate value will be the operating point

In actual practice there are several possible combinations of pressure set point and RPM ranges. For example one range can be a subset of another (in this case the subset range will act as the operating range) or the ranges can overlap (here the overlap region will be the operating range). If there is no common region between the two ranges then the pump routine will use the rated mass flow rate and report a warning in the error file.

6.5 Results

6.5.1 Description of input file

To check the operation of the subroutine a simple test file is created in EnergyPlus. This input file has no building side components. Figure 6-6 shows a schematic diagram of the plant loop used to test the new EnergyPlus pump model. On the demand side, a plant load profile object[19] with a load schedule is placed. A pump with the associated pump curve is placed on the supply side inlet branch. To check the pressure simulation, pressure information is added as a 'pumping load' on the supply side outlet branch.

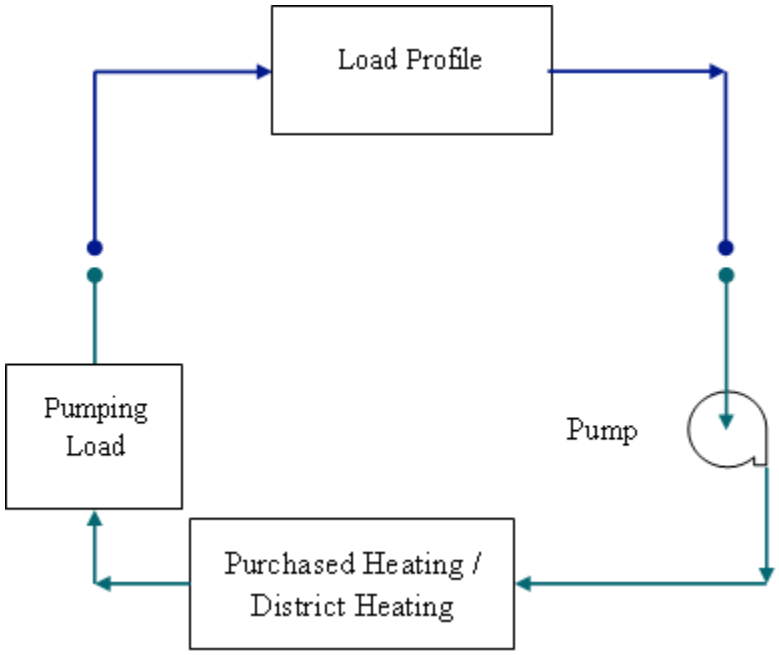

Figure 6-6 EnergyPlus test file schematic

The following pressure information is used in the test file to calculate the pumping load:

[19] The plant load profile object allows a scheduled load to be connected to the plant demand side loop. This is useful when the building plant load profile is already known. It's also useful for testing the operation of plant supply side components.

Table 6-2 Pressure information for test file

Pipe Length	L	80	m
Pipe Diameter	D	40	mm
Roughness	ε	0.045	mm
Loss Coefficients	K	50	-

6.5.2 Pressure simulation with no pump curve

To check the operation of the subroutine, the system is simulated with and without a pump curve. Using information in Table 6-2 and a program in VBA, a generic system curve is found:

$$\Delta p = 30952\dot{m}^2$$

A Bell and Gossett Series 60, 2 X 2 X 5.25 pump is selected which operates at a nominal flow rate of 6.28 kg/s (100 gpm) (which approximately satisfies the load on the demand side of the plant loop), a nominal pressure head of 77.4 kPa (26 ft) and a nominal power consumption of 1050 W. Figure 6-7 shows the system curve and the pump curve of Bell and Gossett Series 60, 2 X 2 X 5.25.

When the system simulation is performed without the benefit of the pump curve (the old EnergyPlus model) the nominal flow rate of. 6.28 kg/s and the nominal pumping power of 1050 W are used in the simulation. Following the pump curve, the system should run at 1.7 kg/s consuming 330 W as shown in Figure 6-7.

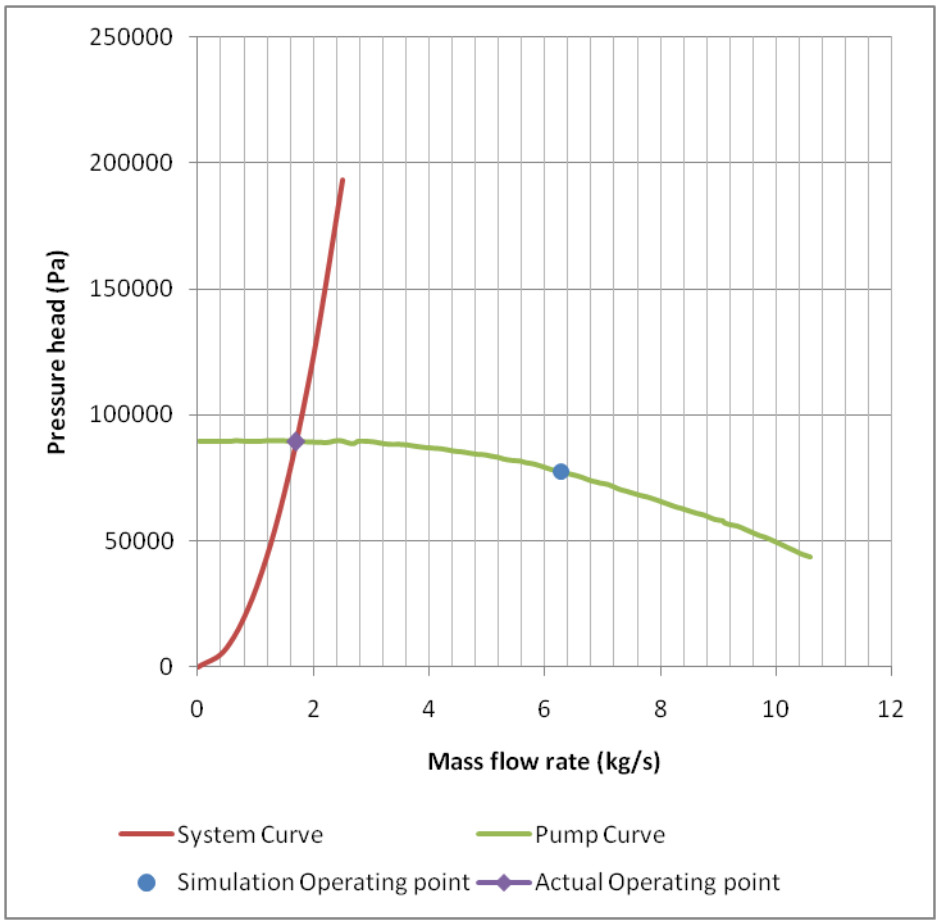

Figure 6-7 Result using previous EnergyPlus model

6.5.3 Pressure simulation with constant speed pump and its pump curve

From the simulation results in Section 6.5.2 it is clear that in the previous version of EnergyPlus, the system is simulated even if the pump cannot satisfy the required flow rate for the given system curve and the load profile. When the same system, pump and load profile is simulated with the Bell and Gossett Series 60, 2 X 2 X 5.25, the simulation ends with warnings stating 'Plant loop falling below lower temperature limit' and in the result file the fluid temperatures are unrealistically lower than freezing temperature. This is because the flow rate provided by the pump is not calculated from rated mass flow rate (i.e. 6.28 kg/s) but resolved from the pump and system curves. Since the calculated mass flow rate (i.e. 1.7 kg/s) is much lower than the required mass flow rate at peak loads in load profile, the pump can't satisfy the heating load on the

demand side, which leads to low temperatures.

The same system is then simulated with a Bell & Gossett Series 80SC 1.5 X 1.5 X 7B pump with a nominal flow rate of 6.6 kg/s (105 gpm), a nominal head of 596000 Pa (200 ft) and a nominal power of 8000 W. This time the simulation is run using the new model and the pressure calculation.

According to the simulation output file, the system mass flow rate is 4.63 kg/s at a pressure head, 635905 Pa and power consumption of 5560 W. Total energy consumed by the pumping system in one day is 133.5 kWhr. Figure 6-8 shows the Bell & Gossett Series 80SC 1.5 X 1.5 X 7B pump curve with the system curve. It can be observed that the operating point calculated by EnergyPlus matches that shown in Figure 6-8 (calculated by MS-Excel).

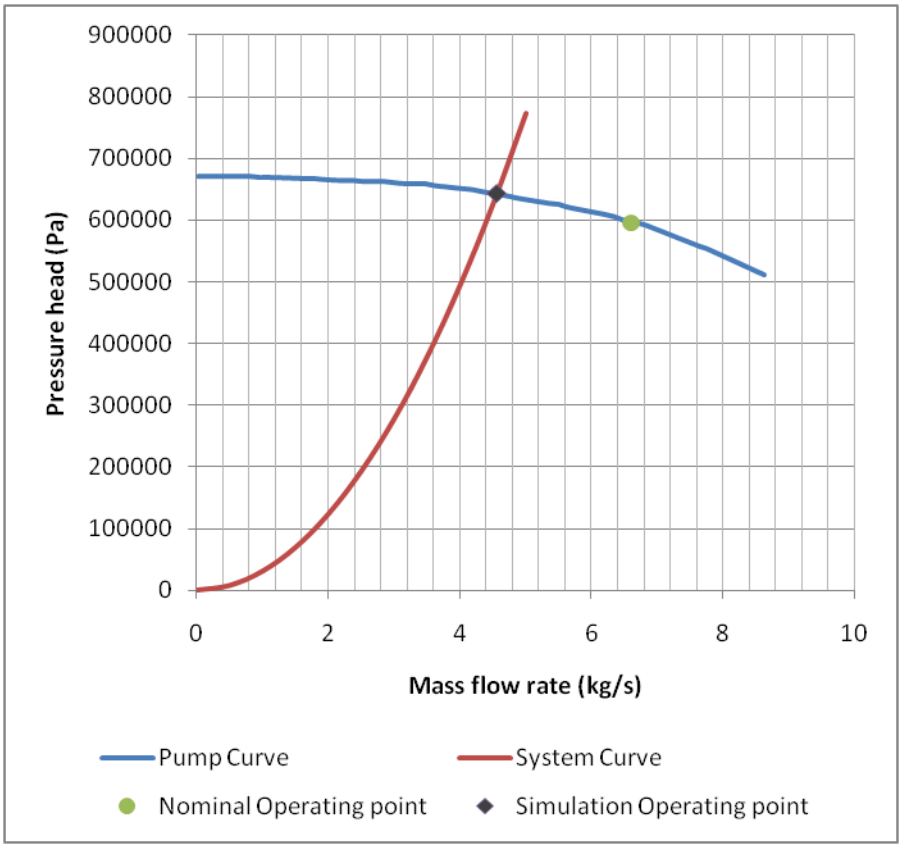

Figure 6-8 Simulation result with flow resolution

To crosscheck the values, the dimensional form of the pump curve:

$$\Delta p = -245.4\dot{m}^3 + 220.96\dot{m}^2 - 2059.3\dot{m} + 671272$$

is numerically solved with the system curve:

$$\Delta p = 30952\dot{m}^2$$

And it gives the result as:

$$\Delta p = 643221\ Pa;\ \dot{m} = 4.56\ kg/s$$

Results from flow resolver of EnergyPlus:

$$\Delta p = 636000\ Pa;\ \dot{m} = 4.63\ kg/s$$

The calculated values match the results from the simulation within 2% for both pressure and flow rate. Thus, the flow resolution works for a constant speed pump and the nominal operating point (or pump BEP) doesn't significantly affect the simulation result.

6.5.4 Pressure simulation using VFD with manual control

To check the operation of a variable speed pump, the constant speed pump is replaced by a variable speed pump with a VFD which is operated in manual control mode. For manual control, an RPM schedule is added. Rotational speeds in this RPM schedule are adjusted with load profile so that the pump will provide required mass-flow rates to satisfy the load on the demand side of the plant loop. Figure 6-9 shows the results of the simulation with the variable speed pump with VFD control. Figure 6-9 shows that with a change in RPM, the resolved mass flow rate changes linearly. Since the flow rate in this cases varies with time, the pressure drop and pump power consumption also varies accordingly.

In this case the energy consumed by the pumping system in a day is 22.7 kWhr, which is much lower than the energy consumption predicted by constant speed pump operation (i.e. 133.5

kWhr). Effectiveness of VFD manual control operation depends on how well the RPM schedule is tuned to the load requirement.

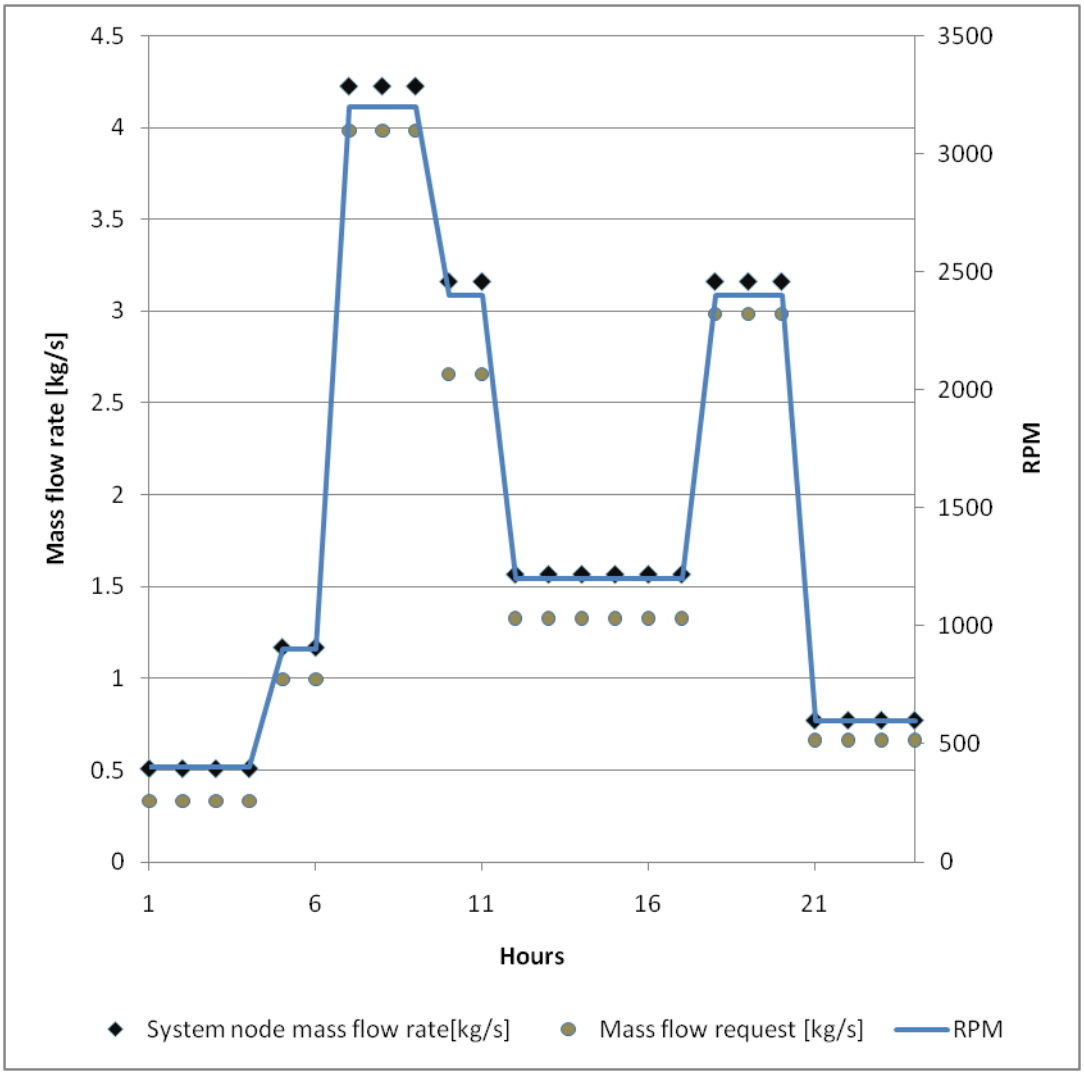

Figure 6-9 Operation of variable speed pump with scheduled rotational speed

From Figure 6-9 it can be observed that the scheduled system mass flow rate is always higher than the optimal mass flow request. For manual control, the schedule will typically be adjusted so that the system flow rate is always slightly higher than required mass flow rate.

6.5.5 Pressure simulation using VFD with pressure set-point control

In this mode of operation the flow request by the system is read by the VFD. Pressure set-point control logic calculates the operating range of the pump from the given conditions (i.e. the minimum-maximum pressure drop range and the minimum-maximum rotational speed range) as explained in section 6.4.3. The mass flow request is then compared with the pump operating range; and if it is within the range, the system mass flow rate is set to the optimal mass flow request.

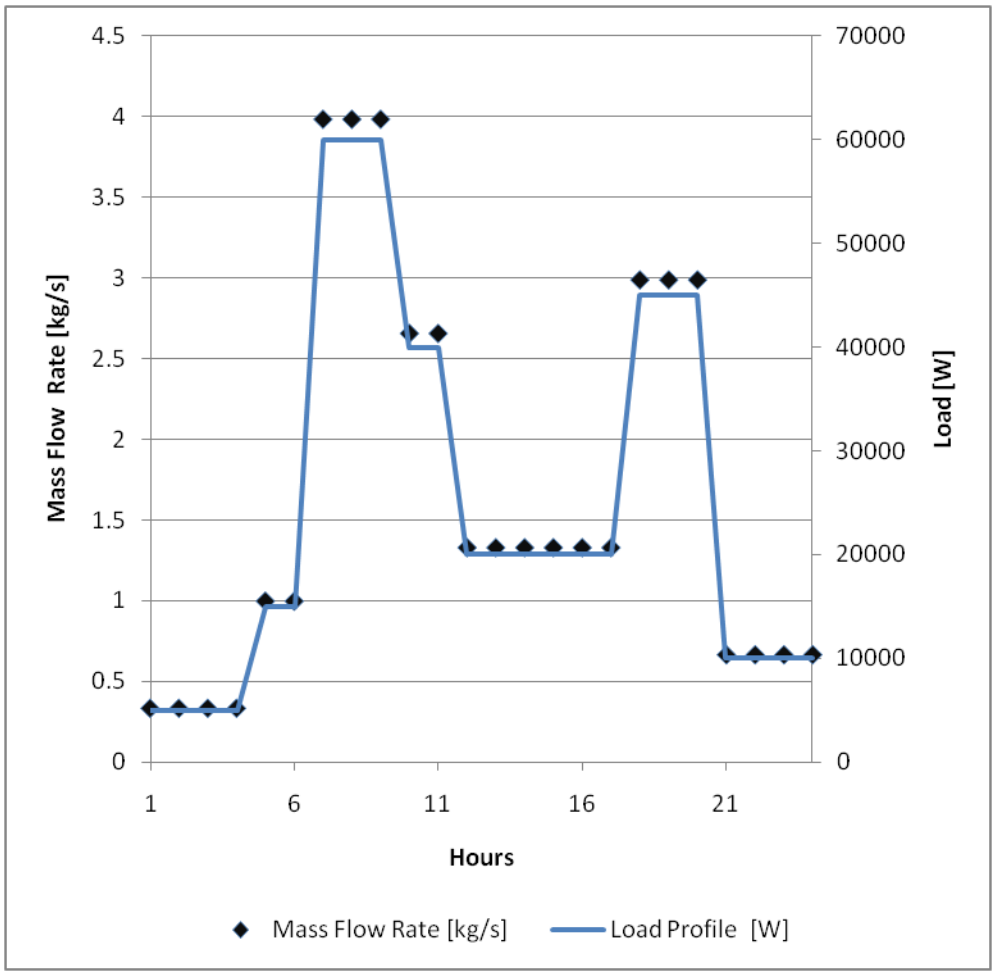

Figure 6-10 Operation of variable speed pump with pressure setpoint control

Figure 6-10 shows the variation in mass flow rate with variation in load. Since in this type of

control, the pump provides exactly the required flow rate, the energy consumed by the pumping system is minimum (18.9 kWhr) compared to other modes of pump operation.

Table 6-3 Summary of results

Operation mode no.	Type of operation	Mass flow rate	Energy Consumption (kWhr)
1	No pressure simulation with constant speed pump	6.28 (Constant, rated mass flow rate)	192
2	Pressure simulation constant speed pump	4.63 (Constant, calculated from pump and system curves)	133.5
3	VFD (RPM schedule)	0.51 - 4.22 (Variable, depends on RPM schedule)	22.7
4	VFD (Pressure set-point control)	0.33 - 3.98 (Variable, depends on flow request)	18.9

Table 6-3 summarizes and compares the results of simulation when same system and pump are used in different operation.

It can be observed that the pump energy consumption calculated by the pressure simulation is significantly lower than the energy calculated with no pressure simulation. The magnitude of the difference will depend on how far the actual operating point if from nominal operating conditions.

In Table 6-3, operation mode 3 and 4 show variable speed pump results. In these modes, the pump operates at the design mass flow rate only when required. The rest of the time the mass flow rate provided by the pump is much lower than the design flow rate. Since the decrease in mass flow rate leads to a significant decrease in energy consumption, mode 3 and 4 show a significant decrease in energy consumption compared to mode 1 and 2.

Energy consumption by the pump in pressure set-point control is lower than for manual control. The energy consumption in manual mode is greater than or equal to that in pressure set-point control mode. The difference in energy consumption between these types of control will depend on the RPM schedule.

Chapter 7. Conclusions and Future Work

Conclusions of the research with respect to the objectives are listed as follows:

7.1 Theoretical study of pump performance

7.1.1 Analytical Pump Performance Curve Models

From results of Tuzson J. (2000) and Spannhake (1934) models and Figure 3-7, we can conclude that skin friction hardly affects the pump performance. Very high surface finish will not help in improving pump performance. Pump material and surface finish should be selected according to application, environmental conditions and cost.

Results of Tuzson J. (2000) and Spannhake (1934) models match closely with manufacturer's data. For the pump taken into consideration, the Spannhake (1934) model results in errors ranging from -28% to 7% while the Tuzson (2000) model results in errors ranging from -10% to 4%.

When assumed parameters are kept constant and impeller diameter is varied the results of both models match with manufacturer's data for varied impeller diameter (Figure 3-10 and Figure 3-11).

Both models provide a rough idea about the effects of pump parameters on the performance curve. Increase in impeller width and impeller inlet diameter leads to an increase in flow passage area and hence a decrease in pump losses. With an increase in impeller width, pump losses decrease slightly and pump performance improves. But, there are geometrical limitations on increasing impeller width, and also significant improvement in pump performance is not observed in the results shown in Figure 3-12. On the other hand, a slight increase in inlet diameter leads to a significant improvement in pump performance due to a drop in shock loss at the entrance. The

effect of an increase in inlet diameter on pump performance is verified with manufacturer's data in Figure 3-13.

An increase in impeller diameter shifts the pump curve upwards (i.e. along the y-axis); this effect is similar to adding pumps in series. While an increase in impeller inlet diameter flattens the pump curve thereby increasing the overall flow rate (for almost the same pressure head); this effect is similar to adding pumps in parallel.

From the equations and the results of the models, it was observed that impeller inlet and exit angles, impeller diameter, impeller inlet diameter and rotational speed all affect the pump performance considerably.

Even if the pump models are approximate and the unavailability of data is a major issue, these models can be used to predict the performance curves of pumps in the same family after calibration.

Neither of the discussed models is convenient to use in a HVAC simulation program when the pump has been specified and pump curves are available. For this situation, the models can be used to determine the effect of each individual parameter on the performance curve. When the size of the pump is unknown, such as in a hydronic system sizing calculation, these models can be used to predict the inlet and outlet diameters of the pump impeller, assisting the designer in sizing the pump for the system. These diameters can be calculated explicitly using the equations developed in this study.

From the observation that the pump shut-off head is approximately 30% of the theoretical head a sizing equation for impeller diameter is derived:

$$d_2 = \frac{1.524}{n} \times \frac{1}{2\pi} \sqrt{\frac{P}{0.3\rho}} \qquad (7\text{-}1)$$

From the results of the models it was observed that the design flow rate of the pump is directly proportional to the impeller inlet diameter. Using this observation a sizing equation for the inlet diameter of the pump is also derived:

$$d_1 = 0.002\sqrt{\frac{kq_{BEP}}{nd_2}} \qquad (7\text{-}2)$$

Efforts were made to find a value of 'k' but it was observed that it varies from 0.02 to 0.05 for different pumps. Since, the equation considers the flow corresponding to best efficiency point; a conservative value of k (≈ 0.03) will provide an approximate value for impeller inlet diameter for known value of flow rate and impeller diameter from Equation 7-1.

7.1.2 Non-Dimensional Pump Model

The non-dimensional π-group gives good results for variation in rotational speed. Using the non-dimensional curve, pump curves at different rotational speeds can be generated from a single set of manufacturer's data.

If geometrical similarity is maintained, the non-dimensional π-groups derived from dimensional analysis will predict the pump performance for variation in pump parameters. But, when the pump impeller is trimmed to match the pump performance, this similarity is not maintained and a unique pump curve for various impeller diameters is not obtained. Thus, these π-groups must be modified to comply with pump affinity laws.

Even after modification of the non-dimensional π-groups, deviation from a single curve is observed. Maximum deviation is observed at higher flow rates and it is minimum near the pump shutoff head. This deviation increases with reduction in impeller diameter from the actual design size. Thus, the non-dimensional model does not completely eliminate the effect of the pump diameter.

When this deviation is measured for pumps with a wide range of flow rates (35 gpm to 1600 gpm), rotational speeds and shapes, a maximum deviation of 30% is observed. No generalized trend is observed between reduction in impeller diameter and deviation from the non-dimensional curve. For example for a 32% reduction in impeller diameter a maximum deviation of 18% is observed for the Bell & Gossett Series 60 - 1 x 1 x 5.25 pump; whereas in the case of the Series 80 - 6 x 6 x 7 pump, a 15% reduction in diameter results in a 27% deviation from the manufacturer's data.

Compared with the analytical pump performance prediction models, the non-dimensional model provides results with comparable accuracy and minimum inputs. One advantage of the non-dimensional model over the affinity laws is that it also considers the variation in fluid density which accounts for temperature variation and the use of anti-freezing agents like Ethylene Glycol. The non-dimensional model first presented by Clark (1985) is only appropriate if the geometrical similarity of the pump is maintained. It is incorrect for use with a single pump housing and trimmed impellers. For this case, the modified model presented in this chapter should be used.

7.2 Experimental validation of affinity laws and non-dimensional model

From the experimental data it was observed that pressure across the pump was almost constant for all flow rates. This lead to the conclusion that the pump is oversized for the system and the mass flow rate through the pump was not close to the design flow rate.

Non-dimensional flow and pressure coefficients of experimental data at various rotational speeds were plotted and found to be in agreement. These non-dimensional curves also validated the manufacturer's pump curve. Due to over-sizing of the pump the experimental data does not represent the complete pump curve.

When mass flow rate and the non-dimensional flow coefficient (φ) were plotted with the variation in rotation speed, it was observed that the mass flow rate is directly proportional to rotational

speed and flow coefficient remains fairly constant (as expected) up to 550 rpm. Below this rotational speed the flow rate through the system deviates from expected results and the value of flow coefficient is no longer constant. This drop in the flow rate is due to recirculation in the pump at low rotational speeds. When this occurs, the flow coefficient from the non-dimensional model does not accurately predict the flow.

When the experimentally determined pressure rise and non-dimensional head coefficient (ψ) were plotted with variation in rotation speed, it was observed that the experimental data points match the theoretically predicted values and the non-dimensional head coefficient remains constant over a wide range of rotational speed. Thus, we can conclude that the experimental results comply with the affinity law and the non-dimensional model for pressure rise across the pump even at low rotational speed.

Deviation of the mass flow rate from the theoretical curve is reflected in experimental data points for output power. Thus, the value of power coefficient follows the flow coefficient and does not remain constant below 550 rpm. Even though percentage wise the deviation in theoretical and experimental value of output power at low rotational speeds is high; the quantitative value of the error is negligible when compared with power consumption in regular HVAC systems. Thus, it is safe to use affinity laws to predict output pump power at low rotational speeds.

Pump output power and input power to the pumping system does not necessarily exhibit a linear relation. Pump power savings depend on a decrease in pump input power with a reduction in pump speed. Thus, extending the results of the non-dimensional model and the affinity law to predict power savings, over wide range of rotational speed is not necessarily correct. A large deviation (percentage wise and quantitatively) in pump input power is observed when compared with estimated input power at low rotational speeds. Thus, at low rotational speeds, the predicted power savings using affinity laws are optimistic.

In the region where $\eta_{wire\_to\_water}$ is relatively constant, the pump output power and the input power to the pumping system will exhibit a linear relationship. The $\eta_{wire\_to\_water}$ depends on individual component efficiencies. Thus, using Figure 5-13 approximate ranges where the non-dimensional model and the affinity law can be applied are found and presented in Table 5-2.

7.3 Implementation of pump model in EnergyPlus

7.3.1 Results and conclusions

When successive substitution and Newton-Raphson methods were compared to solve pump and system curves, the successive substitution was found to be most suitable for the application. The stability and speed of the successive substitution method is further improved by the addition of a damping factor (β). The damping factor not only improves the stability but reduces the number of iterations required for the convergence of the system.

In the successive substitution, the calculation sequence and the information flow determines the stability of the solution. In most cases, the pump and system curve converge when the pressure value is passed on to the next iteration (this flow sequence is implemented in the EnergyPlus pump flow resolution function).

Passing the pressure value between successive substitution iterations usually leads to convergence because; in general, the absolute value of slope of a pump curve is less than that of the system curve at the operating point. If it is other way round (which is rare in practical applications), the same flow of information will lead to divergence. In such cases, the divergence of the system is detected by comparing the resolved mass flow rates from the last two iterations. If divergence is detected the value of damping factor is reduced by 10% and after the next three iterations convergence is checked again. The value of β is reduced until convergence of the system is achieved.

The new EnergyPlus pump model was tested using a simple input data file. Test results for both constant and variable speed pumps showed that the new EnergyPlus model performed correctly.

7.3.2 Future work

While calculating the power consumption, the current EnergyPlus pump model takes into consideration the mass flow rate and pressure drop in the system which is more realistic compared to use of rated power consumption value. But, current model does not include efficiency curves for the pump, the electric motor or the VFD.

The current model uses constant efficiency for power calculations. Thus, the current pump model in EnergyPlus does not take into consideration the variation in efficiency with the change in mass flow rate (or shaft load in case of pump). The efficiency curves for highly efficient electrical motors and VFDs are provided by Bernier & Lemire (1999). Curves from this reference can be added to EnergyPlus as default curves which will be used when no efficiency curves are provided by the user.

Appendix: Derivation of Dimensionless Numbers

There are six basic variables which are concerned with pump performance and their dimensions are shown in Table 0-1:

Table 0-1 Variables in Non-Dimensionalization

Symbol	Variable	Dimension
p	Pressure	$M^1L^{-1}T^{-2}$
m	Mass flow rate	M^1T^{-1}
N	Rotational speed of impeller	T^{-1}
D	Characteristic length / Impeller Diameter	L
ρ	Liquid density	M^1L^{-3}
μ	Liquid viscosity	$M^1L^{-1}T^{-1}$

These six variables are based on three fundamental quantities length (L), mass (M) and time (T). Therefore there will be three (6 – 3 = 3) dimensionless products.

We write dimensionless products in following form:

$$\pi_1 = \rho^{x1} N^{y1} D^{z1} \dot{m}$$

$$\pi_2 = \rho^{x2} N^{y2} D^{z2} p$$

$$\pi_3 = \rho^{x3} N^{y3} D^{z3} \mu$$

Dimensional equation:

π_1: $$M^0L^0T^0 = (M^1L^{-3}T^0)^{x1}\ (M^0L^0\ T^{-1})^{y1}(M^0L^1\ T^0)^{z1}(M^1L^0T^{-1})$$

Algebraic equations for exponents of above equation:

M: $x_1 + 1 = 0$

L: $-3x_1 + z_1 = 0$

T: $-y_1 - 1 = 0$

Solving: $\Rightarrow\ x_1 = -1, y_1 = -1, z_1 = -3$

Substituting: $\Rightarrow\ \pi_1 = \rho^{-1}N^{-1}D^{-3}\dot{m}$

$$\Rightarrow\ \pi_1 = {\dot{m}}/{\rho N D^3} \qquad (8\text{-}1)$$

Similarly:

π_2: $M^0L^0T^0 = (M^1L^{-3}T^0)^{x2}\ (M^0L^0\ T^{-1})^{y2}(M^0L^1\ T^0)^{z2}(M^1L^{-1}T^{-2})$

Algebraic equations for exponents of above equation:

M: $x_2 + 1 = 0$

L: $-3x_2 + z_2 - 1 = 0$

T: $-y_2 - 2 = 0$

Solving: $\Rightarrow\ x_2 = -1, y_2 = -2, z_2 = -2$

Substituting: $\Rightarrow\ \pi_2 = \rho^{-1}N^{-2}D^{-2}P$

$$\Rightarrow\ \pi_2 = {P}/{\rho N^2 D^2} \qquad (8\text{-}2)$$

And,π_3: $M^0L^0T^0 = (M^1L^{-3}T^0)^{x3}\ (M^0L^0\ T^{-1})^{y3}(M^0L^1\ T^0)^{z3}(M^1L^{-1}T^{-1})$

Algebraic equations for exponents of above equation:

M: $x_3 + 1 = 0$

L: $-3x_3 + z_3 - 1 = 0$

T: $-y_3 - 1 = 0$

Solving: $\Rightarrow x_3 = -1, y_3 = -1, z_3 = -2$

Substituting: $\Rightarrow \pi_3 = \rho^{-1}N^{-1}D^{-2}\mu$

$$\Rightarrow \pi_3 = {}^{\mu}/_{\rho N D^2} \tag{8-3}$$

If we multiply Equation 4-10 and Equation 4-11 we will get power coefficient;

$$\pi_4 = \left({}^{\dot{m}}/_{\rho N D^3} \times {}^{p}/_{\rho N^2 D^2}\right)$$

$$\Rightarrow \pi_4 = \left({}^{\dot{m}p}/_{\rho}\right) \times {}^{1}/_{\rho N^3 D^5}$$

$$\Rightarrow \left({}^{\dot{m}}/_{\rho}\right) \times {}^{p}/_{\rho N^3 D^5} = Q \times {}^{p}/_{\rho N^3 D^5}$$

$$\Rightarrow \pi_4 = {}^{P}/_{\rho N^3 D^5} \tag{8-4}$$

References

ASHRAE Handbook. (1996). *HVAC Systems and Equipements (Chapter 38 Centrifugal Pumps)*. American Society of Heating Refrigeration and Air-Conditioning Engineers, Inc.

Bell & Gossett - Series 60 . (2006, 3 17). *SUBMITTAL B-131.5E*. Retrieved 11 30, 2010, from Bell & Gossett: http://www.bellgossett.com/literature/files/1567.pdf

Bell & Gossett, Series 80-SC. (2005, 03). Spacer-Coupled Vertical In-line Centrifugal Pump, ITT Industries, B-180B. Morton Grove, IL, USA.

Bernier, M., & Lemire, N. (1999). Non-Dimensional Pumping Power Curves for Water Loop heat Pump Systems. *ASHRAE Transactions V. 105, Pt. 2* .

Bourret, B., & Bernier, M. A. (1999). Pumping Energy and Variable Frequency Drive. *American Society of Heating Refrigerating and Air-Conditioning Engineers (ASHRAE) Journal* , 37-40.

Brandemuhl, M. J. (1993). Detailed Flow Components - Detailed Pump (Pressure Dependent). In M. J. Brandemuhl, S. Gabel, & I. Andersen, *HVAC 2 Toolkit - A Toolkit for Secondary HVAC System Energy Calculations* (pp. 3-3, 3-14). Atlanta, Georgia: American Society of Heating, Refrigerating and Air-Conditioning Engineers, Inc.

Chua, L. P., & Akamatsu, T. (2000). Measurement of gap pressure and wall shear stress of a blood pump model. *Medical Engineering & Physics* , 175-188.

Clark, D. R. (1985). *HVACSIM+ Building Systems and Equipment Simulation Program: Reference Manual* . Washington, D.C.: U.S. Department of Commerce.

Eldridge, D. S. (1998). *The Validation of Cooling Load Calculation Procedures* . Stillwater:

Oklahoma State University.

Elliot, R. N., & Nadel, S. (2003). *Realizing Energy Efficiency Opportunities in Industrial Fan and Pump Systems (page 1).* Washington, D.C. 20036: American Council for Energy-Efficiency Economy.

EnergyPlus Engineering Reference. (2010, October 11). *EnergyPlus Engineering Reference - The Reference to EnergyPlus Calculations* . USA: University of Illinois and the Ernest Orlando Lawrence Berkeley National Laboratory.

European Association of Pump Manufacturers. (1999). *Attainable Efficiencies of Volute Casing Pumps: a reference guide.* Surrey: Reed Electronics Research.

EuroPump and Hydraulic Institute. (2004). Control Principles of Variable Speed Pumping. In EuroPump and Hydraulic Institute, *Variable Speed Pumping - A Guide to Successful Applications* (pp. 67-77). Kidligton, Oxford: Elsevier Advanced Technology.

(2004). Variable Speed Drive. In Europump And Hydraullic Institute, *Variable Speed Pumping - A Guide To Successful Applications* (pp. 59-66). Kidlington, Oxford: Elsevier Advanced Technology.

Gao, X., Mclnerny, S. A., & Kavanaugh, S. P. (2008). Developement of a Correlation for System Efficiency of Variable Speed Pumping System. *American Society of Heating, Refrigerating and Air-Conditioning Engineers Transactions (Vol. 114, Part 1)* , 387-391.

Hern, S. A. (2002). *Design of an Experimental Facility for Hybrid Ground Source Heat Pump System.* Stillwater: Okolahoma State University .

Hodge, B. K., & Taylor, R. P. (1999). Prime Movers. In *Analysis and Design of Energy Systems (Third Edition)* (pp. 252-338). Prentice Hall Inc., Upper Saddle River, New Jersey 07458.

Integrated Publishing, Inc. (1993). *Nuclear Power Training - DOE FUNDAMENTALS HANDBOOK - Volume 1 of 2.* Retrieved 12 2, 2010, from http://www.tpub.com: http://www.tpub.com/content/doe/h1018v1/css/h1018v1_102.htm

Lazarkiewicz, S., & Troskolanski, A. (1965). Pump Characteristics. In *Impeller Pumps* (pp. 397-448). New York: Pergamon Press.

Lazarkiewicz, S., & Troskolanski, A. T. (1965). Theory of Dynamical Similarity of Impeller Pumps. In *Impeller Pumps* (pp. 101-121). New York: Pergamon Press.

Manivannam, A. (2010). Computatuional Fluid Dynamics Analysis of a Mixed Flow Pump Impeller. *International Journal of Engineering Science and Technology (Vol. 2, No. 6)* , 200-206.

McCoy, G. A., Litman, T., & Douglass, J. G. (1993). *Energy-Efficient Electric Motor Selection Handbook (Rev. 3)*. Olympia, Washington: Department of Energy.

McQuiston, F. C., Parker, J. D., & Spitler, J. D. (2005). Flow, Pumps, and Piping Design. In F. C. McQuiston, J. D. Parker, & J. D. Spitler, *Heating, Ventilating, and Air Conditioning Analysis and Design* (p. 316). John Wiley & Sons, Inc.

Olson, R. M. (1998). Fuid Mechanics. In M. Kutz, *Mechanical Engineers' Handbook* (p. 1317). New York: John Wiley & Sons, Inc.

Shepherd, D. G. (1956). Dimensional Analysis (Page 10 - 48). In D. G. Shepherd, *Principles of Turbomachinery* (pp. 24 - 25). New York: The Macmillan Company.

Sherstyuk, A. N., Trulev, A. V., & Ermolaeva, T. A. (2002). Determination of the Exit Angle of Impeller Blades of a Submersible Oil Pump. *Chemical and Petroleum Engineering, Vol. 38, Nos. 9-10* , 610-612.

Singh, G., & Mitchell, J. W. (1998). Energy Savings from Pump Impeller Trimming. *American*

Society of Heating, Refrigerating and Air-Conditioning Engineers (ASHRAE), , 60-64.

Spannhake, W. (1934). Calculation of the Behavior of Turbo-Machines Under Changing Conditions of Operation, Using the Energy Balance. In *Centrifugal Pumps, Turbines and Propellers* (pp. 149-153). Cambridge: The Technology Press, Massachusetts Institute of Technology.

Stoecker, W. F. (1971). Steady State Simulation of Large Systems. In *Design of Thermal Systems* (pp. 331-357). McGraw-Hill Book Company.

The Fab Lab program, C. f. (2000, 10 16). *Pulse-width modulation*. Retrieved 11 29, 2010, from FabCentral: http://fab.cba.mit.edu/classes/MIT/961.04/topics/pwm.pdf

Timar, P. (2005). Dimensionless Characteristics of Centrifugal Pump. *32nd International Conference of the Slovak Society of Chemical Engineering* (pp. 500-503). Tatranské Matliare: Slovak Society of Chemical Engineering.

Tuzson, J. (2000). Performance Calculation. In J. Tuzson, *Centrifugal Pump Design* (pp. 121-131). New York: John Wiley & Sons, Inc.

Tuzson, J., & Iseppon, A. (1997). Centrifugal Pump Design Teaching Tool. *ASME Pumping Machinery Symposium* .

Wiesner, F. J. (1967). A Review of Slip Facctors for Centrifugal Impellers. *ASME Journal of Engineering for Power* , 558-572.

www.industrial-electronics.com. (n.d.). *Pulse-Width Modulation*. Retrieved 11 29, 2010, from Industrial Electronics Information for Manufacturing Applications - Articles: http://www.industrial-electronics.com/output_devices_amplifiers_valves_relays_variable-frequency_drives_stepper_motors_servomotors/AC-drives-5-2_Pulse-Width-Modulation-

Waveforms-Variable-Frequency-Drives.html

VITA

Kaustubh Pradeep Phalak

Candidate for the Degree of

Master of Science

Thesis: DEVELOPMENT, IMPLEMENTATION AND VALIDATION OF A NON-DIMENSIONAL PUMP MODEL IN ENERGYPLUS

Major Field: Mechanical Engineering

Biographical:

Personal Data: Born in Jalgaon, Maharashtra, India on September 7, 1985.

Education:

Completed the requirements for the Master of Science in Mechanical Engineering at Oklahoma State University, Stillwater, Oklahoma in August, 2011.

Received Bachelor of Technology in Mechanical Engineering at University of Pune – College of Engineering Pune, Maharashtra, India in 2007.

Experience:
Worked as Graduate Research Assistant at Mechanical and Aerospace Engineering Department, Oklahoma State University, Stillwater, Oklahoma from January 09 to December 10

Worked as Graduate Teaching Assistant at Mechanical and Aerospace Engineering Department, Oklahoma State University, Stillwater, Oklahoma from August 08 to May 09

Worked as Design Engineer at Design and Estimation, Process Equipments, Alfa Laval India Ltd., Pune, India from October 07 to June 08.

Name: Kaustubh Phalak Date of Degree: December, 2011

Institution: Oklahoma State University Location: Stillwater, Oklahoma

Title of Study: DEVELOPMENT, IMPLEMENTATION AND VALIDATION OF A NON-DIMENSIONAL PUMP MODEL IN ENERGYPLUS

Pages in Study: 140 Candidate for the Degree of Master of Science

Major Field: Mechanical Engineering

Scope and Method of Study: In HVAC plant simulation software, a pump model is required to carry out pressure based simulation, which will govern flow rate in system and predict accurate power consumption. To implement a pump model in EnergyPlus, which will predict pump performance with varied pump parameters such as rotational speed and pump diameter pump performance models and non-dimensional model was studied. Their applicability and accuracy was checked experimentally and with manufacturer's data. Using the pump performance prediction model effect of pump parameters on its performance was observed. Also applicability of affinity laws to predict pump power savings was studied.

Findings and Conclusions: It was observed that performance prediction models calculate the pump performance with sufficient accuracy but are not suitable to implement in energy simulation programs when the pump has been specified and pump curves are available. These models can be used to determine the effect of each individual parameter on the performance curve. When the size of the pump is unknown, in a hydronic system sizing calculation, these models can be used to predict the inlet and outlet diameters of the pump impeller, assisting the designer in sizing the pump for the system. Due to simplicity, less number of input requirements and accuracy a non-dimensional model was found to be suitable for energy simulation purpose. But, when checked with manufacturer's data it was observed that these non-dimensional models cannot be used directly for variation in impeller diameter. A modified non-dimensional model was suggested which not only satisfied the pump affinity laws but also gave better results as compared to earlier non-dimensional model suggested by Clark (1985). This modified non-dimensional model with VFD control is implemented in EnergyPlus. It was also found that pump affinity laws can be used for predicting power savings only if there is linear relationship between input and output power of the pumping system. The ranges for applicability of the pump affinity laws to predict power savings were found using standard electrical motor efficiency curves.

ADVISER'S APPROVAL: Dr. Daniel Fisher